J. Phys.: Condens. Matter 10 (1998) 1013–1032. Printed in the UK PII: S0953-8984(98)82516-2

Crossover from semiconductor to magnetic metal in semi-Heusler phases as a function of valence electron concentration

J Tobołaţ, J Pierre‡, S Kaprzykţ, R V Skolozdra§ and M A Kouacou‡

ţ Faculty of Physics and Nuclear Techniques, Academy of Mining and Metallurgy, alica Mickiewicza 30, 30-059 Kraków, Poland

‡ Laboratoire de Magnetisme L Néel, CNRS, 166X, 38042 Grenoble, France

§ Chemistry Department, I Franko University, Lviv 290005, Ukraine

Received 10 March 1997, in final form 4 November 1997

Abstract. Experimental and theoretical investigations of intermetallic semi-Heusler compounds (CoTiSn, FeTiSb, CoTiSb, NiTiSn, CoNbSn, CoVSb, NiTiSb) and their solid solutions ($CoTiSn_{1-x}Sb_x$, $CoTi_{1-x}Nb_xSn$) are presented. The physical properties of these systems are found to be mostly determined by the number of valence electrons. Resistivity experiments show that compounds with 18 valence electrons are either semiconductors (CoTiSb, NiTiSn) or semi-metals (CoNbSn). The electronic structure calculations performed on 18-valence-electron systems by the KKR method show nine valence bands below the Fermi level and a gap of order 0.4–0.9 eV. A decrease or increase of the number of valence electrons in CoTiSb, NiTiSn or CoNbSn leads in either case to a metallic state and either ferromagnetic (CoTiSn, CoVSb) or paramagnetic (FeTiSb, NiTiSb) properties. The KKR results concerning 17- and 19-valence-electron systems correspond well with experimental characteristics, except in the case of CoVSb which KKR calculations predict to be a half-metallic ferromagnet, which conflicts with experimental data.

Magnetization and resistivity measurements indicate that semiconductor–metal crossovers occur together with the appearance of ferromagnetism in the $CoTiSn_{1-x}Sb_x$ and $Co_{1-x}Ni_xTiSn$ series, for x near 0.4. This behaviour is discussed in the context of the KKR-CPA results.

1. Introduction

Heusler phases are well known ternary intermetallic compounds, with general formula X_2YZ, where X and Y are transition metals and Z is an sp element. Semi-Heusler phases have the same cubic structure, except that one of the X sites is empty, giving a formula XYZ. Due to the vacant site, the overlap between the d wave-functions is smaller, which gives rise to narrower bands and to the appearance of gaps in the energy spectra. This family of compounds attracted wide interest after the discovery for the NiMnSb and PtMnSb ferromagnets [1, 2] of peculiar electronic structure properties, collectively known as half-metallic ferromagnetism. The half-metallic character arises from the magnetic splitting of the bands, which leads to the occurrence of an energy gap at E_F for down-spin electrons, together with a metallic state for up-spin electrons [3, 4].

In this paper we focus on the physical properties of some XYZ compounds, where the transport and magnetic properties are governed by the number of valence electrons (EC). Compounds such as NiTiSn, CoTiSb with EC = 18 were found to be semiconductors (SC) [5, 6]. In the following, we consider how the electronic and magnetic properties are modified

0953-8984/98/051013+20$19.50

on passing to EC = 19 and EC = 17 systems, by adding (removing) one electron to (from) the different crystallographic sites. We shall see how a crossover from a semiconducting to a metallic state occurs, and how it may be related to the onset of weak ferromagnetism.

Measurements of resistivity and magnetization, as well as band-structure calculations by the Korringa–Kohn–Rostoker (KKR) method, were performed for the following ordered samples: CoTiSn, FeTiSb, CoTiSb, NiTiSn, CoNbSn, CoVSb and NiTiSb. Recently [6, 7], insulator–metal crossovers related to the onset of ferromagnetic ordering were detected in $Co_{1-x}Ni_xTiSn$ and $CoTiSn_{1-x}Sb_x$ solid solutions for x near 0.4. However, the concentration dependencies of the magnetic moments and Curie temperatures are not the same in these two series. In this paper the new series of solutions $CoTi_{1-x}Nb_xSn$ is also described, where the substitution is at the Y site, and compared with the previous $Co_{1-x}Ni_xTiSn$ and $CoTiSn_{1-x}Sb_x$ series. As will be shown, the variations of the physical properties with concentration are again different, as it is not equivalent to add one electron to the X site (filling the d shell of Co), to the Y site (enhancing the density of d states at this site), or to the Z site. In order to get a deeper insight into the influence of alloying on electronic structure, band-structure calculations were performed for the above-mentioned alloys using the KKR method with the coherent potential approximation (CPA). As far as possible, the ground-state KKR-CPA results will be compared to observed properties, and some interpretations will be proposed for these series concerning insulator–metal transitions and the onset of ferromagnetism.

Table 1. The lattice parameter (at RT), Curie and Curie–Weiss temperatures, spontaneous magnetization at 0 K and effective paramagnetic moment (per Co/Fe atom), or constant paramagnetic susceptibility (emu mol^{-1}) for XYZ semi-Heusler compounds. The crystallographic positions of inequivalent atoms in the unit cell can be easily derived, since the chemical formula is written as XYZ, where X is at (0, 0, 0), Y is at (1/4, 1/4, 1/4) and Z is at (3/4, 3/4, 3/4) in the unit cell.

Compound XYZ	a (Å)	T_C (K)	$M(0)$ (μ_B)	θ_p (K)	μ_{eff}	$10^4\chi_p$
CoTiSn	5.997	135	0.357	176	1.35	—
CoTiSb	5.884	—	—	—	—	1.7
CoNbSn	5.947	—	—	—	—	0.53
NiTiSn	5.941	—	—	—	—	1.3
CoVSb	5.791	58	0.18	75	1.26	0
NiTiSb	5.872	—	—	—	—	1.4

2. Crystallography and physical properties

Let us first describe some structural aspects of Heusler systems. The unit cell of the true Heusler X_2YZ structure (space group: $Fm\bar{3}m$) consists of four inter-penetrating f.c.c. sublattices. If one of the two equivalent sites (0, 0, 0) or (1/2, 1/2, 1/2) (here, occupied by X atoms) is empty, the semi-Heusler XYZ structure (space group: $F\bar{4}3m$) appears [5, 8]. As we see from table 1, d atoms occupy X and Y sites, while metalloids are located at Z positions. The smallest d metal generally occupies the site (0, 0, 0) related to the vacancy site (1/2, 1/2, 1/2). The XYZ systems are far from compact, and thus are subject to lattice instabilities. From a chemical point of view, they can be stabilized only through covalent bonding. Thus they are encountered when Z = Sn or Sb, and then only within a restricted range of peripheral electron number. The ideal valence electron concentration (EC) is 8 or 18 electrons per formula unit, which corresponds to AgMgAs, NiTiSn, ZrNiSn,

CoTiSb, CoNbSn, etc. It leads to the formation of tetrahedral bonds and sp^3 hybridization around the p element and favours bonding between d metals. Semiconducting properties occur for EC = 18 for some of the above-mentioned compounds, and disappear for other values of EC.

As always for Heusler compounds, the physical properties are strongly dependent on the crystallographic order. Disorder generally occurs between d metals, the more so the closer they are in the periodic table. Some atoms may also occupy a vacancy site. For these reasons, all of the samples investigated in the present work were annealed for a long time (one week to one month) at temperatures between 650 and 800 °C. Nevertheless, some atomic disorder is still observed. It is not possible for instance to obtain intrinsic semiconductors in these systems and band gaps cannot be determined properly from transport experiments below 300 K. Similarly, the residual resistivity of metallic phases remains significant.

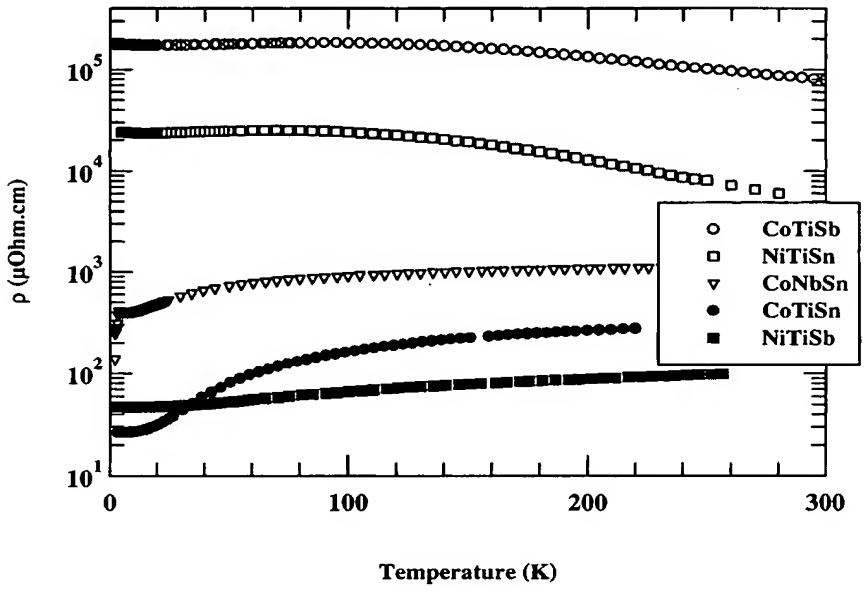

Figure 1. The resistivity for some semi-Heusler compounds.

2.1. The $Co_{1-x}Ni_xTiSn$ series

This series has already been described in previous papers [5, 6]. Here, we recall its basic properties. NiTiSn is a narrow-gap semiconductor (E_g = 0.42 eV according to the KKR calculations [9]). Resistivity measurements show that the intrinsic regime is probably not reached even at room temperature. The experimental gap deduced between 200 and 300 K is only 80 meV, much smaller than calculated. This value may be representative of the activation energy of donor or acceptor levels (figure 1). The susceptibility is nearly constant between 15 and 300 K ($\chi = 1.3 \times 10^{-4}$ emu mol^{-1}) (see table 1). Replacing Ni by Co leads first to the narrowing of the gap, then to metallic conduction and finally to the appearance of weak ferromagnetism for a Co (or hole) concentration of about 0.45. No sharp transition occurs between the SC and metallic phases. The limit between semiconducting and metal-

like behaviours was somewhat arbitrarily set to be the concentration at which the temperature derivative of the resistivity changes from negative to positive, or where the low-temperature resistivity is of the order of the (now historical) Mott limit for metallic resistivity, i.e. a few mΩ cm.

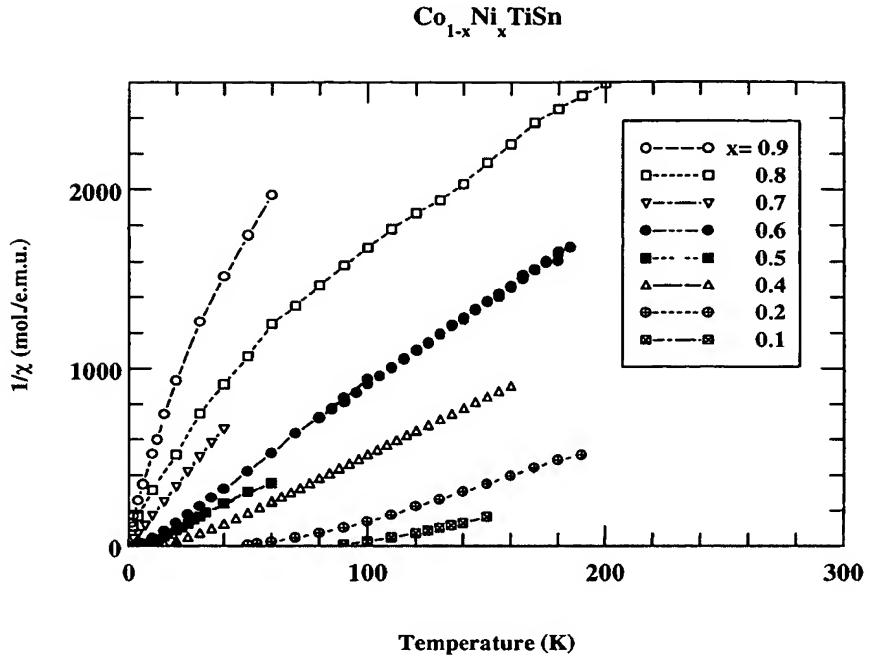

Figure 2. Reciprocal susceptibilities for the $Co_{1-x}Ni_xTiSn$ series.

CoTiSn is a weak ferromagnet, ordering at $T_C = 135$ K, with a moment at low temperature of $M(0) = 0.35\ \mu_B$ (table 2). Co atoms retain a localized moment when diluted in NiTiSn, as shown by the susceptibility of the solutions (figure 2), which exhibit both Curie–Weiss-like and temperature-independent contributions: $\chi = (1-x)C/T + \chi_0$. The Curie constant C per Co ion gives an effective (paramagnetic) moment of Co close to 1.1 μ_B, a value similar to that for pure CoTiSn (1.35 μ_B). Thus the Co paramagnetic moment localizes without a significant change in magnitude when diluted in NiTiSn. In the ferromagnetic range, T_C scales as $M(0)^{1.7}$, which is close to the quadratic behaviour generally observed for localized systems.

2.2. The $CoTiSn_{1-x}Sb_x$ series

Experimental results for this series have already been partly described elsewhere [10]. In this series the solid solution is not continuous: the lattice parameter first decreases regularly on adding Sb up to $x = 0.5$, the phases being metallic. A two-phase region, with two cubic Heusler phases, exists between $x = 0.5$ and $x = 0.6$, then the second semiconducting phase with the smaller lattice parameter continues up to the compound CoTiSb. The SC phase is more compact, which should be ascribed to the bonding mechanism and to the distribution of valence electrons. This SC–metal crossover cannot be a classical Mott transition, since

the SC phase here has a smaller volume than the metallic one and is not magnetically ordered.

The Sn-rich phases order ferromagnetically for $x < 0.5$, but the solutions turn paramagnetic for larger Sb contents. The susceptibility behaviour changes from Curie–Weiss-like in the ferromagnetic range, with an effective moment per Co proportional to the Sn content, to the characteristic behaviour of enhanced paramagnets, with a maximum value in the range 50 to 100 K (figure 3) for SC solutions. A nearly constant susceptibility $\chi = 1.7 \times 10^{-4}$ emu mol^{-1} is observed for the CoTiSb, a result which is close to that ($\chi = 1.14 \times 10^{-4}$ emu mol^{-1}) obtained by Terada *et al* [11]. The magnetic susceptibility of this series as a function of concentration behaves like that of $ZrZn_2$ under pressure [12]. In the ferromagnetic range, T_C is proportional to $M(0)$, a behaviour which was also observed in the metallic solutions between Co_2TiSn and Ni_2TiSn [13].

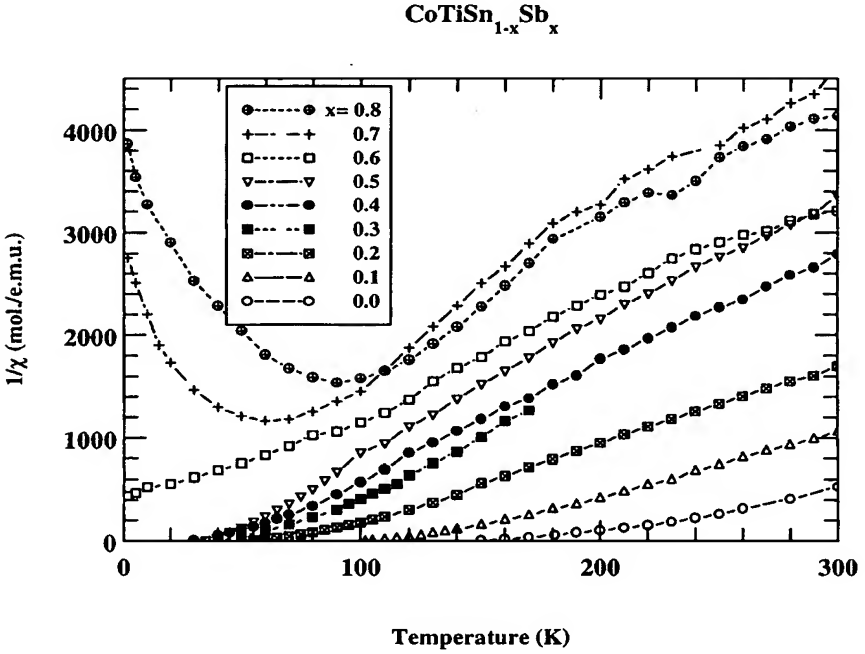

Figure 3. Reciprocal susceptibilities for the $CoTiSn_{1-x}Sb_x$ series.

The resistivity curves of the solutions have a complex behaviour [10]: in the metallic range, the magnetic part of the resistivity becomes larger and larger as the concentration approaches the magnetic–non-magnetic boundary, giving a large T^2-term at low temperature; the S shape of the resistivity is typical of spin fluctuations. For $x > 0.6$, the SC behaviour is recovered.

Thus striking differences are observed between the $CoTiSn_{1-x}Sb_x$ and the $Co_{1-x}Ni_xTiSn$ series. A puzzling feature is that CoTiSb does not order magnetically, and does not even exhibit any localized magnetism (Curie–Weiss susceptibility) whereas Co atoms diluted in NiTiSn do so. A first interpretation would be that an extra electron added to the Z site can be transferred to Co and fills the d shell. We shall see below that this picture is not accurate, and that another interpretation should be given.

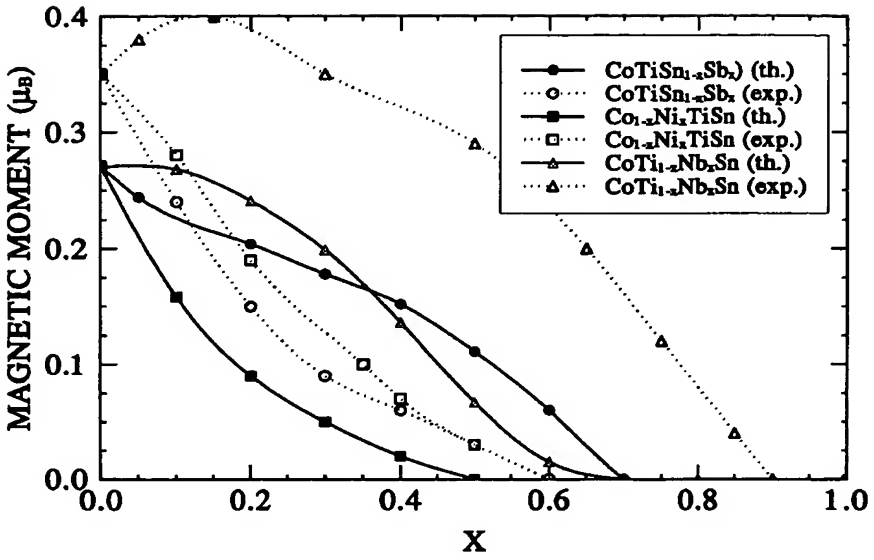

Figure 4. Total magnetic moment variations versus alloy compositions for three isoelectronic series: $Co_{1-x}Ni_xTiSn$ (squares), $CoTiSn_{1-x}Sb_x$ (circles) and $CoTi_{1-x}Nb_xSn$ (triangles). The measured and KKR-CPA points are linked by dotted and solid lines, respectively.

Table 2. Magnetic data for solutions in the $CoTi_{1-x}Nb_xSn$ series.

x (Nb)	T_C (K)	$M(0)$ (μ_B)	θ_p (K)	μ_{eff}
0	135	0.357	158	1.35
0.05	141	0.38	165	1.44
0.15	155	0.40	180	1.51
0.3	120	0.35	151	1.33
0.5	112	0.29	146	1.15
0.65	90	0.20	No CW	—
0.75	23	0.17	—	—
0.85	17	0.12	—	—
0.9	0	0	—	—
1.0	0	0	—	—

2.3. The $CoTi_{1-x}Nb_xSn$ series

A third way to change EC from 17 to 18 is to operate on the third crystallographic site, and to replace Ti by V or Nb. Nb was chosen, since the atomic size of V is smaller than that of either Ti and Nb. In this case, adding a 'd electron' to the Y site should enhance the density of states and correlations on this site. Indeed, the effective moment μ_{eff} per formula unit, θ_p, T_C and $M(0)$ all start to increase with Nb content (table 2, figure 4) up to $x = 0.15$. For $x > 0.15$ all of these quantities decrease, and the ferromagnetism disappears for x between 0.85 and 0.9. The susceptibility of CoNbSn (table 1) is nearly temperature independent and is lower than for other compounds with EC = 18, which may be due to the larger diamagnetic susceptibility of the 4d-metal core. For ferromagnetic samples, the square of the spontaneous magnetization $M(T)$ varies as T^2 for x lower than 0.3, but as

Table 3. The quantities from the band-structure calculations: energy gap E_g, total number of electrons (N_X, N_Y and N_Z), number of d states ($N_{X,d}$, $N_{Y,d}$) inside muffin-tin spheres as well as magnetic moments per formula unit.

Compound	E_g (eV)	N_X	N_Y	N_Z	$N_{X,d}$	$N_{Y,d}$	M (μ_B)
CoTiSn		26.68	20.36	47.83	7.56	1.87	0.28
FeTiSb		25.57	20.38	48.61	6.53	1.96	0.78
CoTiSb	0.95	26.64	20.34	48.52	7.51	1.93	
CoNbSn	0.4–0.6	26.74	38.72	47.82	7.54	2.51	
NbCoSn		39.19	26.42	48.04	2.86	7.44	
NiTiSn	0.42	27.73	20.34	47.87	8.50	1.94	
CoVSb		26.61	21.50	48.41	7.48	2.95	1.00
NiTiSb		27.70	20.33	48.44	8.48	1.96	0.0

$T^{4/3}$ for larger x. This last behaviour was already predicted by Moriya and Kawabata [14] and Lonzarich and Taillefer [15], and attributed to the fluctuations of the order parameter close to the magnetic–non-magnetic crossover.

The resistivity measurements indicate that the metallic character is maintained throughout the series, although the resistivity is much higher for CoNbSn than for metallic CoTiSn or NiTiSb (figure 1). The behaviour observed for CoNbSn implies either a semi-metallic state with a low density of states, or a large atomic disorder which prevents a true semiconducting behaviour. Several CoNbSn samples have been prepared, but even the best one (shown in the figure 1) has a superconducting transition at 3.5 K, a transition temperature which is close to that of Sn. It is probable that some Sn filaments exist between grains and that the stoichiometry of the Heusler phase is not exact. The presence of this spurious phase (undetected by x-rays) may thus explain the metallic-like shape of the resistivity, due to the short-circuit of the primary CoNbSn phase. It may be due to the large difference between the melting points of Sn and Nb, although Co and Nb were first melted together to produce a eutectic with a lower melting point.

Band-structure calculations (see below) show that the inversion of Nb and Co atoms gives rise to a semi-metallic phase instead of a SC one.

2.4. Summary of the experimental results and other compounds

The variation of the ordered magnetic moment $M(0)$ in the three series is plotted in figure 4 as a function of the concentration x (or versus the valence electron number: $17 < EC < 18$). $M(0)$ decreases continuously and almost at the same rate in the $Co_{1-x}Ni_xTiSn$ and $CoTiSn_{1-x}Sb_x$ series, and the ferromagnetic state disappears for x close to 0.6 (EC = 17.6). For the $CoTi_{1-x}Nb_xSn$ series, the magnetization and the Curie temperature first increase as a function of EC, and then drop to zero for EC close to 17.9. As previously mentioned, the last feature is due to the increase in the d DOS at the Y site which reinforces the magnetic interactions.

Compounds like NiTiSb and CoVSb have 19 valence electrons, and thus a reappearance of metallic conduction may be expected. The magnetic properties of these systems have been investigated by Terada *et al* [11]. NiTiSb is a Pauli paramagnet, with $\chi = 1.56 \times 10^{-4}$ emu mol^{-1} as deduced from measurements between 25 and 250 K ($\chi = 1.37 \times 10^{-4}$ emu mol^{-1} from reference [11]). Resistivity measurements show that this compound is a normal metal. The Debye temperature obtained by a Bloch–Grüneisen fit is estimated to be 220 ± 20 K.

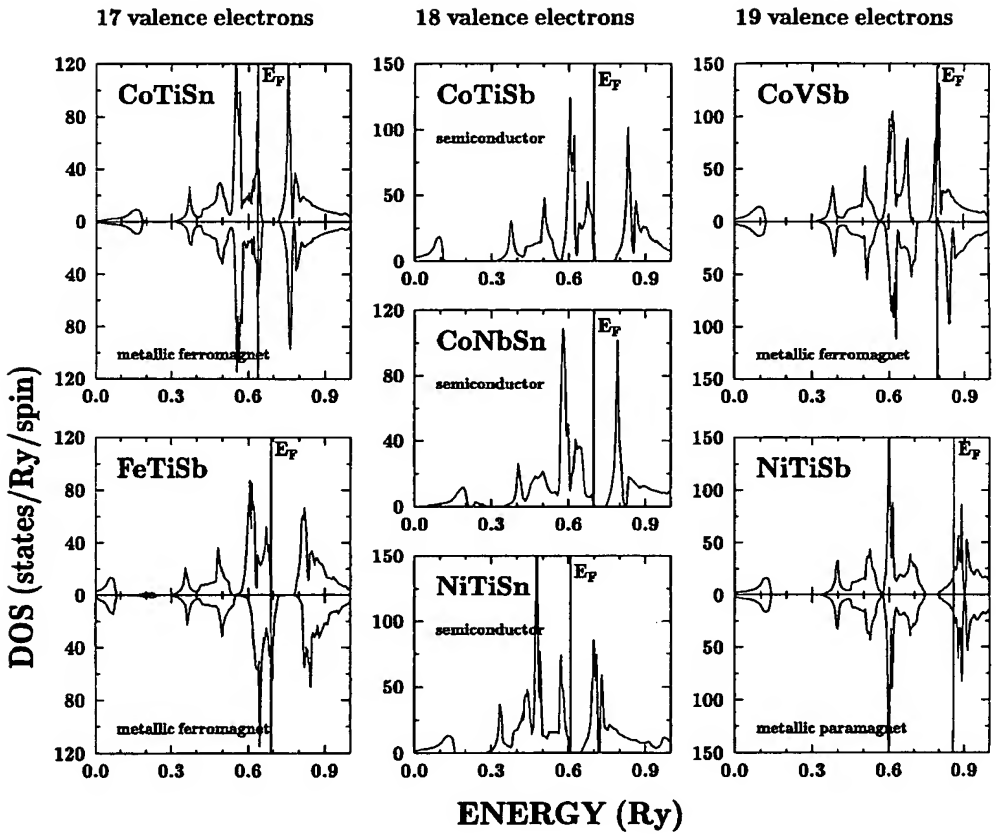

Figure 5. Total densities-of-states spectra of semi-Heusler compounds with various numbers of valence electrons (EC). Each column represents isoelectronic systems. CoTiSn and FeTiSb (EC = 17) are metals, CoTiSb, CoNbSn and NiTiSn (EC = 18) are semiconductors, while CoVSb and NiTiSb (EC = 19) are again metals.

CoVSb is a weak ferromagnet, with $M(0) = 0.18\ \mu_B$, and $T_C = 58$ K [11]. Its effective paramagnetic moment is $1.26\ \mu_B$, close to the values found for CoTiSn and Co diluted in NiTiSn. As for CoTiSn, a fairly large ratio of the paramagnetic to the ferromagnetic moment is observed, which is typical of weak itinerant systems. Finally we observed that FeTiSb (EC = 17) is metallic and exhibits a Curie-like behaviour at low temperatures, but without magnetic order down to 1.5 K.

3. Band-structure studies

We have implemented fully charge and spin self-consistent KKR calculations for CoTiSn, FeTiSb, CoTiSb, CoNbSn, NiTiSn, CoVSb and NiTiSb ordered systems. The computations for $CoTiSn_{1-x}Sb_x$ and $CoTi_{1-x}Nb_xSn$ and the previous ones [9] for $Co_{1-x}Ni_xTiSn$ (with $x = 0.0, \ldots, 1.0$) solid solutions were performed by the KKR-CPA method [16–19]. For compounds as well as for alloys, muffin-tin potentials were constructed within the local spin-density (LSD) approach, using the exchange–correlation part of the von Barth–Hedin

formula [20]. The KKR-CPA self-consistency cycles were repeated for each composition until the difference between input and output potentials was less than 1 mRyd. For the final muffin-tin potentials, the total density of states (DOS), the site-decomposed densities of states (CDOS) and l-decomposed (with $l_{max} = 2$) partial densities of states (PDOS) were computed on a 201-energy-point mesh for the alloys and on a 601-point mesh for the compounds. The integration in k-space was performed using 192 small tetrahedra in (1/48)th of the Brillouin zone, applying the method described in reference [21]. The KKR-CPA code contains the generalized Lloyd formula which permits the precise determination of the Fermi energy, using an elliptic contour in the complex energy plane. In our computations the contour contained 48 energy points and the CPA Green function was computed on a mesh of 75 special k-points in the irreducible part of the BZ for each of the 48 above-mentioned energy points.

In our calculations the experimental lattice constants were generally used. The KKR-CPA calculations for disordered $CoTiSn_{1-x}Sb_x$ were performed with lattice constants corresponding to the values of CoTiSn and CoTiSb compounds successively. This allowed the influence of the lattice parameter to be checked on the electronic structure, an important feature in this case due to the discontinuity of the solid solution. In the $CoTi_{1-x}Nb_xSn$ series the variation of the cell parameter is quite small (table 1). An empty sphere was added at the (1/2, 1/2, 1/2) position in order to improve the filling factor of the WS cell for filling by non-overlapping muffin-tin spheres (for semi-Heusler systems, when using equal radii, this factor is less than 50%; it increases to 68% on adding extra spheres). The radius $r_{mt} = \frac{\sqrt{3}}{8}a$ was chosen for all non-equivalent atoms in the WS cell, although some numerical trials were done for the CoTiSn compound using various muffin-tin radii for Co, Ti and Sn atoms.

The electronic structure of the end-point compounds was also computed using the KKR-CPA code. Such calculations allow the results obtained by the two methods to be compared and show the DOS characteristics for a vanishing or near-vanishing concentration of one dopant. The limit cases ($x = 0$ and $x = 1$) mean that from the KKR-CPA calculations one may recover for instance the DOS of the Nb atom (one-impurity properties) diluted in the pure CoTiSn, i.e. the $CoTi_{1-x}Nb_xSn$ ($x = 0$) case.

The electronic structure of the present semi-Heusler systems is roughly divided into three groups, according to the number of valence electrons (17-, 18- and 19-electron systems). Figure 5 is a kind of phase diagram, which illustrates the electronic structure of systems and their corresponding ground-state properties. CoTiSn and FeTiSb (EC = 17) are found to be metallic ferromagnets, CoTiSb, CoNbSn and NiTiSn (EC = 18) semiconductors, while NiTiSb and CoVSb (EC = 19) are again metals in the paramagnetic and ferromagnetic state, respectively. From a brief comparison we observe that, even for isoelectronic compounds, the magnetic and transport properties strongly depend on the constituent atoms and their crystallographic positions. From the set of pictures in figure 5, we can easily draw all possible 'paths' between the ordered systems, guessing properties of possible solid solutions. Nevertheless, as observed in our experiments, some phase diagrams do not show a continuous solution. In this paper we focus on the series of solid solutions $CoTiSn_{1-x}Sb_x$ and $CoTi_{1-x}Nb_xSn$, which seem the most attractive for our purposes. The $CoV_{1-x}Ti_xSb$ series has not yet been investigated experimentally and will not be presented in this paper.

3.1. CoTiSn and FeTiSb

The spin-projected DOS picture for CoTiSn (the top-left-hand panel in figure 5, also in reference [9]) shows a weak polarization corresponding to a magnetic moment of about

0.28 μ_B per formula, which is mainly localized on the Co site (0.15 μ_B inside the muffin-tin sphere). The conduction band is formed essentially from d states of Co with some admixture of Sn p states and Ti d states, but part of them are observed above a gap. The DOS for spin up abruptly decreases in the vicinity of the Fermi level, whereas for spin down E_F falls almost precisely at a peak of the DOS. Electronic structure calculations close to the SC–metal limit and close to the magnetic instability are highly sensitive to the determination of the Fermi level. The DOS spectra for CoTiSn (the left-hand column in figure 5) and the position of E_F are deduced from the KKR-CPA method (using the generalized Lloyd formula, when determining E_F). The KKR computations of ordered CoTiSn show stronger polarization of bands and result in magnetic moments both on Co (0.41 μ_B) and Ti (0.30 μ_B) atoms. As stated above, the relevant KKR-CPA calculations for CoTiSn show the magnetization to be of order 0.3 μ_B, mainly due to the magnetic moments at Co sites. Recently, the electronic structure calculations have been performed for the Co_2TiSn and Co_2TiAl Heusler systems with the use of the FP-LAPW and the ASW-ASA methods [22]. The comparison shows that the full-potential LAPW computations lead to a total magnetic moment in agreement with experiment in contrast to the ASW-ASA method, which gives non-magnetic ground states for these systems. This result may be influenced by the use of overlapping spheres (ASA) around atoms, which probably cancel some spin-density contributions. The calculations presented in this paper (using muffin-tin potentials inside non-ovelapping spheres) indicate that CoTiSn and Co_2TiSn [9] are weak ferromagnets with the total magnetic moments 0.28 μ_B and 0.90 μ_B (per Co atom) respectively. These values are close to the experimental data (0.35 and 0.96 μ_B [6]) and to the FP-LAPW results [22].

The electronic structure of FeTiSb (the left-hand column in figure 5) is presented for comparison with that of the isoelectronic CoTiSn. FeTiSb is found to be a metallic ferromagnet with a total magnetic moment per formula unit of 0.78 μ_B; the calculated local magnetic moments at the Fe(X) and Ti(Y) sites are 0.66 μ_B and 0.10 μ_B, respectively. As for CoTiSn, E_F lies at the peak of the spin-down DOS. When comparing the component DOS of these two systems (not drawn here), we notice that the d states of Ti more strongly contribute to the conduction band in the FeTiSb system, resulting among other things in a small magnetic moment on Ti. The integrated partial DOS of the Ti d shell up to E_F (table 2) exhibits a higher value for FeTiSb ($N_{Y=Ti,d} = 1.96$) than for CoTiSn ($N_{Y=Ti,d} = 1.86$). This compound indeed exhibits a Curie-like behaviour typical of local magnetic moments at low temperature, with a nearly vanishing Curie–Weiss temperature. However, no magnetic order was detected experimentally down to 1.5 K. As reported in reference [23], the refinement of the diffraction data for FeTiSb seems to show more complex crystallographic structure than the semi-Heusler one (a super-cell or disordered structure). When assuming a disorder on X sites within the X_2YZ-type structure, the KKR-CPA computations show a non-magnetic ground state of $(Fe_{0.5}E_{0.5})_2TiSb$ (E denotes a vacancy), in agreement with the present experiments.

3.2. CoTiSb, CoNbSn and NiTiSn

The KKR studies of semi-Heusler systems possessing 18 valence electrons show the presence of a semiconducting ground state. The basic difference between CoTiSb, NiTiSn and CoNbSn compounds concerns the value of the energy gap E_g, which is biggest ($E_g = 0.95$ eV) for CoTiSb (see table 2). As can be seen from the dispersion curves, bands for CoTiSb (figure 6) and NiTiSn [9] exhibit an indirect Γ–X gap, while E_g for CoNbSn appears between the W and X points in the Brillouin zone.

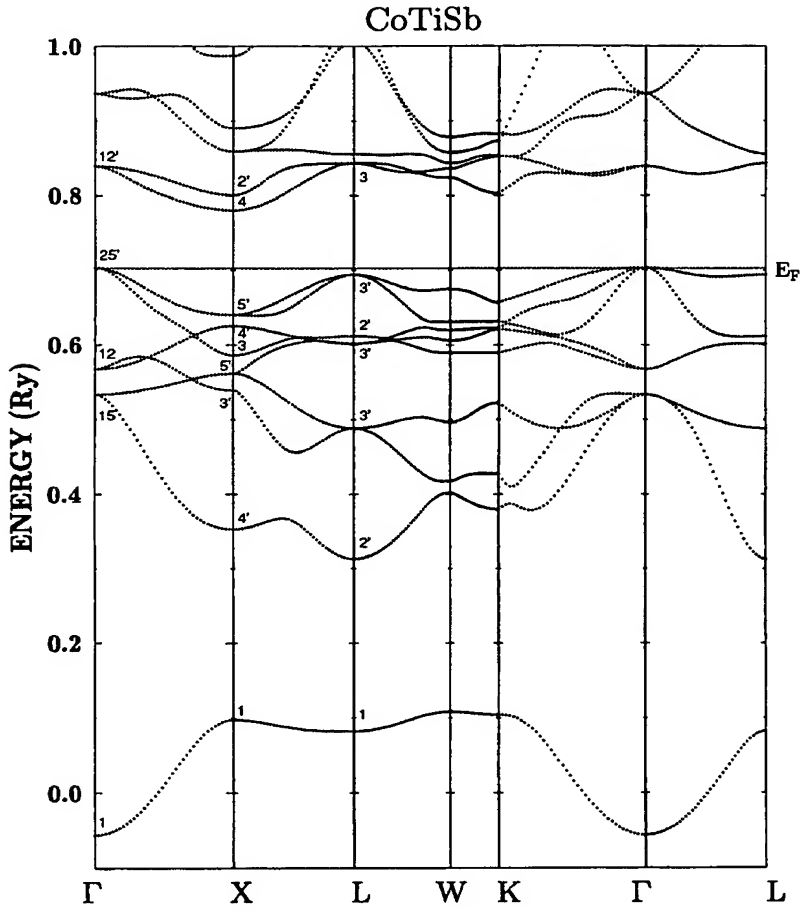

Figure 6. The dispersion curves along high-symmetry BZ directions in the semiconducting CoTiSb. The symmetry labels are assigned according to reference [28].

In this context we recall some limits of the LSD approach in the description of semiconductors. The value of the computed energy gap may be also modified when including the spin–orbit coupling, which is not considered in the present KKR calculations. We expect that upon inclusion of the spin–orbit interaction, the band gaps in semi-Heusler systems may be reduced by about 10–15%, as concluded in reference [24] with respect to the half-metallic PtMnSb.

On the other hand, transport measurements do not give reliable values for the gaps, due to the extrinsic character of the samples (at present, optical measurement results are not available for these systems). Nevertheless, the resistivity values for the three compounds vary in the same sense as the calculated values of the gap (see figure 1 and figure 5).

The CoNbSn compound is near the metal–SC limit, as observed in resistivity measurements. The band-structure studies give an energy gap E_g of the order of 0.4 eV (KKR-CPA) and 0.6 eV (KKR). The disagreement with experiment may arise from the disorder between Co and Nb sites: the KKR computations performed for NbCoSn with

inverted sites (Nb at the X site, while Co is at the Y site) give a semi-metallic state (table 3), with a small DOS at E_F (13 states Ryd^{-1}) mainly due to the Co d contribution.

Both for NiTiSn and for CoTiSb, a dominant character of the electrons (larger mobility, or more donor centres than acceptors) has been observed in the Hall effect. The larger electron mobility may be attributed to the curvature of the valence and conduction bands and to the threefold degeneracy of hole orbitals near the Γ point (the top of the valence band in figure 6), which limits the hole mobility.

For NiTiSn, the main DOS peaks below E_F are principally formed from Ni d states, while above the gap they are due to Ti d states. The situation observed for CoTiSb is slightly different. Here, the gap is two times larger; the electronic spectra deduced from KKR computations also differ from the DOS of NiTiSn. The d states of Co are separated by a gap, and only about 80% of the Co d states are filled below E_F. The main peak of the Co d PDOS is shifted to higher energies, relative to the Ni d PDOS for NiTiSn, due to Co possessing a less attractive potential than Ni. The exact position of the Co d PDOS peak relative to the Fermi energy is also slightly different for CoTiSb and CoNbSn. Moreover, the filling of the d shell of Co in CoNbSn ($N_{Y=Co,d} = 7.54$) is like that in CoTiSb ($N_{Y=Co,d} = 7.51$) (see table 3).

From the DOS spectra for the Y and Z sites in the above-mentioned systems (not drawn here), we see, that replacing Ti by Nb and Sb by Sn leads to a higher increase of d states below E_F than the corresponding decrease of p states at the Z site. Consequently, d states from X and Y sites in CoTiSb and CoTiSn are less hybridized than in CoNbSn.

In this comparison we cannot neglect the influence of the Z position on the formation of the energy gap. The degree of hybridization between d states at X and Y sites and p states at the Z site may control the value of the gap. As can be observed from the p PDOS at the Z site, the hybridization is stronger if Z = Sb than if Z = Sn. Thus CoTiSb (with higher electronegativity of Sb) has a wider E_g than NiTiSn and CoNbSn systems. Nevertheless, the d PDOS are very large on both sides of the gap, and hence its value may also be related to the splitting between bonding/anti-bonding wave-functions of transition metals (see the discussion).

3.3. NiTiSb and CoVSb

Adding one electron more to the semi-Heusler EC = 18 compounds, at either the X or the Z position, turns the system metallic, with only one conduction electron per formula unit. When the density of states at the Fermi level is sufficient, as in CoVSb, Stoner's criterion is met and a ferromagnetic ground state occurs. Calculations show that, surprisingly, the magnetization arises from vanadium atoms. This behaviour may be explained by the fact that E_F falls at a high peak of the d DOS for vanadium. The corresponding density for Co is significantly smaller, and thus the local Stoner criterion is not fulfilled.

Both KKR and KKR-CPA methods indicate that the bands are fully polarized; thus CoVSb should be a half-metallic system (the right-hand column in figure 5) with a magnetic moment per Wigner–Seitz cell equal to 1.00 μ_B. The calculated local magnetic moments on Co, V and Sb are found to be -0.02, 1.03 and -0.03 μ_B, respectively. However, this magnetization value is larger than that observed by Terada *et al* [11]. This disagreement may be due to the very rapidly varying DOS in this compound near E_F: from the total DOS for CoVSb, we also conclude that the half-metallic ferromagnetism here is linked to the highly localized conduction states (a large peak of the DOS at E_F). A different ground state may be favoured in a real system; thus an analysis of the total energy variation as a function of polarization should be undertaken. One other reason for the discrepancy

between experiment and theory may be the atomic disorder between Co and V atoms: V has a smaller radius than other 3d metals which occupy the Y sublattice. It is close to that of Co and this may permit greater disorder.

Now, passing to the NiTiSb system, we notice clearly that adding one electron at the X site (Co replaced by Ni) does not have the same effect as increasing the number of electrons at the Y site by replacing Ti by V. The electronic structure of NiTiSb (figure 5) shows striking differences when compared to that of CoVSb. Spin-polarized KKR computations indicate that the ground state of NiTiSb is non-magnetic. In contrast to the Co d states in CoVSb, the Ni d shell in NiTiSb is more or less filled (as in NiTiSn), and the states above the gap are formed with Ti d states. Due to a small value of the DOS at the Fermi level, neither Ni nor Ti atoms in NiTiSb retain magnetic moments. This result is in agreement with magnetization and resistivity measurements, which indicate vanishing magnetization and metallic character in NiTiSb.

3.4. $CoTiSn_{1-x}Sb_x$ and $CoTi_{1-x}Nb_xSn$ alloys

In this section we compare the electronic structure and magnetic properties derived from KKR-CPA computations for the isoelectronic series of alloys $CoTi_{1-x}Nb_xSn$ and $CoTiSn_{1-x}Sb_x$ (figure 7). In the $CoTi_{1-x}Nb_xSn$ series (the right-hand column in figure 7) an increase of valence electron number is brought about by substitution at the Y site by a d element from the next group in the periodic table (Nb), while in the $CoTiSn_{1-x}Sb_x$ series (the left-hand column in figure 7) it is effected by doping the Z site with Sb.

Due to the different origins of the electrons at the two substitution sites, we expect different behaviours of the electronic structure and magnetism for the series, upon alloying the parent compounds. The total magnetic moment (μ_{tot}) variations versus composition are presented in figure 4 for three series (the $Co_{1-x}Ni_xTiSn$ series was investigated in [9]). As in experiments, the variations of μ_{tot} (more or less proportional to μ_{Co}) change non-linearly in all cases. The alloy compositions for which ferromagnetic ordering disappears are also different for the different series. Taking into account the weak ferromagnetism in all of the samples investigated, the critical concentrations found from KKR-CPA calculations are not far from the experimental results. The starting value of 0.28 μ_B for the magnetic moment of CoTiSn at $x = 0$ also slightly differs from the experimental value (0.35 μ_B), which may modify $\mu_{tot}(x)$ dependencies.

First let us consider $CoTi_{1-x}Nb_xSn$ alloys. Here, an interesting observation concerns the concentration-dependent variation of the total magnetic moment, which exhibits a maximum in experiment and a plateau in the KKR-CPA calculations for Nb concentrations of about 0.1–0.2. This is related to an increase in the d states at Y sites, which generates a small induced magnetic moment at this site for $0 < x < 0.2$. It can be seen from the component DOS (the middle and right-hand columns in figure 8), which exhibits some polarization both at the Co site as well as at the Y site (mainly the Ti site) for $x < 0.3$. For higher Nb content, it is mainly the magnetic moment at the Co site that contributes to the total magnetization, which reaches zero for x-values of about 0.6–0.7. Surprisingly, both the gap between the conduction and valence bands in the $CoTi_{1-x}Nb_xSn$ series (the right-hand column in figure 7 and figure 8) and the exchange splitting become smaller as x increases.

For $x > 0.5$ the density of states at the Fermi level subsequently decreases, reaching zero for $x = 1.0$ (an energy gap of about 0.4 eV occurs). This is supported by resistivity measurements, which show an increase of the resistivity in Nb-rich $CoTi_{1-x}Nb_xSn$ samples although, experimentally, CoNbSn appears to be more or less semi-metallic (see section 2.3).

Crystallographic studies have shown that the solid solution was not continuous between

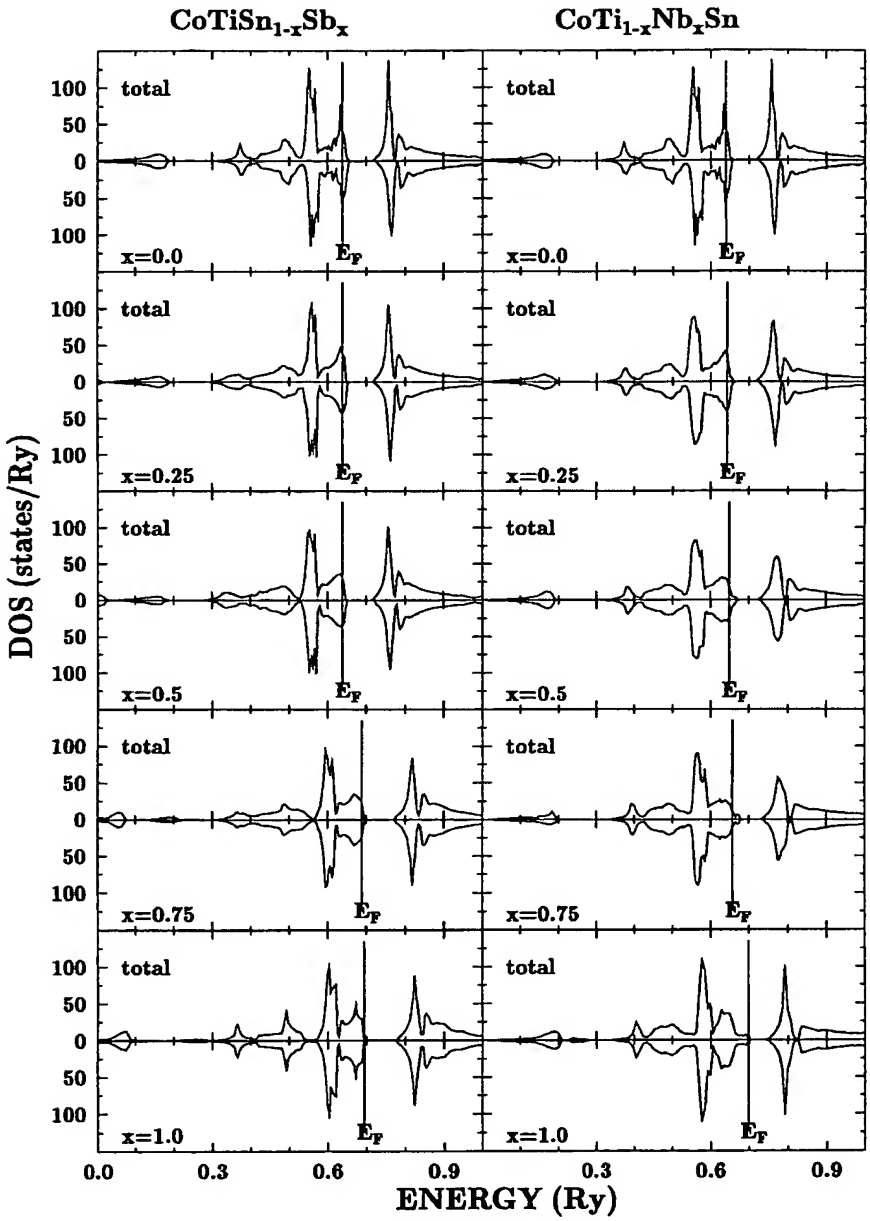

Figure 7. Total densities of states (from the KKR-CPA method) for two disordered series: $CoTi_{1-x}Nb_xSn$ and $CoTiSn_{1-x}Sb_x$.

CoTiSn and CoTiSb. In order to investigate the influence of the lattice parameter on the SC–metal transition, calculations were performed for the $CoTiSn_{1-x}Sb_x$ series with the true parameter (figure 7 and figure 9). The overall DOS shape is not significantly changed (for $x > 0.5$); only a global shift of energies is observed. In the $CoTiSn_{1-x}Sb_x$ series

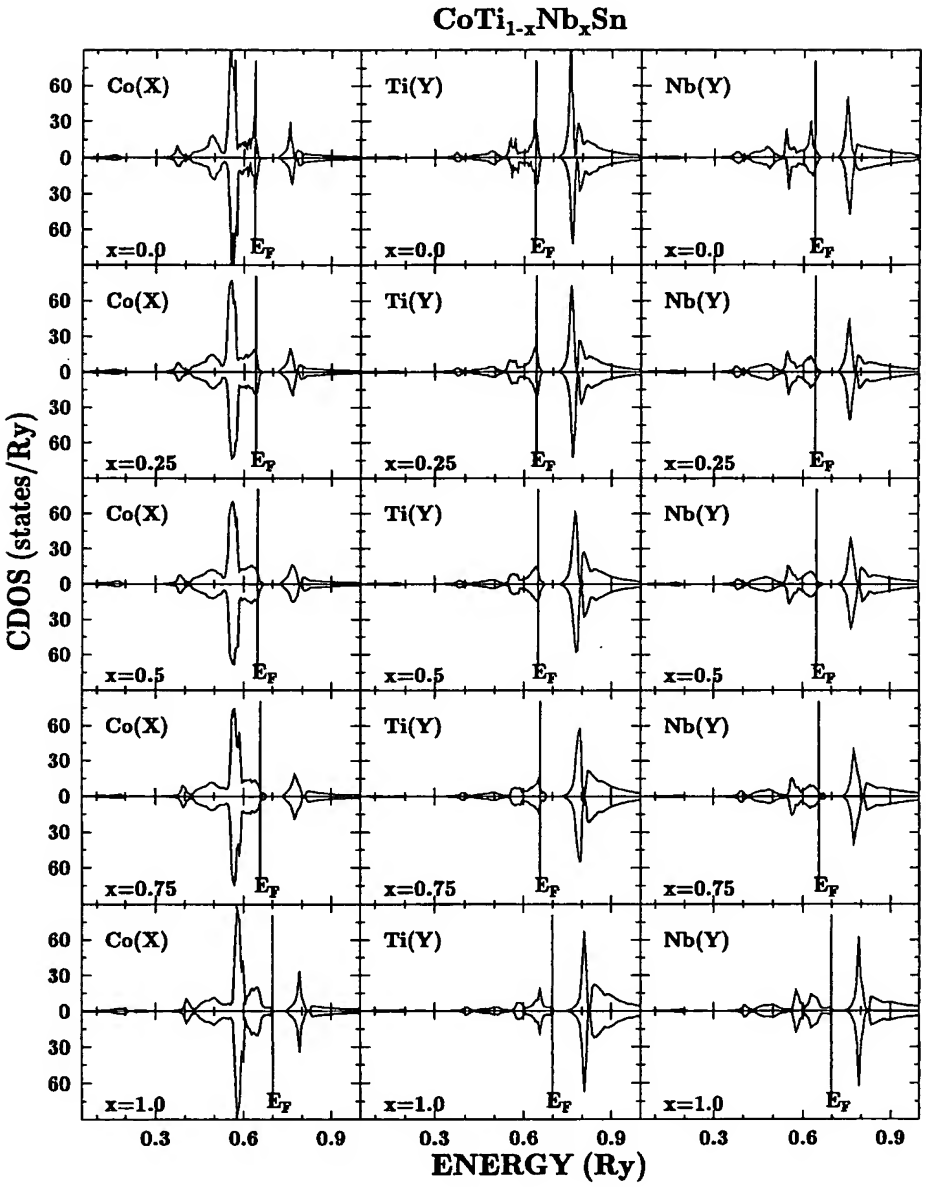

Figure 8. Component densities of states for X and Y sites in the disordered $CoTi_{1-x}Nb_xSn$ series. For borderline concentrations the CDOS of one impurity in the matrix is shown, i.e. Nb in CoTiSn ($x = 0$) and Ti in CoNbSn ($x = 1$).

(oppositely to the previous case), the gap between the conduction and valence bands slightly increases on approaching the CoTiSb compound (the left-hand column in figure 7). The spin polarization continuously decreases, reaching zero for $x \approx 0.7$, which corresponds well to magnetization measurements ($x = 0.6$). Nevertheless, in contrast to the results of the

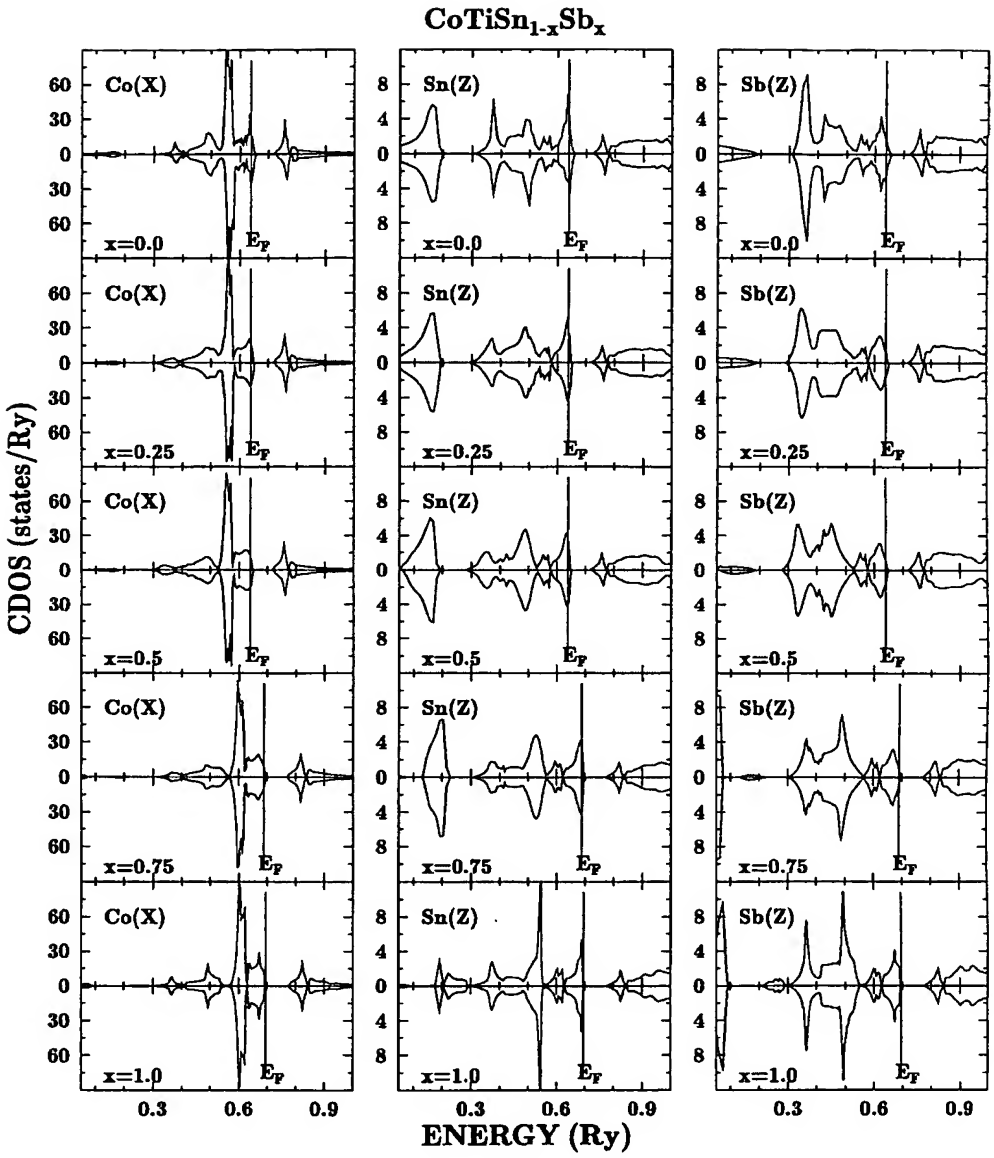

Figure 9. Component densities of states for X and Z sites in the disordered $CoTiSn_{1-x}Sb_x$ series. For borderline concentrations the CDOS of one impurity in the matrix is shown, i.e. Sb in CoTiSn ($x = 0$) and Sn in CoTiSb ($x = 1$).

transport experiments, the crossover to the semiconducting state is not observed in KKR-CPA spectra for intermediate concentrations, mainly due to non-zero contributions of states from Co and Sn atoms (figure 9).

This rigid-band behaviour is a due to eight bands, which are filled for $x = 1.0$, so E_F cannot fall into the gap for $x < 1$. Weakly doped samples probably still have a

semiconducting-like resistivity due to localization arising from the atomic disorder, which will be discussed in the next section.

4. Discussion

Some properties, such as the ferromagnetic–paramagnetic or metal–semiconductor crossovers, can be directly understood from electronic structure calculations, but other results are much less clear and need a more detailed discussion. We will first discuss the transport properties, and next the magnetic properties of these systems.

4.1. Transport properties

We first recall that the gap in the semiconducting phases cannot be properly estimated from our transport experiments below 300 K, due to their extrinsic character. Thus we must rely on the values calculated for the ideal structure within the LSD framework. Nevertheless we observe that the order of magnitude of the measured resistivity goes in the same sense as the calculated value of the gap, both values decreasing from CoTiSb, through NiTiSn, to CoNbSn. This can be simply due to the fact that CoTiSb is better ordered, having fewer impurity states, and CoNbSn is more disordered. One discrepancy between experiments and calculations is the following: when the electron concentration is decreased starting from a SC phase (EC = 18), the resistivity retains a semiconducting-like behaviour (negative temperature derivative) and a large magnitude at low temperatures up to a quite large value for the hole concentration in the lattice. Conversely, in most cases, the CPA calculations indicate that there is a finite DOS at E_F, which implies a metallic state. This should be interpreted in the following way: the CPA calculations do not completely take into account the inhomogeneities in the sample—that is, the different local potentials experienced by carriers due to the chemical disorder—since the environment at an atom is replaced by a mean potential. The resistivity behaviour is indeed caused by the disorder. Anderson and Mott [25] have treated the case of disordered semiconductors, argued for the existence of a mobility edge, and described the mechanism of variable-range hopping (VRH) of carriers, due to localization at the deepest potential wells. In the present system, the typical VRH law: $\ln(R)$ varying as $1/T^{1/4}$ or $1/T^{1/2}$, cannot be observed due to the extrinsic character, but hopping is the common mode of conduction in disordered semiconducting systems [26].

Different types of behaviour are indeed encountered in the present solid solutions. In the case of the $Co_{1-x}Ni_xTiSn$ series, calculations as well as the experimental evidence for a localized moment on Co show that Co levels fall into the former gap of NiTiSn, which is a shortcoming of the rigid-band model. This can explain why the systems remains SC until either a percolation limit is reached, or the Fermi level falls below (for hole doping) the mobility edge, when Co levels collapse into a band. In the case of the $CoTiSn_{1-x}Sb_x$ series, the discontinuity of the lattice parameter of the solid solutions shows that local environment effects must be larger. Conversely, the $CoTi_{1-x}Nb_xSn$ series looks correspondingly more homogeneous and the SC behaviour is indeed rapidly replaced by a metallic state close to the CoNbSn composition.

4.2. Magnetic properties

One first problem is to explain why some compounds present a constant paramagnetism and others a Curie–Weiss behaviour. Moriya and Kawabata [14] have shown that the existence of

strictly localized magnetic moments is not a necessary condition for the existence of Curie–Weiss behaviour. Generally, the Curie–Weiss behaviour has been found to be associated with a sharp peak of the DOS at E_F. Thus we will try to relate magnetic properties to the density of states. We must also explain why localized states of Co diluted in NiTiSn have a small effective moment, why CoTiSb does not show any localized magnetic moments, and also why itinerant magnetic features are observed for narrow bands and, thus, close to a SC–metal transition.

The first observation is that the semiconducting phases NiTiSn and CoTiSb as well as metallic NiTiSb present a susceptibility which does not depend on temperature, whereas CoTiSn and CoVSb present a weak ferromagnetism with a Curie–Weiss behaviour in the paramagnetic range.

Let us first ask what the nature is of the semiconducting phase CoTiSb (charge-transfer, Mott–Hubbard, or another type of semiconductor), and why there is no Curie–Weiss magnetism in this compound. In contrast to the case of Ni in NiTiSn, the d shell of the Co atom is not filled. Electronic structure calculations show (table 3) that there is no more charge transfer from Sb to Co than from Sn to Co in CoTiSn: the number of electrons within the muffin-tin (MT) sphere of Co is the same for the two compounds, and from the partial d DOS the configuration of Co is about $3d^8$. Large electronic correlations within the d shell should maintain a strong intra-atomic coupling. Since Sb p levels are centred well below the gap and have a weak partial DOS on both sides of the gap, we conclude that this gap does not arise only from the charge transfer between Sb and metals. On the other hand, the energy bands (figure 6) show that the splitting between $\Gamma_{25'}$ (occupied t_{2g} states of Co and Ti below E_F) and the unoccupied level Γ_{12} (e_g states above the gap) is about 2 eV. The Co d PDOS is dominant below the gap, and Ti levels dominate above. Thus the gap seems to be due mainly to the hybridization between Co and Ti and the energy difference between bonding and anti-bonding states.

The splitting of d states also indicates that the crystal field around Co is fairly large. In this case, according to Goodenough [27], the spin of the ground state resulting from the crystal field and spin–orbit coupling may be quenched. For a $3d^8$ configuration in a tetrahedral interstice, it has been predicted that the ground state is a non-magnetic singlet (Γ_1 representation), followed by a Γ_4 triplet [27]. This non-magnetic ground state expected for the ionic configuration may tentatively explain why CoTiSb fails to exhibit any Curie–Weiss behaviour, although this ionic picture should be treated with caution due to the strong hybridization with ligands. The hybridization itself, splitting the last occupied bands around the gap, may give rise to this non-magnetic situation.

The constant paramagnetism for other semiconducting phases can be explained as for CoTiSb by a non-magnetic ground state or weak correlations (NiTiSn, CoNbSn), whereas for the NiTiSb metallic phase the more or less uniform Pauli susceptibility is related to a low density of states at E_F.

Conversely, the Curie–Weiss behaviour observed in CoTiSn (or CoVSb) is obviously associated with the presence of a high local density of states at E_F, as revealed by band calculations, and can be rather well understood within the framework of itinerant-electron magnetism. Due to the presence of the gap, only one hole (or electron) participates in conduction and in magnetic ordering, which favours a ferromagnetic type of order. Surprisingly, the magnetic moment in CoVSb is expected to lie on the V atom which has the highest DOS at E_F, rather than on the Co atom. Such a situation should be verified by polarized neutron experiments on single crystals, which is the only way to measure such low ferromagnetic moments.

For solid solutions like $Co_{1-x}Ni_xTiSn$, we pass progressively from one regime to the

other, and the susceptibility can be described by the superposition of a Curie-like term plus a constant susceptibility: $\chi = (1 - x)C/T + \chi_0$. The Curie term comes from the rather well localized Co contribution, the other from other d electrons. This is a typical example of localization without a large change in the Co effective moment (1.1 μ_B for Co diluted in NiTiSn, compared to 1.35 for pure CoTiSn). The KKR-CPA band calculations [9] show that the Co d levels tend to form acceptor levels in the gap of NiTiSn (a shortcoming of the rigid-band model), which gives rise to a non-homogeneous magnetism localized at the Co sites. The ferromagnetic order appears when these impurity states are close enough to give rise to a band and thus to a large enough density of states at E_F. A percolation limit can be defined which corresponds to about 0.4 of a hole per formula unit.

The picture of spin quenching by the crystalline field can also explain, together with the weak ferromagnetism expected from the itinerant model, why the magnetic moment is so low for CoTiSn or for $Co_{1-x}Ni_xTiSn$ solutions. Crystal fields and hybridization give rise to a strong breakdown of Hund's rule and to a low-spin state. One interesting feature is that the effective moment remains close to 1.2 μ_B for CoTiSn, for CoVSb and also for some other weak ferromagnets.

Another peculiar feature is the observation of a susceptibility maximum in the $CoTiSn_{1-x}Sb_x$ series close to CoTiSb. Such a behaviour has also been observed for some enhanced paramagnets (YCo_2 for instance) as for $ZrZn_2$ under pressure [12]. Most probably it is related to a pronounced minimum in the DOS at E_F, giving a positive second derivative $n''(E_F)$; the existence of such a minimum is expected as a consequence of the former gap.

4.3. Conclusions and further developments

In summary, many very different behaviours have been observed in these semi-Heusler phases, from semiconductor to metal, from Pauli-like to Curie–Weiss paramagnet, from paramagnetic to ferromagnetic ground state. An overall agreement has been observed between experimental data and electronic band calculations. Some discrepancies remain, since calculations predict for example a ferromagnetic state for FeTiSb (but a non-magnetic state for $(Fe_{0.5}E_{0.5})_2TiSb$) and a fully polarized state for CoVSb which are not observed. Some of the discrepancies may be attributed to the crystallographic disorder in the real lattices and others to the extreme instability of the magnetic polarization near the magnetic–non-magnetic crossover.

Further experiments are planned to investigate in more detail the appearance of magnetism at the Y site, and to follow by substituting for atoms from Ti to Mn the evolution of the ferromagnetic state from the weak-ferromagnet case to the case of complete ferromagnetic polarization and half-metallic behaviour, as found for NiMnSb.

Acknowledgment

This work was partly realized at CNRS Grenoble thanks to a TEMPRA grant allotted to JT by the Rhone-Alpes Region.

References

[1] de Groot R A, Mueller F M, van Engen P G and Buschow K H J 1983 *Phys. Rev. Lett.* **50** 2024
[2] de Groot R A and Buschow K H J 1986 *J. Magn. Magn. Mater.* **54–57** 1377
[3] Kübler J, Williams A R and Sommers C B 1983 *Phys. Rev.* B **28** 1745
[4] Ishida S, Asano S and Ishida J 1984 *J. Phys. Soc. Japan* **53** 2718

[5] Aliev F G, Kozyrkow V V, Moshchalkov V V, Skolozdra R V and Durczewski K 1990 *Z. Phys.* B **80** 353
[6] Pierre J, Skolozdra R V, Gorelenko Yu K and Kouacou M A 1994 *J. Magn. Magn. Mater.* **134** 95
[7] Pierre J, Skolozdra R V and Stadnyk Yu V 1993 *J. Magn. Magn. Mater.* **128** 93
[8] Booth J G 1988 *Ferromagnetic Materials* vol 4, ed E P Wohlfarth and K H J Buschow (Amsterdam: Elsevier Science) p 211 and references therein
[9] Toboła J, Pierre J, Kaprzyk S, Skolozdra R V and Kouacou M A 1996 *J. Magn. Magn. Mater.* **159** 192
[10] Kouacou M A, Pierre J and Skolozdra R V 1995 *J. Phys.: Condens. Matter* **7** 7373
[11] Terada M, Endo K, Fujita Y and Kimura R 1972 *J. Phys. Soc. Japan* **32** 91
[12] Grosche F M, Pfleiderer C, McMullan G J, Lonzarich G G and Berhoeft N R 1995 *Physica* B **206–207** 20
[13] Pierre J, Skolozdra R V and Kouacou M A 1995 *Physica* B **206–207** 844
[14] Moriya T and Kawabata A 1973 *J. Phys. Soc. Japan* **34** 639
[15] Lonzarich G G and Taillefer L 1985 *J. Phys. C: Solid State Phys.* **18** 4339
[16] Kaplan Th, Leath P L, Gray L J and Diehl H W 1980 *Phys. Rev.* B **21** 4230 and references therein
[17] Kaprzyk S and Bansil A 1990 *Phys. Rev.* B **42** 7378
[18] Bansil A, Kaprzyk S and Toboła J 1992 *Applications of Multiple Scattering Theory in Material Science (MRS Symp. Proc. 253)* (Pittsburgh, PA: Materials Research Society) p 505
[19] Kaprzyk S 1997 *Acta Phys. Pol.* A **91** 135
[20] von Barth U and Hedin L 1972 *J. Phys. C: Solid State Phys.* **5** 1629
[21] Kaprzyk S and Mijnarends P E 1986 *J. Phys. C: Solid State Phys.* **19** 1286
[22] Mohn P, Blaha P and Schwarz K 1995 *J. Magn. Magn. Mater.* **140–144** 183
[23] Szytuła A, Tomkowicz Z and Turowski M 1973 *Acta Phys. Pol.* A **44** 147
[24] Continenza A, de Pascale T M, Meloni F and Serra M 1993 *Japan. J. Appl. Phys.* **32** 240
[25] Mott N F 1974 *Metal–Insulator Transitions* (London: Taylor and Francis)
[26] Pollack M and Shklovskii B (ed) 1991 *Hopping Transport in Solids* (Amsterdam: North-Holland)
[27] Goodenough J B 1963 *Magnetism and the Chemical Bond* (New York: Wiley–Interscience) p 67
[28] Bouckaert L P, Smoluchowski R and Wigner E 1936 *Phys. Rev.* **50** 58

THERMOELECTRIC ELEMENT AND ELECTRIC APPARATUS WITH THERMOELECTRIC ELEMENT

Patent number:	JP8037324
Publication date:	1996-02-06
Inventor:	SUZUKI MINAKO; others: 01
Applicant:	SEIKO INSTR INC
Classification:	
- international:	H01L35/32; G01K7/02; G04C10/00; G04G1/00
- european:	
Application number:	JP19940169729 19940721
Priority number(s):	

Abstract of **JP8037324**

PURPOSE:To provide a small thin thermoelectric element with good efficiency, by making a radiating-side insulating plate larger in surface area than an endothermic-side insulating plate.
CONSTITUTION:A radiating-side insulating body 102 is made larger in surface area than an endothermic-side insulation body 101 and the radiating-side insulating plate 102 has good radiation. At the same time, a sufficient difference in temperatures can be obtained, because the endothermic-side insulating plate 101 is put at a high temperature, while the insulation body 101 on the radiating side is put at a low temperature. The heat is conducted from the insulating body 101 to the insulating body 102, and the thermal transfer is converted into an electric current. Then, the electricity caused by electromotive force is generated at an end terminal 106. In this way, only by forming a difference of surface area in first and second insulating bodies, a small thin thermoelectric element with good efficiency can be obtained without using a heat collective body or a radiating body.

---

(19)日本国特許庁（ＪＰ）　(12) 公開特許公報（A）　(11)特許出願公開番号

特開平8－37324

(43)公開日　平成８年(1996)２月６日

(51)Int.Cl.[6]	識別記号	庁内整理番号	ＦＩ	技術表示箇所
Ｈ０１Ｌ　35/32		Ａ		
Ｇ０１Ｋ　7/02		Ｚ		
Ｇ０４Ｃ　10/00		Ｃ		
Ｇ０４Ｇ　1/00	３１０	Ｙ	9109－2F	

審査請求　未請求　請求項の数６　ＯＬ　（全７頁）

(21)出願番号　特願平6－169729

(22)出願日　平成６年(1994)７月21日

(71)出願人　000002325
セイコー電子工業株式会社
千葉県千葉市美浜区中瀬１丁目８番地

(72)発明者　鈴木　美奈子
東京都江東区亀戸６丁目31番１号　セイコー電子工業株式会社内

(72)発明者　津端　佳介
東京都江東区亀戸６丁目31番１号　セイコー電子工業株式会社内

(74)代理人　弁理士　林　敬之助　（外１名）

(54)【発明の名称】　熱電素子及び熱電素子を用いた電子機器

(57)【要約】

【目的】　小型、薄型で、高効率な熱電素子を得る。

【構成】　複数のｎ型半導体１０３と複数のｐ型半導体素子１０４を接続部１０５により交互に電気的に直列になるように接続する。接続部１０５を固定した放熱側に設けた絶縁体１０２の表面積が、吸熱側に設けた絶縁体１０１の表面積よりも広くなるように形成すると温度差が生じ、起電力を得ることができる。

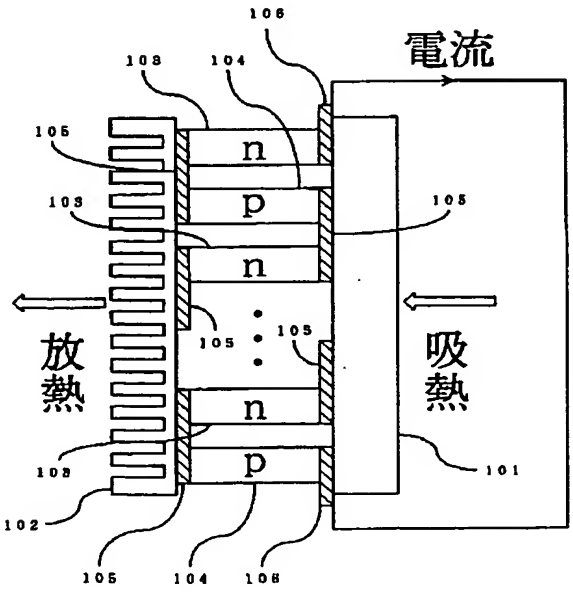

1

【特許請求の範囲】
【請求項１】　複数のｎ型半導体（１０３）と複数のｐ型半導体（１０４）を交互に電気的に直列になるように接続する複数の接続部（１０５）と、
接続部（１０５）を１つおきに固定するとともに、酸化膜を付けたアルミニウムからなる第一の絶縁体（１０１）と、
第一の絶縁体（１０１）で固定していない接続部（１０５）を固定するとともに、酸化膜を付けたアルミニウムからなる第二の絶縁体（１０２）と、
起電力を取り出すための出力端子部（１０６）とを有し、
第一の絶縁体（１０１）と第二の絶縁体（１０２）の表面積が異なることを特徴とする熱電素子。
【請求項２】　複数のｎ型半導体（２０３ａ）から構成される複数のｎ型半導体複合素子（２０３）と、
複数のｐ型半導体（２０４ａ）から構成される複数のｐ型半導体複合素子（２０４）を有し、
複数のｎ型半導体複合素子（２０３）と複数のｐ型半導体複合素子（２０４）を交互に電気的に直列になるように接続する複数の接続部（２０５）と、
接続部（２０５）を１つおきに固定するとともに、酸化膜を付けたアルミニウムからなる第一の絶縁体（２０１）と、
第一の絶縁体（２０１）で固定していない接続部（２０５）を固定するとともに、酸化膜を付けたアルミニウムからなる第二の絶縁体（２０２）と、
起電力を取り出すための出力端子部（２０６）とを有し、
第一の絶縁体（２０１）と第二の絶縁体（２０２）の表面積が異なることを特徴とする熱電素子。
【請求項３】　動力源を有する電子機器において、請求項１又は請求項２のいずれか１項に記載する熱電素子を動力源として用いた電子機器。
【請求項４】　動力源を有する電子時計において、請求項１又は請求項２のいずれか１項に記載する熱電素子を動力源として用いた電子時計。
【請求項５】　請求項４に記載の電子時計において、腕に接する側に吸熱側の第一の絶縁体を配置し、腕に接しない側に放熱側の第二の絶縁体を配置したことを特徴とする電子時計。
【請求項６】　請求項５に記載の電子時計において、放熱側の第二の絶縁体は、時計の６時側に近い位置に配置される複数の直線上の凹凸を有することを特徴とする電子時計。
【発明の詳細な説明】
【０００１】
【産業上の利用分野】本発明は、動力源として電池を使用しない電子機器を実現するための熱電素子、及び動力源として熱電素子を用いた電子機器に関するものである。

2

【０００２】
【従来の技術】従来は図３に示すように、熱電材料からなる第一の素子１１と第二の素子１２を、導電材料で作られた第一の接合体１３で結び付けた熱電対を複数個用意し、熱電対が電気的に直列になるように第二の接合体１４で結合して熱電堆１を構成している。さらに、熱電堆１の第一の接合体１３は絶縁材１５を介して集熱体２２に固着されており、第二の接合体１４は絶縁材１５を介して放熱体３２に固着されている。ここで、集熱体２２はその外周を熱の散逸を防ぐ保護部材で覆われ、また、放熱体３２は放熱効果を高めるためにひれ３２ａ～３２ｆを有している。例えば特開昭５７－１８９５８４号公報にこのような従来の構造が開示されている。
【０００３】
【発明が解決しようとする課題】しかし、従来の構造では、図３に示すように、熱電堆１に集熱体２２とひれ３２ａ～３２ｆを有する放熱体３２を固着することで熱電素子に温度差を生じさせていた。この構造によると、より高い発電能力を得ようとした場合、熱電素子全体の小型、薄型化が困難であり、集熱体、放熱体の材質により、発電効率が低下する等の課題を有していた。
【０００４】そこで、本発明は、小型、薄型で、高効率な熱電素子を得ることを目的としている。
【０００５】
【課題を解決するための手段】上記の、熱電堆に集熱体とひれを有する放熱体を固着させることにより、発電効率が低下する等という課題を解決するために、本発明は、熱電素子において、集熱体、放熱体を用いることなく、第一の絶縁体と第二の絶縁体そのものの表面積を異なる構造とすることで、小型、薄型で、高効率な熱電素子を実現した。
【０００６】
【作用】上記のように構成された熱電素子においては、図１において、複数のｎ型半導体１０３と複数のｐ型半導体素子１０４は、複数の接続部１０５により交互に電気的に直列になるように接続される。さらに、複数のｎ型半導体１０３と複数のｐ型半導体素子１０４が接続された接続部１０５を酸化膜を付けたアルミニウムからなる第一の絶縁体１０１により固定されるとともに、吸熱側に設けられる。また、第一の絶縁体１０１で固定していない接続部１０５は、酸化膜を付けたアルミニウムからなる第二の絶縁体１０２により固定されるとともに、放熱側に設けられる。
【０００７】この際、一方の放熱側に設けられた絶縁体１０２の表面積が、もう一方の吸熱側に設けられた絶縁体１０１の表面積よりも広くなるように形成すると、吸熱側が高温、放熱側が低温となるような温度差を与えた場合、絶縁体１０１から絶縁体１０２の方向に熱が伝達され、その際にｎ型半導体１０３の中では電子が、ｐ型

半導体１０４の中では正孔がそれぞれ放熱側に設けられた絶縁体１０２の方向に移動する。ｎ型半導体１０３とｐ型半導体１０４は接続部１０５を介して電気的に直列に接続されているため、熱の伝達が電流に変換され、両端の出力端子部１０６の間に起電力が生じる。

【０００８】さらに、本発明の熱電素子を電子機器の動力源として用いた場合は、図４において、熱電素子４００に温度差が与えられ、起電力が発生すると、蓄電機構４０８に電気が蓄えられる。蓄電機構４０８に蓄えられた電気の電圧が駆動機構４０９を駆動するのに十分な大きさに達すると、駆動機構４０９により、動作表示機構４１０が駆動される。

【０００９】

【実施例】以下に本発明の実施例を図面に基づいて説明する。

（１）第一実施例

図１は、本発明の熱電素子の第一の断面図及び発電原理を示した図である。図１において、複数のｎ型半導体１０３と複数のｐ型半導体素子１０４は、複数の電極１０５により交互に電気的に直列になるように接続される。さらに、複数のｎ型半導体１０３と複数のｐ型半導体素子１０４が接続された電極１０５は、例えば酸化膜を付けたアルミニウムからなる絶縁体１０１により固定されるとともに、吸熱側に設けられる。また、絶縁体１０１で固定していない電極１０５は、例えば酸化膜を付けたアルミニウムからなる第二の絶縁体１０２により固定されるとともに、放熱側に設けられる。この際、放熱側に設けられた絶縁体１０２は、吸熱側に設けられた絶縁体１０１の表面積よりも広くするための直線状の凹凸を形成している。

【００１０】ここで、放熱側に設けられた絶縁体１０２は、吸熱側に設けられた絶縁体１０１よりも表面積が広くなるため、より放熱しやすい状態となる。このため、吸熱側に設けられた絶縁体１０１が高温、放熱側に設けられた絶縁体１０２が低温となり、十分な温度差が得られることになる。そして、絶縁体１０１から絶縁体１０２の方向に熱が伝達され、その際にｎ型半導体１０３例えばビスマステルル系あるいはナマリーテルル系の中では電子が、ｐ型半導体１０４例えばビスマステルル系あるいはナマリーテルル系の中では正孔がそれぞれ放熱側に設けられた絶縁体１０２の方向に移動する。ｎ型半導体１０３とｐ型半導体１０４は電極１０５を介して電気的に直列に接続されているため、熱の伝達が電流に変換され、両端の出力端子部１０６に起電力が生じる。

【００１１】なお、図５乃至図７は、本発明の熱電素子の第三実施例、第四実施例、第五実施例の断面図であるが、図１に示す第一実施例の構造と同様に、放熱側に設けられた絶縁体５０２、６０２、７０２は、吸熱側に設けられた絶縁体５０１、６０１、７０１の表面積よりも広くするための直線状または曲線状の凹凸を形成することにより同様な効果が得られる。

【００１２】（２）第二実施例

図２は、本発明の熱電素子の第二実施例の断面図及び発電原理を示した図である。図２において、先の第一実施例との相違点は、複数のｎ型半導体２０３ａから複数のｎ型半導体複合素子２０３が構成されている点であり、また、複数のｐ型半導体２０４ａから複数のｐ型半導体複合素子２０４が構成されている点である。第一実施例と同様に、複数のｎ型半導体複合素子２０３と複数のｐ型半導体複合素子２０４が交互に電気的に直列になるように接続された電極２０５は、例えば酸化膜を付けたアルミニウムからなる絶縁体２０１により固定されるとともに、吸熱側に設けられる。また、絶縁体２０１で固定していない電極２０５は、例えば酸化膜を付けたアルミニウムからなる絶縁体２０２により固定されるとともに、放熱側に設けられる。この際、放熱側に設けられた絶縁体２０２は、吸熱側に設けられた絶縁体２０１の表面積よりも広くするための直線状または曲線状の凹凸を形成することにより同様な効果が得られる。

【００１３】（３）第六実施例

図８は、本発明の熱電素子の第六実施例の断面図である。図８において、放熱側に設けられた絶縁体８０２は、電極８０５が固定されている面と平行に穴部８０２ａを形成している。このため、放熱側に設けられた絶縁体８０２の表面に凹凸を形成した場合と同様な効果が得られる。

【００１４】（４）第七実施例

図９は、本発明の熱電素子に蓄電素子を設けた場合の第七実施例の断面図及び発電原理を示した図である。図９において、先の第一実施例との相違点は、蓄電素子９０８を備えた点である。絶縁板９０１と絶縁体９０１の表面積よりも広くするための直線状の凹凸を形成している絶縁板９０２との間に温度差が生じることで得た起電力は、蓄電素子９０８に蓄電され、電子機器の動力源として用いることができる。

【００１５】（５）第八実施例

図１０は、本発明の熱電素子を動力源として用いた電子機器の第八実施例の電子腕時計の動作原理を示したブロック図である。図１０において、熱電素子１０００に温度差が与えられ、起電力が発生すると充電制御回路１００７を介して蓄電素子１００８に電気が蓄えられる。蓄電素子１００８に蓄えられた電気により駆動制御回路１００９が駆動し、表示機構１０１０に時刻が表示される。

【００１６】図１１は、本発明の熱電素子を動力源として用いた電子機器の第八実施例の電子腕時計の外観図である。図１１において、絶縁体１１０２は、放熱されやすいように直線状の凹凸を形成するとともに、表面に露出している。絶縁体１１０２は、例えば絶縁のために酸化膜を付けたアルミニウムで構成されている。

【００１７】図１２は、本発明の熱電素子を動力源として用いた電子機器の第八実施例の電子腕時計の断面図である。図１２に示すように、絶縁板１２０１は一般に気温よりも高温である腕側、すなわち、吸熱側に設けられ、絶縁板１２０１の表面積よりも広くするための直線状の凹凸が形成された絶縁板１２０２は、大気中、すなわち、放熱側に設けられる。絶縁板１２０１及び絶縁板１２０２は、例えば酸化膜を付けたアルミニウムで構成されている。ここで、例えば携帯者の体温が３６度で、気温２０度の環境にて使用し、電子腕時計全体が腕の温度に近くなると、絶縁板１２０１と絶縁板１２０２との間に生じる温度差は２度前後である。温度差が生じると、熱は絶縁板１２０１から絶縁板１２０２に伝えられ大気に放熱される。このときゼーベック効果により起電力が生じ、蓄電機構１２０８、例えばリチウム２次電池あるいはバナジウムーリチウム２次電池に蓄電される。この蓄えられた電気により、輪列とモータからなる運針動作を行なうムーブメント１２１１が駆動する。

【００１８】このような構成とすることにより、集熱体、放熱体を用いることなしに、熱電素子の小型、薄型化がはかれるとともに、発電効率を低下させることなく、高効率な熱電素子が実現できる。このため、本発明による熱電素子を電子機器に用いることにより、電子機器を小型化することが可能となる。

【００１９】

【発明の効果】本発明による熱電素子によれば、第一の絶縁体と第二の絶縁体の表面積が異なるという簡単な構成で、必要とする起電力を得るための熱電素子として、小型、薄型で、高効率な熱電素子を実現することができる。さらにこの熱電素子を電子機器に用いることにより、電子機器を小型化することが可能になるといった効果を有する。

【図面の簡単な説明】

【図１】本発明の熱電素子の第一実施例の断面図及び発電原理を示した図である。

【図２】本発明の熱電素子の第二実施例の断面図及び発電原理を示した図である。

【図３】従来の熱発電器の断面図である。

【図４】本発明の熱電素子を動力源として用いた電子機器の動作原理を示したブロック図である。

【図５】本発明の熱電素子の第三実施例の断面図である。

【図６】本発明の熱電素子の第四実施例の断面図である。

【図７】本発明の熱電素子の第五実施例の断面図である。

【図８】本発明の熱電素子の第六実施例の断面図である。

【図９】本発明の熱電素子に蓄電素子を設けた場合の第七実施例の断面図及び発電原理を示した図である。

【図１０】本発明の熱電素子を動力源として用いた電子腕時計の第八実施例の動作原理を示したブロック図である。

【図１１】本発明の熱電素子を動力源として用いた電子腕時計の第八実施例の外観図である。

【図１２】本発明の熱電素子を動力源として用いた電子腕時計の第八実施例の断面図である。

【符号の説明】

１　熱電堆
１１、１２　素子
１３、１４　接合体
１５　絶縁材
２２　集熱体
３２　放熱体
３２ａ～３２ｆ　ひれ
１０１、２０１、５０１、６０１、７０１、８０１、９０１、１２０１　第一の絶縁体
１０２、２０２、５０２、６０２、７０２、８０２、９０２、１１０２、１２０２　第二の絶縁体
１０３、２０３ａ、５０３、６０３、７０３、８０３、９０３、１２０３ｎ型半導体
１０４、２０４ａ、５０４、６０４、７０４、８０４、９０４、１２０４ｐ型半導体
１０５、２０５、５０５、６０５、７０５、８０５、９０５　接続部、電極
１０６、２０６、５０６、６０６、７０６、８０６、９０６　出力端子部
２０３　ｎ型半導体複合素子
２０４　ｐ型半導体複合素子
４０８、１２０８　蓄電機構
４００、１０００　熱電素子
４０９　駆動機構
４１０　動作表示機構
８０２ａ　第二の絶縁体の穴部
９０８、１００８　蓄電素子
１００９　駆動制御回路
１００７　充電制御回路
１０１０　表示機構
１２１１　ムーブメント

【図1】

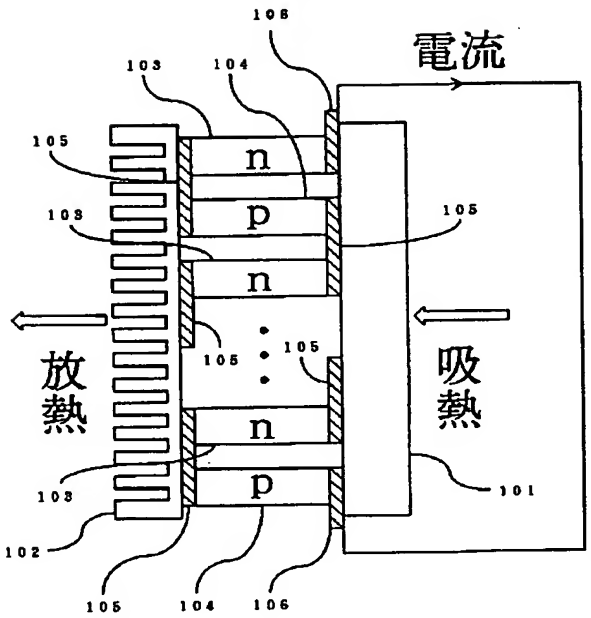

【図2】

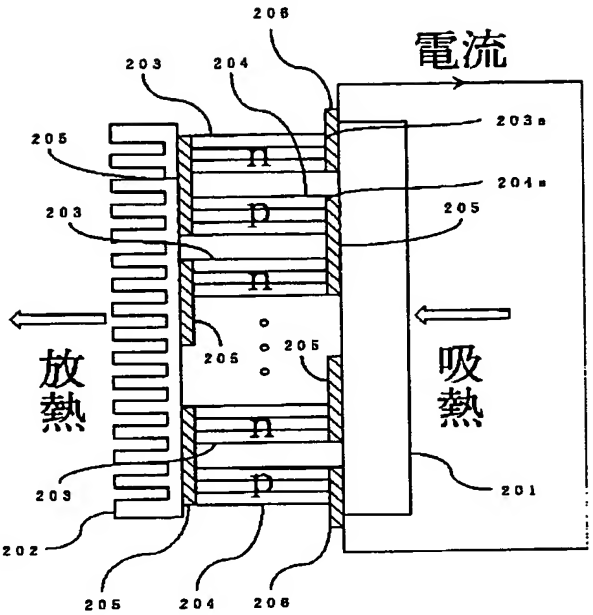

【図3】

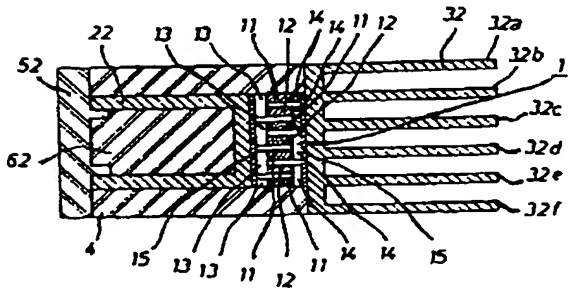

【図4】

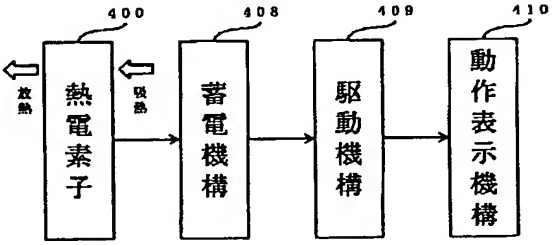

【図10】

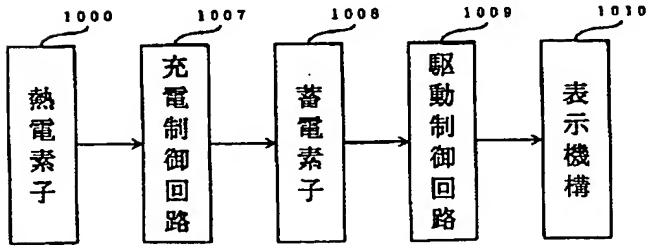

【図11】

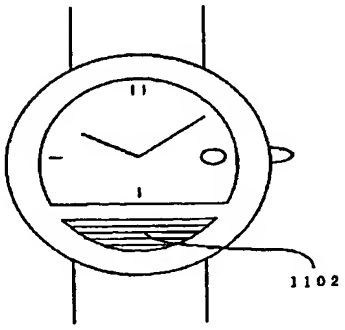

【図5】

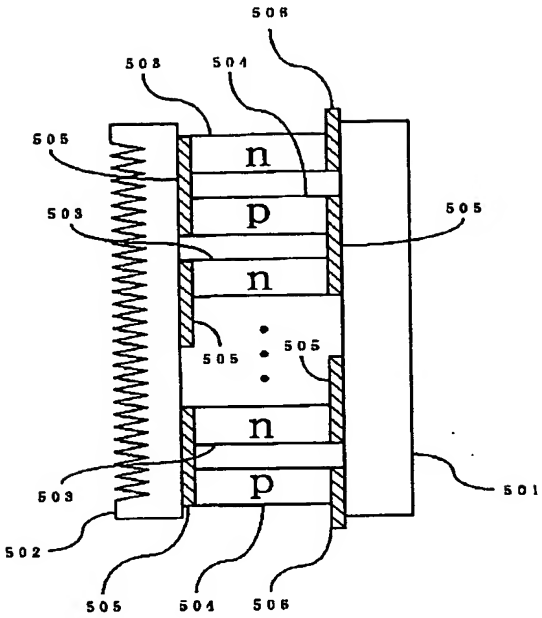
506
508
504
505
n
p
n
505
505
n
p
503
502
505
504
506
501

【図6】

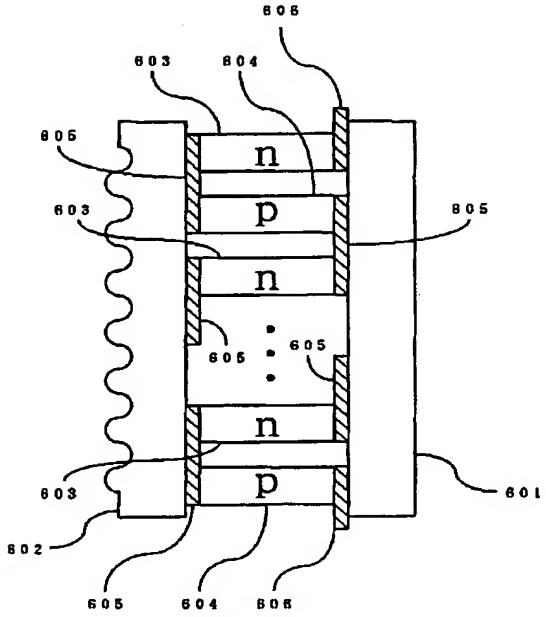
806
603
804
805
n
p
603
805
n
605
605
n
p
603
802
601
605
604
806

【図7】

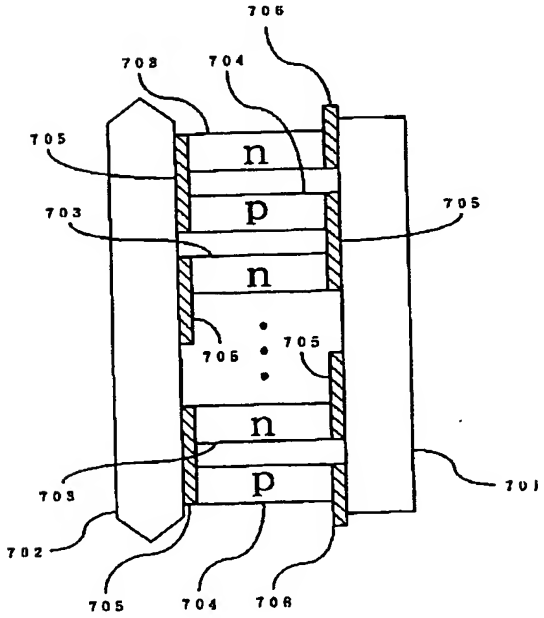
706
708
704
705
n
p
703
705
n
705
705
n
p
703
702
701
705
704
706

【図8】

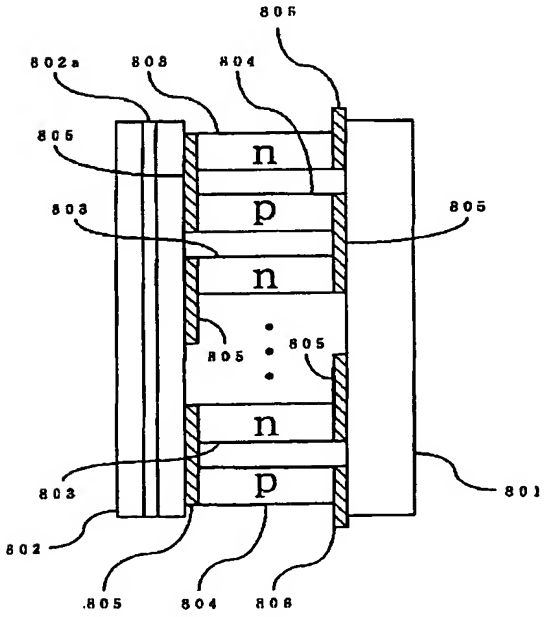
806
802a
808
804
805
n
p
803
805
n
805
805
n
p
803
802
801
805
804
808

【図9】

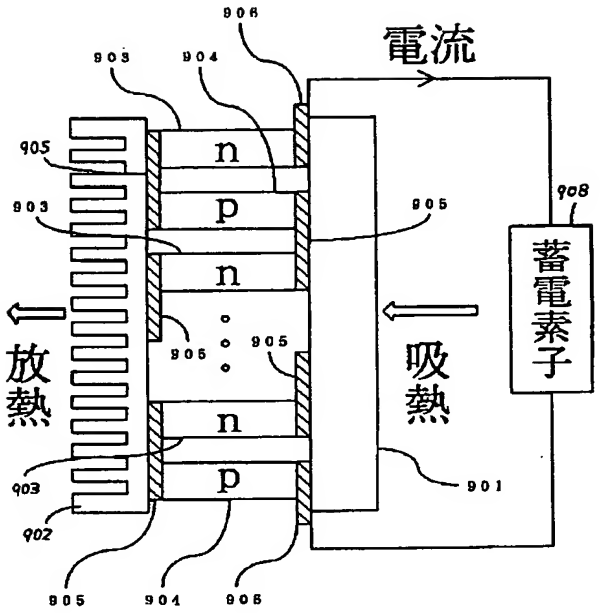
906
電流
903
904
905
n
p
n
903
905
908
蓄電素子
放熱
905
905
吸熱
n
p
903
901
902
905
904
906

【図12】

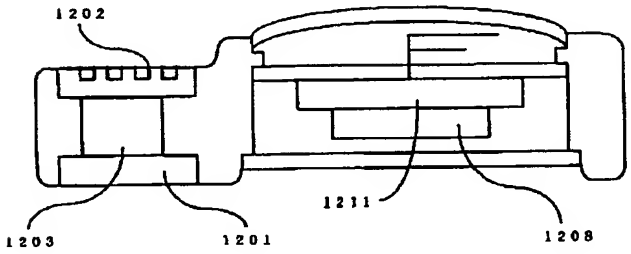
1202
1211
1203
1201
1208

METHOD FOR COMBINING THERMOELECTRIC CONVERSION MATERIAL CONFIGURATION ATOM

Patent number: JP2001189495

Publication date: 2001-07-10

Inventor: MATSUBARA KAKUEI; ABU HIROAKI

Applicant: YAMAGUCHI INDUSTRIAL PROMOTION FOUNDATION

Classification:

- international: H01L35/18; H01L35/14; H01L35/34

- european:

Application number: JP19990373288 19991228

Priority number(s):

Abstract of **JP2001189495**

PROBLEM TO BE SOLVED: To give a guide for combining the configuration atoms of a thermoelectric conversion material for constituting a Heusler-type compound.

SOLUTION: Neutral atom configuration atoms for composing neutral atoms by eliminating insufficient electron-filled state in the s, p, and d orbitals of electron orbitals, a cation configuration atom for composing a cation by eliminating insufficient electron-filled state in the s, p, and d orbits of the electron orbitals, an anion configuration atom for composing an anion by eliminating insufficient electron-filled state in the s, p, and d orbitals of the electron orbitals are combined so that the charge balance, based on the anion configuration atom and the cation configuration atom can be balanced, thus constituting the thermoelectric conversion material of a Heusler-type compound.

---

(19)日本国特許庁（ＪＰ）　(12) 公開特許公報（Ａ）　(11)特許出願公開番号
特開2001－189495
（P2001－189495A）
(43)公開日　平成13年７月10日(2001.7.10)

(51)Int.Cl.⁷	識別記号	ＦＩ	ﾃｰﾏｺｰﾄﾞ(参考)
Ｈ０１Ｌ 35/18		Ｈ０１Ｌ 35/18	
35/14		35/14	
35/34		35/34	

審査請求　未請求　請求項の数９　ＯＬ　（全 ７ 頁）

(21)出願番号　特願平11－373288

(22)出願日　平成11年12月28日(1999.12.28)

(71)出願人　391025660
財団法人やまぐち産業振興財団
山口県山口市熊野町１番10号
(72)発明者　松原　覚衛
山口県宇部市芝中11－46－701
(72)発明者　阿武　宏明
山口県宇部市大字東須恵４－７　ラークハイツ厚南201号
(74)代理人　100080001
弁理士　筒井　大和　（外２名）

(54)【発明の名称】　熱電変換材料構成原子の組合せ方法

(57)【要約】
【課題】　ホイスラー型化合物を構成する熱電変換材料の構成原子の組合せ指針を与えること。
【解決手段】　電子軌道のｓ軌道、ｐ軌道、およびｄ軌道における不十分な電子充填状態を解消して、中性原子を構成する中性原子構成原子と、電子軌道のｓ軌道、ｐ軌道、およびｄ軌道における不十分な電子充填状態を解消して、陽イオンを構成する陽イオン構成原子と、電子軌道のｓ軌道、ｐ軌道、およびｄ軌道における不十分な電子充填状態を解消して、陰イオンを構成する陰イオン構成原子とを、前記陽イオン構成原子と前記陰イオン構成原子とに基づく電荷バランスを平衡させるように組み合わせて、ホイスラー型化合物の熱電変換材料を構成する。

図　4

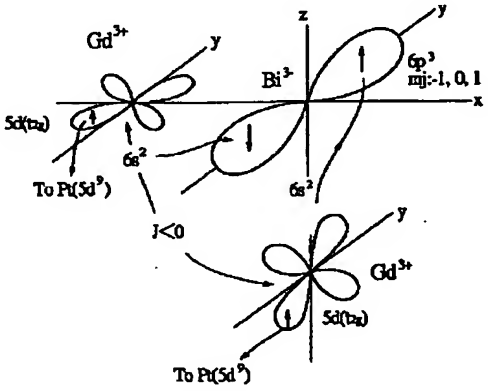

Gd	→ 4f⁷	5s²,5p⁶,5d①	6s②	→Gd³⁺:4f⁷
Pt	→	→5d⑨	6s①	→閉殻を構成
Bi	→	→	6s²,6p③	→Bi³⁻

1

【特許請求の範囲】

【請求項１】　電子軌道における不十分な電子充填状態を解消して、中性原子を構成する中性原子構成原子と、電子軌道における不十分な電子充填状態を解消して、陽イオンを構成する陽イオン構成原子と、
電子軌道における不十分な電子充填状態を解消して、陰イオンを構成する陰イオン構成原子とを、
前記陽イオン構成原子と前記陰イオン構成原子とに基づく電荷バランスが平衡するように組合せて、ホイスラー型化合物を構成することを特徴とする熱電変換材料構成原子の組合せ方法。

【請求項２】　電子軌道における不十分な電子充填状態を解消して、中性原子を構成する中性原子構成原子と、電子軌道における不十分な電子充填状態を解消して、陽イオンを構成する陽イオン構成原子と、
電子軌道における不十分な電子充填状態を解消して、陰イオンを構成する陰イオン構成原子とを、
前記陽イオン構成原子と前記陰イオン構成原子とに基づく電荷バランスが平衡するように組合せてホイスラー型化合物を構成し、
前記中性原子構成原子がＮｉ、前記陽イオン構成原子がＴｉ、ＺｒまたはＨｆ、前記陰イオン構成原子がＳｉ、Ｇｅ、ＳｎまたはＰｄであることを特徴とする熱電変換材料構成原子の組合せ方法。

【請求項３】　電子軌道における不十分な電子充填状態を解消して、中性原子を構成する中性原子構成原子と、電子軌道における不十分な電子充填状態を解消して、陽イオンを構成する陽イオン構成原子と、
電子軌道における不十分な電子充填状態を解消して、陰イオンを構成する陰イオン構成原子とを、
前記陽イオン構成原子と前記陰イオン構成原子とに基づく電荷バランスが平衡するように組合せてホイスラー型化合物を構成し、
前記中性原子構成原子がＰｔ、前記陽イオン構成原子がＧｄ、Ｔｂ、Ｌｕ、Ｐａ、UまたはＣｍであり、前記陰イオン構成原子がＰ、Ａｓ、ＳｂまたはＢｉであることを特徴とする熱電変換材料構成原子の組合せ方法。

【請求項４】　請求項１～３のいずれか１項に記載の熱電変換材料構成原子の組合せ方法において、
前記ホイスラー型化合物には、０．１～５０原子%の不純物がドーピングされていることを特徴とする熱電変換材料構成原子の組合せ方法。

【請求項５】　請求項１～４のいずれか１項に記載の熱電変換材料構成原子の組合せ方法において、
不十分な電子充填状態を解消して中性原子を構成するに際しては、前記中性原子構成原子の前記陽イオン構成原子からの電子の受領と、前記中性原子構成原子からの前記陰イオン構成原子への電子の供与とにより行われると見なされることを特徴とする熱電変換材料構成原子の組合せ方法。

2

【請求項６】　請求項１～４のいずれか１項に記載の熱電変換材料構成原子の組合せ方法において、
不十分な電子充填状態を解消して陽イオンを構成するに際しては、前記陽イオン構成原子からの前記中性原子構成原子への電子の供与と、前記陽イオン構成原子からの前記陰イオン構成原子への電子の供与とにより行われると見なされることを特徴とする熱電変換材料構成原子の組合せ方法。

【請求項７】　請求項１～４のいずれか１項に記載の熱電変換材料構成原子の組合せ方法において、
不十分な電子充填状態を解消して陰イオンを構成するに際しては、前記陰イオン構成原子の前記中性原子構成原子からの電子の受領と、前記陰イオン構成原子の前記陽イオン構成原子からの電子の受領とにより行われると見なされることを特徴とする熱電変換材料構成原子の組合せ方法。

【請求項８】　請求項５～７のいずれか１項に記載の熱電変換材料構成原子の組合せ方法において、
電子の受領および供与には、同一主量子数の電子軌道間の電子移動が関与していると見なされることを特徴とする熱電変換材料構成原子の組合せ方法。

【請求項９】　請求項５～７のいずれか１項に記載の熱電変換材料構成原子の組合せ方法において、
電子の受領、および／または供与には、異なる主量子数の電子軌道間の電子移動が関与していると見なされることを特徴とする熱電変換材料構成原子の組合せ方法。

【発明の詳細な説明】

【０００１】

【発明の属する技術分野】本発明は、熱エネルギーと電気エネルギーとの相互変換を行う熱電変換材料に関する。

【０００２】

【従来の技術】近年、熱エネルギーを電気エネルギーに直接変換したり、あるいは電気エネルギーを熱エネルギーに直接変換する熱電変換材料の研究が行われている。かかる熱電変換材料は、ゼーベック効果、あるいはペルチェ効果を利用して熱電変換を行うものであるが、その変換性能は、性能指数と呼ばれる以下の式、

$Z = \alpha^2 (\sigma / \kappa)$

Ｚ：性能指数（K^{-1}）

α：ゼーベック係数（VK^{-1}：単位温度当たりの発生熱起電力）

σ：電気伝導度（Scm^{-1}）

κ：熱伝導度（$Wcm^{-1}K^{-1}$）

で示される。

【０００３】熱電変換は、駆動部分がなく小型軽量であり、メンテナンスフリーで半永久的に使えるなどの優れた特徴がある。その特徴を活かして、例えば、熱電発電では宇宙探査機の電源として、また灯台などの僻地利用の電源として利用されている。

【０００４】一方、ペルチェ効果は、半導体レーザー、センサー、集積回路（ＬＳＩ）などの電子素子の冷却や、小型のクーラーボックスなどの民生用にも利用されている。しかし現状では、変換効率が１０％以下であるので、現有のエネルギー変換系と競合できる段階には至っていない。

【０００５】熱電変換を多くの用途で使えるレベルまで引き上げるには、いくつかの課題を解決することが必要である。中でも変換効率の向上が第一の課題であり、変換効率２０％が達成できれば応用分野は飛躍的に拡大できる。このほかに、熱電変換の優位性、他のエネルギー変換系との競合性、ＣＯＰ（成績係数）、経済性（コスト）などの多面的な検討も必要である。

【０００６】これらの技術的問題点が解決されると、産業分野での用途や民生品での幅広い利用が見えてくる。例えば、自動車のエンジン排熱が電気エネルギーとして回収できる。現行の自動車のエンジンでは燃料の約２６％が動力であり、残りは約６０％は熱として大気中に放出されている。

【０００７】エンジン外壁またはターボチャージャーから放出される約８００℃の排熱で電力をつくり、これをバッテリーに充電すればクーラーやオルタネーターなどの駆動用として利用できる。

【０００８】その他、中小規模焼却炉の高温排熱や燃料電池の反応熱からのエネルギー回収（科学技術庁・航空宇宙研究所）、ヒートパイプに熱電発電モジュールを組み込んだ高速増殖炉（電力中央研究所）の熱交換器など、幅広い分野で実用化が期待できる。

【０００９】

【発明が解決しようとする課題】現在、上記のように種々の分野で熱電変換材料に対する強い実用化の要請があり、変換効率の優れた新規な熱電変換材料の開発は急務である。その中で、ホイスラー型結晶構造をもつ金属間化合物の一部は半導体的性質を示すことから、新規熱電材料として注目されている。

【００１０】しかしながら、これまでホイスラー型金属間化合物は金属伝導を示す磁性材料としての研究が主に進められており、例えば、優れた磁気光学材料としてＰｔＭｎＳｂが得られているものの熱電変換材料としての実用化できる熱電性能を有するホイスラー合金は得られていない。ホイスラー合金の熱電性能は化合物を構成する元素の組合せに依存する。しかし、熱電材料としてのホイスラー型化合物の十分な開発手法は提案されておらず、ある意味では、手探りの状態である。

【００１１】本発明者らは、自ら新規熱電変換材料の開発に携わりつつ、かかる状況に憂慮し、より効率的な開発が行えるように、開発手法に資する基準を見いだすべきと常々考えてきた。

【００１２】本発明の目的は、新規熱電変換材料としての材料開発に際して、ホイスラー型化合物の構成原子の組合せ方法の基準を与えることにある。

【００１３】

【課題を解決するための手段】本発明者らは、かかるホイスラー型熱電変換材料の探索方法において、従来手探りの状態であった問題を見直し、新規熱電変換材料としてのホイスラー型化合物の探索基準を提案する。

【００１４】従来、ホイスラー合金については磁性材料として理論的には電子構造が議論されているものの、熱電変換材料としての見地からは殆ど議論されていない。この点を見直しホイスラー合金の電子結合状態またはバンド構造と、熱電特性の相関について研究を行った中から、本発明に至ったものである。

【００１５】本発明者らは、特にＰｔＧｄＢｉついて、同様の結晶構造を有するホイスラー合金のＰｔＭｎＳｂ、ＰｄＭｎＳｂと比較しつつ、その電子結合状態とバンド構造とに着目し研究を行った結果、ホイスラー型化合物の中で熱電変換材料として良好な特性をもつための構成元素の組合せについて、電子構造論的観点からその選択基準を見出した。かかる基準に沿って原子構成を選択することにより、新規なホイスラー型化合物によって構成される熱電変換材料を効率的に提供することができる。

【００１６】すなわち、本発明のホイスラー型化合物によって構成される熱電変換材料の構成原子の組合せ方法は、電子軌道における不十分な電子充填状態を解消して、中性原子を構成する中性原子構成原子と、電子軌道における不十分な電子充填状態を解消して、陽イオンを構成する陽イオン構成原子と、電子軌道における不十分な電子充填状態を解消して、陰イオンを構成する陰イオン構成原子とを、前記陽イオン構成原子と前記陰イオン構成原子とに基づく電荷バランスが平衡するように組合せて、ホイスラー型化合物を構成することを特徴とする。

【００１７】また、電子軌道における不十分な電子充填状態を解消して、中性原子を構成する中性原子構成原子と、電子軌道における不十分な電子充填状態を解消して、陽イオンを構成する陽イオン構成原子と、電子軌道における不十分な電子充填状態を解消して、陰イオンを構成する陰イオン構成原子とを、前記陽イオン構成原子と前記陰イオン構成原子とに基づく電荷バランスが平衡するように組合せてホイスラー型化合物を構成し、前記中性原子構成原子がＮｉ、前記陽イオン構成原子がＴｉ、ＺｒまたはＨｆ、前記陰イオン構成原子がＳｉ、Ｇｅ、ＳｎまたはＰｄであることを特徴とする。

【００１８】電子軌道における不十分な電子充填状態を解消して、中性原子を構成する中性原子構成原子と、電子軌道における不十分な電子充填状態を解消して、陽イオンを構成する陽イオン構成原子と、電子軌道における不十分な電子充填状態を解消して、陰イオンを構成する陰イオン構成原子とを、前記陽イオン構成原子と前記陰

イオン構成原子とに基づく電荷バランスが平衡するように組合せてホイスラー型化合物を構成し、前記中性原子構成原子がＰｔ、前記陽イオン構成原子がＧｄ、Ｔｂ、Ｌｕ、Ｐａ、ＵまたはＣｍであり、前記陰イオン構成原子がＰ、Ａｓ、ＳｂまたはＢｉであることを特徴とする。

【００１９】上記いずれかに記載の熱電変換材料構成原子の組合せ方法において、前記ホイスラー型化合物には、０．１～５０原子%の不純物がドーピングされていることを特徴とする。

【００２０】前記いずれかに記載の熱電変換材料構成原子の組合せ方法において、不十分な電子充填状態を解消して中性原子を構成するに際しては、前記中性原子構成原子の前記陽イオン構成原子からの電子の受領と、前記中性原子構成原子からの前記陰イオン構成原子への電子の供与とにより行われると見なされることを特徴とする。

【００２１】前記いずれかに記載の熱電変換材料構成原子の組合せ方法において、不十分な電子充填状態を解消して陽イオンを構成するに際しては、前記陽イオン構成原子からの前記中性原子構成原子への電子の供与と、前記陽イオン構成原子からの前記陰イオン構成原子への電子の供与とにより行われると見なされることを特徴とする。

【００２２】前記いずれかに記載の熱電変換材料構成原子の組合せ方法において、不十分な電子充填状態を解消して陰イオンを構成するに際しては、前記陰イオン構成原子の前記中性原子構成原子からの電子の受領と、前記陰イオン構成原子の前記陽イオン構成原子からの電子の受領とにより行われると見なされることを特徴とする。

【００２３】前記いずれかに記載の熱電変換材料構成原子の組合せ方法において、電子の受領および供与には、同一主量子数の電子軌道間の電子移動が関与していると見なされることを特徴とする。前記いずれかに記載の熱電変換材料構成原子の組合せ方法において、電子の受領、および／または供与には、異なる主量子数の電子軌道間の電子移動が関与していると見なされることを特徴とする。

【００２４】上記構成の中性原子構成原子、陽イオン構成原子、陰イオン構成原子の選定は、例えば、中性原子の基底状態の電子配置から、上記構成を満足する原子構成の組み合わせを選択することにより行える。手探り状態で種々の原子の組み合わせを考慮する従来方法の新規熱電変換材料の探索方法に比べて、格段に探索範囲を狭めることができ、優れた熱電変換材料の開発が効率的に行える。

【００２５】本明細書で使用する「軌道」とは、主量子数、方位量子数、磁気量子数の一組の組み合わせで規定され、電子の存在確率を示す波動関数により表示されるものを意味し、オービタル（ｏｒｂｉｔａｌ）とも呼ばれる。各軌道には電子スピンが逆方向（異なるスピン量子数）の電子が最大２個まで入り得る。

【００２６】

【発明の実施の形態】以下、本発明の実施の形態を図面に基づいて詳細に説明する。

【００２７】ＰｔＧｄＢｉなる組成式を有するホイスラー型化合物に属する３元合金を製造し、その熱電特性と結晶構造中の原子配置、電子構造との関係を調べた。Ｇｄは、純度９９．９%の原料を使用した。Ｐｔの原料には、９９．９９%の原料を使用した。Ｂｉの原料には、純度９９．９９９９%の原料を使用した。

【００２８】これらの原料を上記組成式に基づく化学量論的割合に合わせて秤量し、これらをアーク溶解した。アーク溶解により得られた合金物質は、組成が均一となるように、必要回数再溶解を繰り返した。その後、得られたインゴットを熱処理することによってＰｔＧｄＢｉで構成される試料を作製した。得られた結晶の構造は、Ｘ線回析により確認した。

【００２９】このようにして得られた試料について、その熱電特性を測定した。図１は、電気伝導度の温度依存性を示している。比較として、ホイスラー合金のＭｎベースのアンチモナイドであるＰｔＭｎＳｂ、ＰｄＭｎＳｂの電気伝導度も示した。図１に示す電気伝導度からは、ＰｔＭｎＳｂ、ＰｄＭｎＳｂが、通常とは異なる温度依存性を示していることがわかる。かかる温度依存性は、キャリヤー散乱によるものとは考えられず、バンド構造の変化によるものと推測される。

【００３０】かかるＰｔＭｎＳｂ、ＰｄＭｎＳｂに比較して、ＰｔＧｄＢｉでは、半導体のような挙動をとっている。ホール濃度は、室温で$7\times10^{19}cm^{-3}$であった。ホール移動度は、室温で約１２０cm^2／Ｖｓ、１００Ｋで２２０cm^2／Ｖｓであった。

【００３１】図２には、ゼーベック係数の温度依存性を示す。前記図１と同様に、ＰｔＧｄＢｉと共にＰｔＭｎＳｂ、ＰｄＭｎＳｂを比較として示した。ＰｔＭｎＳｂ、ＰｄＭｎＳｂに関しては、３００～８５０Ｋの範囲で、極めて低い値を示しているが、ＰｔＧｄＢｉに関しては、室温で６０μＶ／Ｋ、５５０～７５０Ｋの温度範囲で８２μＶ／Ｋの高い値を示した。

【００３２】ＰｔＧｄＢｉは、図３に示すように、ＰｔＭｎＳｂ、ＰｄＭｎＳｂと同様の$C1_b$対称性の結晶構造を有し、かかる構造はＸ線回析により確認された。図３に示す単位結晶格子中では、ＢｉとＧｄとは副格子を構成して、Ｂｉの両隣に９０°の角度を有してＧｄが配置された原子配置をとっている。かかる様子を、図４に示した。

【００３３】図４では、Ｂｉの$6p_y^1$軌道の両隣に、Ｇｄの$5d_{xy}^1$、$5d_{yz}^1$軌道が９０度の角度を有して配置されている様子を示している。両者の交換積分Ｊは負となりエネルギー的な相互作用が存在してることが計

算からも確認される。

【００３４】Ｐｔは、［Ｘｅ］４ｆ^{14}５ｄ^{9} ６ｓ^{1} の電子配置を有している。すなわち、Ｘｅと同一の電子配置を内殻に有し、外殻に不十分な電子充填状態の５ｄ^{9} ６ｓ^{1}軌道を有した電子配置となっている。異なるスピンの電子を最大１０個まで許容可能な主量子数５のｄ軌道に９個の電子が充填され、電子を最大２個まで許容可能な主量子数６のｓ軌道に１個の電子が充填されて、いずれの軌道も不十分な電子充填状態になっていることがわかる。これらの不十分な電子充填状態を解消することにより、Ｐｔはエネルギー的に安定化する。

【００３５】一方、Ｂｉは、［Ｘｅ］４ｆ^{14}５ｄ^{10}６ｓ^{2} ６ｐ^{3} の電子配置を有している。すなわち、内殻にＸｅの電子配置を有し、外殻の６ｐ^{3} 軌道が不十分な電子充填状態となっている。そのため、外殻の主量子数６のｐ軌道には、他の原子から３個の電子を受けて軌道を満たし、陰イオンを構成することにより、エネルギー的に安定な電子配置を取ろうとする傾向があると言える。

【００３６】Ｇｄは、［Ｘｅ］４ｆ^{7} ５ｄ^{1} ６ｓ^{2} の電子配置を有している。内殻にＸｅの閉殻電子配置を有し、外殻の５ｄ^{1} が不十分な電子充填状態となっている。かかる電子配置を有するＧｄは、５ｄ^{1} 電子軌道から電子を１個放出して、陽イオンになりやすい傾向を有していると言える。なお、Ｇｄでは、４ｆ^{7} 軌道も電子充填状態は不十分ではあるが、５ｄ、６ｓ、６ｐ軌道との電子移動を行う程には相互のエネルギー順位は接近しておらず、本考察からは除外できる。

【００３７】ＰｔＧｄＢｉでは、前述のようにその単位格子中にＢｉ－Ｇｄの副格子が形成されており、かかる副格子では、図３に示すように、Ｂｉの両隣に９０°の角度有して２個のＧｄが配置された構成が形成されている。

【００３８】そこで、かかる結晶格子中の原子配置と、Ｐｔ、Ｇｄ、Ｂｉの上記電子配置とを併せて考えると、Ｇｄの５ｄ^{1} 軌道から１個の電子がＰｔの同じ主量子数の５ｄ^{9} 軌道へ移動して、Ｐｔの５ｄ^{9} 軌道は５ｄ^{10}軌道となり、５ｄ軌道は完全に満たされて５ｄ^{9} 軌道の不十分な電子充填状態が解消されていると考えられる。Ｇｄでは、５ｄ^{1} 軌道から電子が１個放出されて不十分な電子充填状態であった５ｄ軌道は完全に空位となり解消されている。

【００３９】一方、Ｇｄの６ｓ^{2} 軌道からの２個の電子と、Ｐｔの６ｓ^{1} 軌道からの１個の電子とは、Ｂｉの６ｐ^{3} 軌道へ移動することにより、ＧｄはＧｄ$^{3+}$の陽イオンとなり、ＢｉはＢｉ$^{3-}$の陰イオンとなり、陽イオン、陰イオンの電荷バランスの平衡を保ちながら、各原子の不十分な電子充填状態の解消が図られている。

【００４０】すなわち、Ｇｄの６ｓ^{2} 軌道からの２個の電子と、Ｐｔの６ｓ^{1} 軌道からの１個の電子とが、Ｂｉの６ｐ^{3} 軌道へ移動することにより、中性原子のＧｄは、Ｇｄ$^{3+}$となり、その電子配置は、［Ｘｅ］４ｆ^{7} となりｓ軌道、ｐ軌道、ｄ軌道における不十分な電子充填状態が解消されている。

【００４１】中性原子のＰｔも、Ｇｄから１個の電子を受け入れて５ｄ^{9} 軌道が５ｄ^{10}軌道となり、併せて６ｓ^{1} 軌道から１個の電子をＢｉの６ｐ^{3} 軌道へ放出させることにより、その電子配置は、［Ｘｅ］４ｆ^{14}５ｄ^{10}となり、不十分な電子充填状態を解消して、所謂閉殻電子配置を有する中性原子構成原子となっている。

【００４２】Ｂｉでは、Ｇｄの６ｓ^{2} 軌道からの２個の電子と、Ｐｔの６ｓ^{1} 軌道からの１個の電子とを、Ｂｉの６ｐ^{3} 軌道へ受け入れることにより、６ｐ^{3} 軌道の不十分な電子充填状態が解消され、［Ｘｅ］４ｆ^{14}５ｄ^{10} ６ｓ^{2} ６ｐ^{6} の電子配置を有する安定な電子配置を有した陰イオンのＢｉ$^{3-}$となっている。

【００４３】Ｇｄでは、Ｇｄの５ｄ^{1} 軌道からの１個の電子をＰｔの５ｄ^{9} へ、６ｓ^{2} 軌道からの２個の電子をＢｉの６ｐ^{3} 軌道へ供与することにより、５ｄ^{1} 軌道の不十分な電子充填状態が解消され、［Ｘｅ］４ｆ^{7} の電子配置を有する安定な電子配置を有した陽イオンのＧｄ$^{3+}$となっている。

【００４４】このようにＰｔＧｄＢｉでは、Ｐｔ、Ｇｄ、Ｂｉのそれぞれの原子が基底状態の電子配置におけるｓ軌道、ｐ軌道、ｄ軌道の不十分な電子充填状態を解消して、狭いバンドギャップを有するエネルギー的に安定な結晶構造が創出されることから、同一の結晶構造を有するＰｔＭｎＳｂ、ＰｄＭｎＳｂとは異なる熱電特性を示すものと考えられる。

【００４５】すなわち、ＰｔＭｎＳｂでは、Ｍｎは［Ａｒ］３ｄ^{5} ４ｓ^{2} なる電子配置を有し、Ｐｔは［Ｘｅ］４ｆ^{14}５ｄ^{9} ６ｓ^{1} なる電子配置を有し、Ｓｂは［Ｋｒ］４ｄ^{10}５ｓ^{2} ５ｐ^{3} なる電子配置を有しており、ＰｔＧｄＢｉで考察したと同様な各原子間の電子移動に基づき、個々の原子の不十分な電子充填状態を解消させるような電子配置の構成を考えることはできない。

【００４６】また、ＰｄＭｎＳｂでは、Ｐｄは［Ｋｒ］４ｄ^{10}なる電子配置を有し、Ｐｔは［Ｘｅ］４ｆ^{14}５ｄ^{9} ６ｓ^{1} なる電子配置を有し、Ｓｂは［Ｋｒ］４ｄ^{10}５ｓ^{2}５ｐ^{3} なる電子配置を有しているため、ＰｔＭｎＳｂで考察したと同様に、ＰｔＧｄＢｉと同様な各原子間の電子移動に基づく構成原子の不十分な電子充填状態を解消させるような電子配置の構成を考えることはできない。

【００４７】かかるＰｔＭｎＳｂ、ＰｄＭｎＳｂの電子配置のＰｔＧｄＢｉとの相違が、熱電特性の発現の差異につながっていると考えられる。かかる考察から、電子軌道の不十分な電子充填状態を解消して、中性原子を構成する中性原子構成原子と、電子軌道における不十分な電子充填状態を解消して、陽イオンを構成する陽イオン構成原子と、電子軌道における不十分な電子充填状態を

解消して、陰イオンを構成する陰イオン構成原子とを、前記陽イオン構成原子と前記陰イオン構成原子とに基づく電荷バランスを平衡するように含有させることが、新規なホイスラー型化合物を構成する熱電変換材料の原子構成の基準となり得るものと考えられ本発明となしたものである。

【００４８】すなわち、本発明者らはＰｔＧｄＢｉの熱電特性と、結晶構造における原子配置、構成原子の電子構造とを、初めて詳細に検討することにより、電子構造的見地からのホイスラー型化合物の構成原子の組合せ方法を見出し初めて提案するものである。

【００４９】かかる構成を有するホイスラー型化合物としては、既知のＰｔＧｄＢｉ以外に、表１に示すような種々の系の組合せが考えられる。

【００５０】ここで、表中Ａ原子は上記中性原子を構成する中性原子構成原子であり、ＰｔＧｄＢｉを構成するＰｔに相当し、Ｂ原子は上記陽イオンを構成する陽イオン構成原子であり、ＰｔＧｄＢｉを構成するＧｄに相当し、Ｃ原子は上記陰イオンを構成する陰イオン構成原子であり、ＰｔＧｄＢｉを構成するＢｉに相当する。

【００５１】

【表１】

表１

Ａ原子	Ｂ原子	Ｃ原子
Ｎｉ	Ｔｉ Ｚｒ Ｈｆ	Ｓｉ Ｇｅ Ｓｎ Ｐｂ
Ｐｔ	Ｇｄ Ｔｂ Ｌｕ Ｐａ Ｕ Ｃｍ	Ｐ Ａｓ Ｓｂ Ｂｉ

【００５２】本発明は前記の形態に限定されるものではなく、その要旨を逸脱しない範囲で種々変更することができる。

【００５３】例えば、ＰｔＧｄＢｉまたは表１に示した種々の系の組合せからなるホイスラー型化合物に、０．１～５０原子％（ａｔｏｍ％）程度の不純物をドーピング（ｄｏｐｉｎｇ）して、不純物を結晶格子内に挿入したり、あるいは構成原子の一部を置換したりすることも可能である。

【００５４】

【発明の効果】本発明によれば、熱電変換材料としてのホイスラー型化合物の構成原子の組合を、電子構造などに基づき予測することができる。そのため、ホイスラー型化合物を構成する新規な熱電変換材料の効率的な開発が行える。

【図面の簡単な説明】

【図１】ＰｔＧｄＢｉの電気伝導度の温度依存性を示すグラフ図である。

【図２】ＰｔＧｄＢｉのゼーベック係数の温度依存性を示すグラフ図である。

【図３】ＰｔＧｄＢｉの結晶構造を示す説明図である。

【図４】ＰｔＧｄＢｉにおけるＧｄ－Ｂｉ間の電子遷移の様子を示す説明図である。

【図１】

図　1

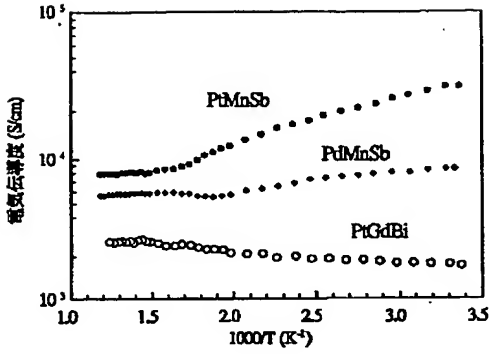

【図２】

図　2

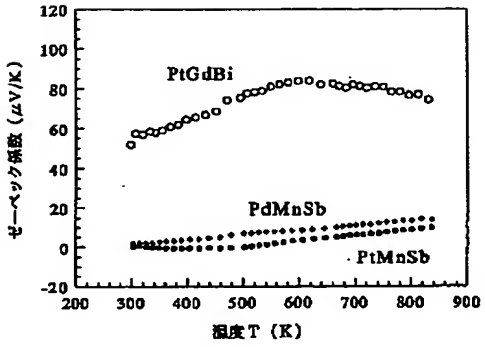

【図３】

図　3

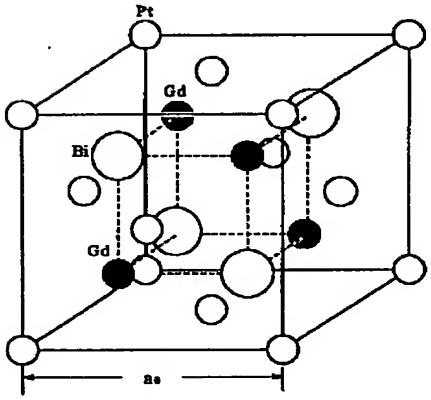

【図４】

図　4

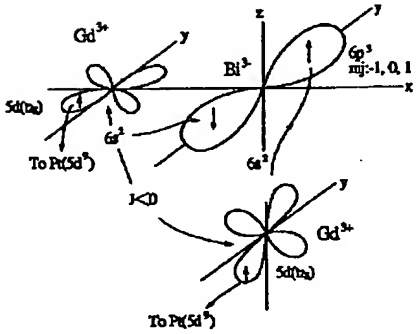

Gd	→4f⁷	5s²,5p⁶,5d①	6s②	→Gd³⁺:4f⁷
Pt		→5d③	6s①	→結合を構成
Bi			6s²,6p③	→Bi³⁻

THERMOELECTRIC ELEMENT AND ELECTRONIC EQUIPMENT USING IT

Patent number:	JP8032127
Publication date:	1996-02-02
Inventor:	TSUBATA KEISUKE
Applicant:	SEIKO INSTR INC
Classification:	
- International:	H01L35/32; G04C10/00; G04G1/00
- european:	
Application number:	JP19940167242 19940719
Priority number(s):	

Abstract of **JP8032127**

PURPOSE:To first insulator 101 is set on a heat absorbing thermoelectric element and reduce the size of the element by specifying the thicknesses of a plurality of n-type semiconductors and a plurality of p-type semiconductors within specific ranges.

CONSTITUTION:A first insulator 101 is set on a heat absorbing side and second insulator 102 is set on a heat radiating side. When a high temperature is given to the heat absorbing side so that the temperature on the heat absorbing side becomes higher than that on the heat radiating side, heat is transmitted from the first insulator 101 to the second insulator 102. When the heat is transmitted, electrons move toward the insulator 102 on the heat radiating side in an n-type semiconductor 103. In a p-type semiconductor 104, holes move toward the insulator 102 on the heat radiating side. Since the semiconductors 103 and 104 are electrically connected in series with each other through a connecting section 105, the heat transmission is converted into an electric current and an electomovtive force can be obtained across output terminals 106 at both ends. When silicon is used for the insulators, the power generating efficiency of this thermoelectric element can be improved 2 the size of the element can be reduced, because the thickn and of the n-and p-type semiconductors can be reduced to 0.2-0.3mm.

(19)日本国特許庁（ＪＰ）　(12) 公開特許公報（A）　(11)特許出願公開番号

特開平8－32127

(43)公開日　平成８年(1996)２月２日

(51)Int.Cl.[6]	識別記号	庁内整理番号	ＦＩ	技術表示箇所
Ｈ０１Ｌ　35/32		Ａ		
Ｇ０４Ｃ　10/00		Ｃ		
Ｇ０４Ｇ　1/00	３１０	Ｙ	9109－2F	

審査請求　未請求　請求項の数６　ＯＬ　（全　６　頁）

(21)出願番号　特願平6－167242

(22)出願日　平成６年(1994)７月19日

(71)出願人　000002325
セイコー電子工業株式会社
千葉県千葉市美浜区中瀬１丁目８番地

(72)発明者　津端　佳介
東京都江東区亀戸６丁目31番１号　セイコー電子工業株式会社内

(74)代理人　弁理士　林　敬之助　（外１名）

(54)【発明の名称】　熱電素子および熱電素子を用いた電子機器

(57)【要約】

【目的】　ｎ型半導体およびｐ型半導体の厚さが発電能力と小型化を考慮して決定された熱電素子、および熱電素子を用いた電子機器を提供する。

【構成】　シリコンの第一の絶縁体１０１を吸熱側、シリコンの第二の絶縁体１０２を放熱側とすると、吸熱側の温度を放熱側と比較して高温となるような温度差を与えた場合、第一の絶縁体１０１から第二の絶縁体１０２の方向に熱が伝達される。その際にｎ型半導体１０３の中では電子が放熱側の絶縁体１０２の方向に移動する。ｐ型半導体１０４の中では正孔が放熱側の絶縁体１０２の方向に移動する。ｎ型半導体１０３とｐ型半導体１０４は接続部１０５を介して電気的に直列に接続されているため熱の伝達が電流に変換され、両端の出力端子部１０６より起電力を得ることができる。

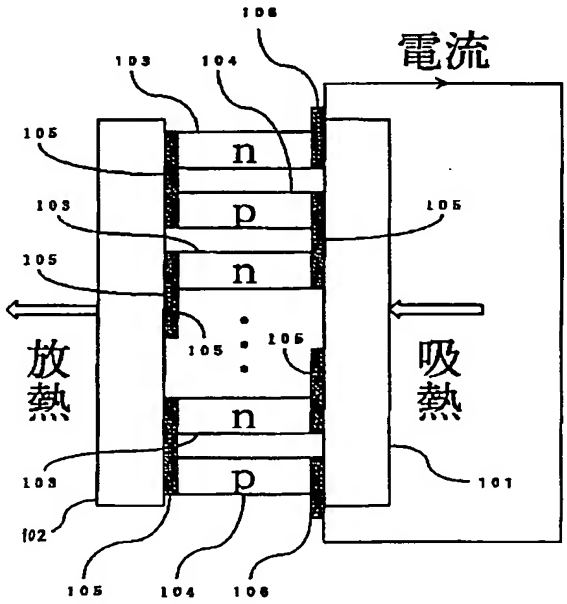

1

【特許請求の範囲】

【請求項１】　複数のｎ型半導体（１０３）と複数のｐ型半導体（１０４）を交互に電気的に直列になるように接続する複数の接続部（１０５）と出力端子部（１０６）とを有し、接続部（１０５）を１つおきに固定するシリコンで構成した第一の絶縁体（１０１）と、第一の絶縁体で接続していない１つおきの接続部（１０５）を固定するシリコンで構成した第二の絶縁体（１０２）とを有し、第一の絶縁体（１０１）と第二の絶縁体（１０２）との間に固定される複数のｎ型半導体（１０３）および複数のｐ型半導体（１０４）のそれぞれの厚さが０．２㎜～３㎜であることを特徴とする熱電素子。

【請求項２】　複数のｎ型半導体から構成されるｎ型半導体複合素子（２０３）を複数有し、複数のｐ型半導体から構成されるｐ型半導体複合素子（２０４）を複数有し、複数のｎ型半導体複合素子（２０３）と複数のｐ型半導体複合素子（２０４）を交互に電気的に直列になるように接続する複数の接続部（２０５）と出力端子部（２０６）とを有し、接続部（２０５）を１つおきに固定するシリコンで構成した第一の絶縁体（２０１）と、第一の絶縁体（２０１）で接続していない１つおきの接続部（２０５）を固定するシリコンで構成した第二の絶縁体（２０２）とを有し、第一の絶縁体（２０１）と第二の絶縁体（２０２）との間に固定される複数のｎ型半導体複合素子（２０３）および複数のｐ型半導体複合素子（２０４）のそれぞれの厚さが０．２㎜～３㎜であることを特徴とする熱電素子。

【請求項３】　請求項１記載の熱電素子において、複数のｎ型半導体（１０３）および複数のｐ型半導体（１０４）のそれぞれの厚さが０．５㎜～２㎜であることを特徴とする熱電素子。

【請求項４】　請求項２記載の熱電素子において、複数のｎ型半導体複合素子（２０３）および複数のｐ型半導体複合素子（２０４）のそれぞれの厚さが０．５㎜～２㎜であることを特徴とする熱電素子。

【請求項５】　エネルギー源を必要とする電子機器において、請求項１乃至請求項４のいずれか１項に記載する熱電素子をエネルギー源として用いた電子機器。

【請求項６】　エネルギー源を必要とする電子時計において、請求項１乃至請求項４のいずれか１項に記載する熱電素子をエネルギー源として用いた電子時計。

【発明の詳細な説明】

【０００１】

【産業上の利用分野】本発明はエネルギー源として電池を使用しない電子機器を実現するための熱電素子、およびエネルギー源として熱電素子を用いた電子機器に関するものである。

【０００２】

【従来の技術】電子機器にはそのエネルギー源として、主に電池が使用されていた。しかし使用者は、使用中に

2

電池切れが起こる心配を常に抱えなくてはならず、万一使用中に電池切れが起こった場合、その損害は大きなものとなる場合もある。そして電池切れを起こした場合には電池を交換する、或は使用者が出来ない場合には他に依頼することを強いられる。更に使用済みの電池は環境破壊の原因となるために、一般の廃棄物と同じ扱で廃棄することが出来ない。

【０００３】電池に変わるエネルギー源として、ゼーベック効果に基づく起電力を発生する熱電素子が最近研究されている。例えば図９は、熱電発電機の発電原理を示す図である。熱電発電機はｐ型熱電素子（９０１）およびｎ型熱電素子（９０２）を直列に多数個接続し、絶縁板（９０３）と放熱板（９０４）および吸熱板（９０５）から構成されている。以上のような熱電発電機が、例えば特開昭５４－１２３０４７号公報に、開示されている。

【０００４】一方熱電素子を用いた電子機器も最近研究されている。例えば図１０は、熱電式腕時計の構成を示す図である。熱電式腕時計は、ムーブメント（１００１）と、熱電式発電器（１００２）と、電気エネルギー畜電器と、金属製底部、フレーム部、金属製の頂部、を備えた多部分からなる腕時計のケーシング（１００３）と、を有する。以上のような熱電式腕時計が、例えば特開昭５５－２０４８３号公報に、開示されている。しかし発電能力及び小型化を考慮した熱電素子モジュールは、まだ実用化には至っていない。

【０００５】

【発明が解決しようとする課題】熱電素子の発電能力は、ｎ型半導体およびｐ型半導体の数に比例し、ｎ型半導体およびｐ型半導体の厚さは厚い方が高い。つまり高い発電能力を得ようとするとｎ型半導体およびｐ型半導体の数を増やし厚くするので熱電素子全体が大きくなってしまう。しかし、この熱電素子を電子機器に搭載する場合には、熱電素子は出来るだけ小さいことが理想であり、発電能力の増大と、熱電素子の小型化は相反する要求となる。

【０００６】そこで本発明の目的は、ｎ型半導体およびｐ型半導体の厚さが発電能力と小型化を考慮して決定された熱電素子、および熱電素子を用いた電子機器を提供することにある。

【０００７】

【課題を解決するための手段】上記課題を解決するために本発明は、熱電素子の発電能力がｎ型半導体およびｐ型半導体の数や厚さだけでなく、絶縁体の熱伝導率によっても左右されることに着目し、絶縁体にシリコンを用いた場合には、ｎ型半導体およびｐ型半導体の厚さを０．２～３㎜、さらに望ましくは０．５～２㎜とした。

【０００８】

【作用】図１は、本発明の第一の熱電素子の構造と発電原理を示す図である。第一の絶縁体１０１を吸熱側、第

二の絶縁体１０２を放熱側とする。吸熱側の温度を放熱側と比較して高温となるような温度差を与えた場合、第一の絶縁体１０１から第二の絶縁体１０２の方向に熱が伝達される。その際に、ｎ型半導体１０３の中では、電子が放熱側の絶縁体１０２の方向に移動する。ｐ型半導体１０４の中では、正孔が放熱側の絶縁体１０２の方向に移動する。ｎ型半導体１０３とｐ型半導体１０４は、接続部１０５を介して電気的に直列に接続されているため、熱の伝達が電流に変換され、両端の出力端子部１０６より起電力を得ることができる。

【０００９】図２は、本発明の第二の熱電素子の構造と発電原理を示す図である。第一の絶縁体２０１を吸熱側、第二の絶縁体２０２を放熱側とする。吸熱側の温度を放熱側と比較して高温となるような温度差を与えた場合、第一の絶縁体２０１から第二の絶縁体２０２の方向に熱が伝達される。その際に、ｎ型半導体複合素子２０３の中では、電子が放熱側の絶縁体２０２の方向に移動する。ｐ型半導体複合素子２０４の中では、正孔が放熱側の絶縁体２０２の方向に移動する。ｎ型半導体複合素子２０３とｐ型半導体複合素子２０４は、接続部２０５を介して電気的に直列に接続されているため、熱の伝達が電流に変換され、両端の出力端子部２０６より起電力を得ることができる。

【００１０】さらに図３は、本発明の熱電素子をエネルギー源として用いた電子機器の動作原理を示すブロック図である。熱電素子３０１に温度差が与えられ、起電力が発生すると、蓄電機構３０２に電気が蓄えられる。蓄電機構３０２に蓄えられた電気の電圧が駆動機構３０３を駆動するのに十分な大きさに達すると、駆動機構３０３が駆動され、動作・表示機構３０４が働き出す。

【００１１】

【実施例】図４は、本発明の熱電素子の一実施例の構造と発電原理を示す図である。第一の絶縁体４０１は、例えばシリコンで構成し吸熱側とする。第二の絶縁体４０２は、例えばシリコンで構成し放熱側とする。吸熱側の温度が放熱側より高温となるような例えば２度程度の温度差を与えた場合、第一の絶縁体から第二の絶縁体の方向に熱が伝達される。その際に、ｎ型半導体４０３例えばビスマスーテルル系、ナマリーテルル系あるいは鉄ーシリサイド系の中では電子が放熱側の第二の絶縁体の方向に移動する。ｐ型半導体４０４例えばビスマスーテルル系、ナマリーテルル系あるいは鉄ーシリサイド系の中では、正孔が放熱側の第二の絶縁体の方向に移動する。ｎ型半導体４０３とｐ型半導体４０４は、接続部４０５例えば電極を介して電気的に直列に接続されているため、熱の伝達が電流に変換され、出力端子部４０６より起電力を得ることができる。出力端子部４０６より得られた起電力は蓄電素子４０９に充電される。

【００１２】図５は、第一の絶縁体及び第二の絶縁体にシリコンを用いた場合のｎ型半導体およびｐ型半導体の

厚さに対する出力電圧の変化を示したグラフである。このとき熱電素子に与えられた温度差は２度、半導体の断面積は０．０１㎟ とした。半導体数はｎ型ｐ型合わせて４０００個、４５００個、５０００個、５５００個、６０００個の場合を示した。１．５ｖ電池の代用となるためには、ｎ型半導体およびｐ型半導体の厚さの誤差による出力電圧のばらつきが少なくなる厚さ１㎜以上において、少なくとも１．４Ｖを得られる５０００個が必要である。さらに製造時の欠陥や、温度差が２度をわずかに下回った場合を考えると５５００個程度必要である。ここで温度差を２度としたのは、本発明の熱電素子を電子腕時計に搭載した場合、得られる温度差が実験により２度程度であったためである。

【００１３】一般のＩＣの動作電圧の実力値を０．７ｖとし、電子機器例えば電子腕時計に搭載する場合には外観上の制約があるためｎ型半導体およびｐ型半導体の厚さは図５より０．２㎜以上３㎜以下とする事が望ましい。さらに望ましくは、一般のＩＣの動作電圧の規格値を１．２ｖとし、より大きな電圧を得ようとした場合ｎ型半導体およびｐ型半導体の厚さの増加に対する出力電圧の増加率が１０％以上であることが効率を考えた上で好ましいので、ｎ型半導体およびｐ型半導体の厚さは図５より０．５㎜以上２㎜以下とする事が望ましい。例えばｎ型半導体およびｐ型半導体の断面積が０．０１㎟、厚さが１㎜、数がｎ型ｐ型合わせて５０００個、ｎ型半導体とｐ型半導体の間隔を約０．２㎜、放熱側及び吸熱側の電極と絶縁板を合わせた厚さがそれぞれ１㎜であるとすると、熱電素子の大きさは全体で約１５㎜×１５㎜×３㎜となり、２度の温度差が与えられた場合約１．４Ｖの起電力を得ることが可能である。

【００１４】図６は、本発明の熱電素子を動力源として用いた電子機器の一実施例として、電子腕時計の動作原理を示すブロック図である。熱電素子６０１に温度差が与えられ起電力が発生すると充電制御回路６０２を介して蓄電素子６０３に電気が蓄えられる。蓄電素子６０３に蓄えられた電気により駆動制御回路６０４が駆動し、表示機構６０５に時刻が表示される。

【００１５】図７は、本発明の電子腕時計の実施例の外観を示す図である。放熱されやすいように放熱板７０１が表面に露出している。放熱板７０１は、例えばシリコンで構成されている。図８は、本発明の電子腕時計の実施例の構造を示す断面図である。絶縁板８０１は一般に気温よりも高温である腕に触れるために吸熱側、絶縁板８０２は大気中にあるために放熱側となる。絶縁板８０１および８０２は、例えばシリコンで構成されている。例えば携帯者の体温が摂氏３６度で、気温摂氏２０度の環境にて使用し電子腕時計全体が腕の温度に近くなると、絶縁板８０１と絶縁板８０２との間に生じる温度差は２度前後である。温度差が生じると、熱は絶縁板８０１からｎ型およびｐ型半導体８０３を通り絶縁板８０２

5

に伝えられ大気中に放熱される。このときゼーベック効果により起電力が生じ蓄電素子８０４、例えばリチウム２次電池、カーボンーリチウム２次電池、あるいはバナジウムーリチウム２次電池に蓄電される。この蓄えられた電気により輪列とモーターから成り運針動作を行うムーブメント８０５が駆動する。

【００１６】

【発明の効果】以上述べてきたように本発明によれば、絶縁体にシリコンを用いた熱電素子のｎ型、ｐ型半導体の厚さを０．２～３㎜、さらに望ましくは０．５～２㎜とする事により、必要とする起電力を得るための熱電素子としては発電効率が良くかつ小型化されたものを得ることができる。さらにこの熱電素子を電子機器に用いることにより、電子機器を小型化することが可能になる。

【図面の簡単な説明】

【図１】本発明の第一の熱電素子の構造と発電原理を示す図である。

【図２】本発明の第二の熱電素子の構造と発電原理を示す図である。

【図３】本発明の熱電素子をエネルギー源として用いた電子機器の動作原理を示すブロック図である。

【図４】本発明の熱電素子の実施例の構造と発電原理を示す図である。

【図５】本発明の熱電素子の半導体数の違いによる半導体の厚さと出力電圧の関係を示す図である。

【図６】本発明の熱電素子を動力源として用いた電子機器の一実施例として、電子腕時計の動作原理を示すブロック図である。

【図７】本発明の一実施例の電子腕時計の外観を示す図

6

である。

【図８】本発明の一実施例の電子腕時計の構造を示す断面図である。

【図９】従来の熱電素子の構造と発電原理を示す図である。

【図１０】熱電素子を動力源として用いた従来の電子腕時計の構造を示す断面図である。

【符号の説明】

１０１、４０１　第一の絶縁体
１０２、４０２　第二の絶縁体
１０３　ｎ型半導体
１０４　ｐ型半導体
１０５　接続部
１０６　出力端子部
２０３　ｎ型半導体複合素子
２０４　ｐ型半導体複合素子
３０１、６０１　熱電素子
３０２　蓄電機構
３０３　駆動機構
３０４　動作、表示機構
４０７、、６０３、８０４　蓄電素子
６０２　充電制御回路
６０４　駆動制御回路
６０５　表示機構
７０１　放熱板
８０１、８０２　絶縁板
８０３　ｎ型およびｐ型半導体
８０５　ムーブメント

【図３】

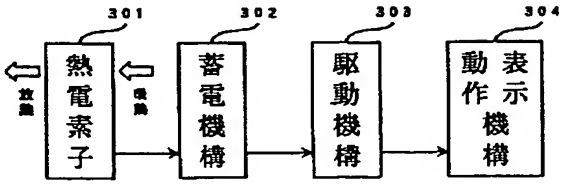

【図７】

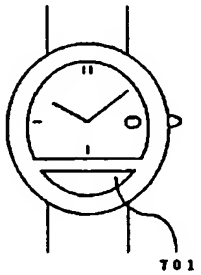

【図６】

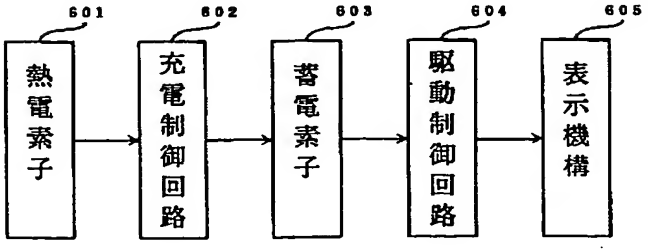

【図１】

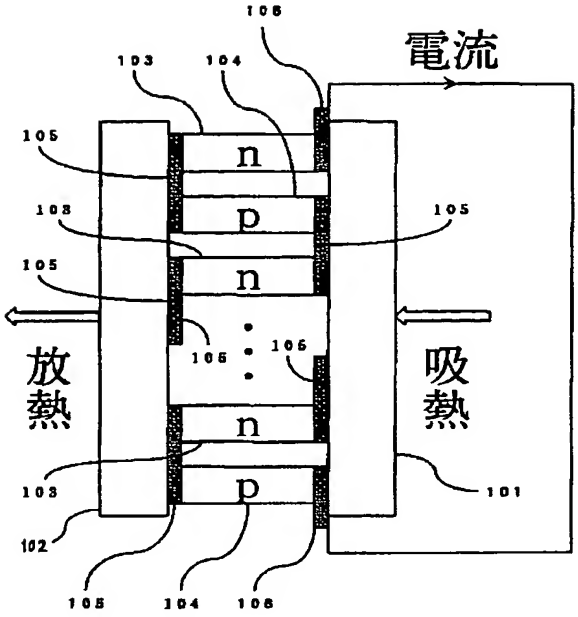

【図２】

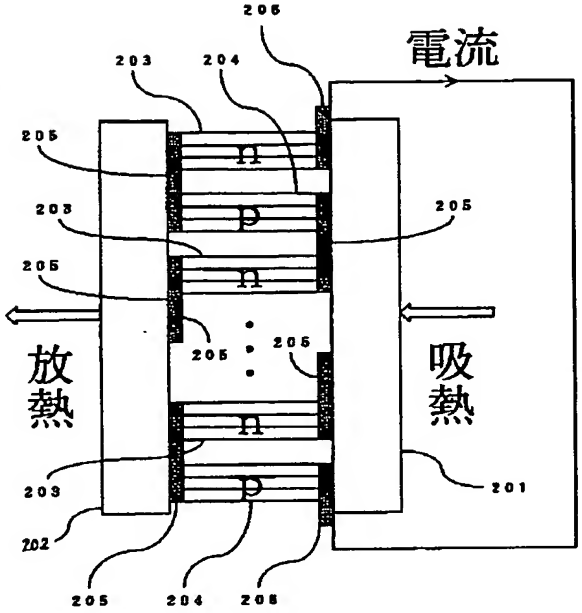

【図４】

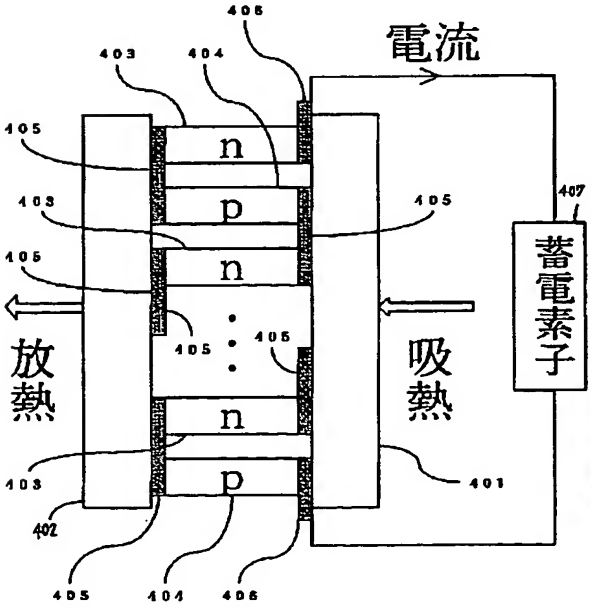

【図８】

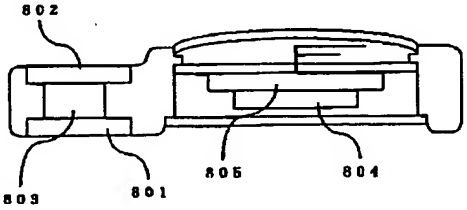

【図１０】

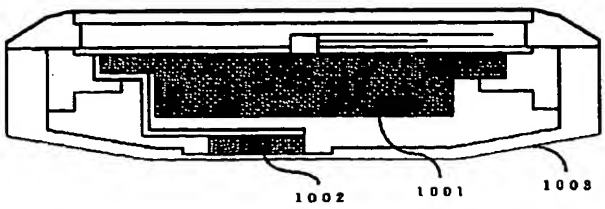

【図５】

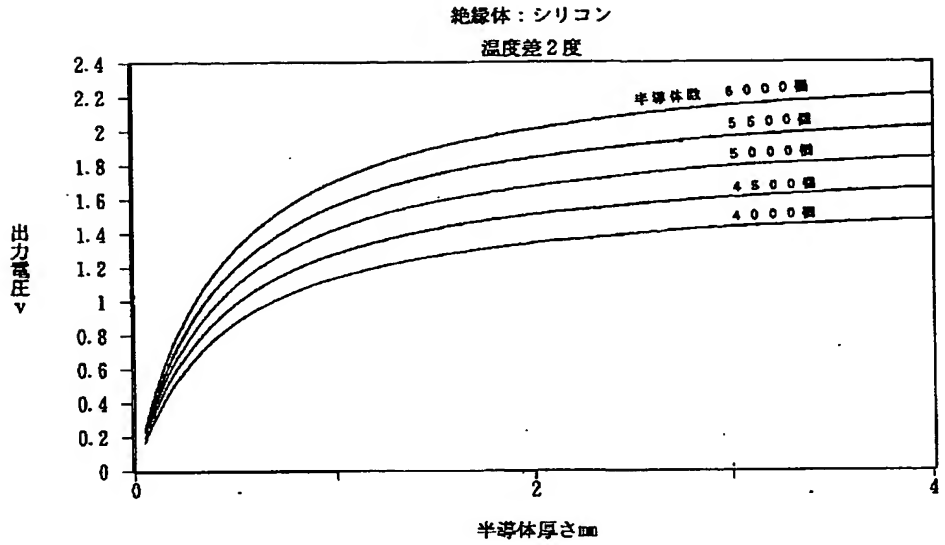
絶縁体：シリコン
温度差２度
出力電圧V
2.4
2.2
2
1.8
1.6
1.4
1.2
1
0.8
0.6
0.4
0.2
0
0
2
4
半導体厚さmm
半導体数　６０００個
５５００個
５０００個
４５００個
４０００個

【図９】

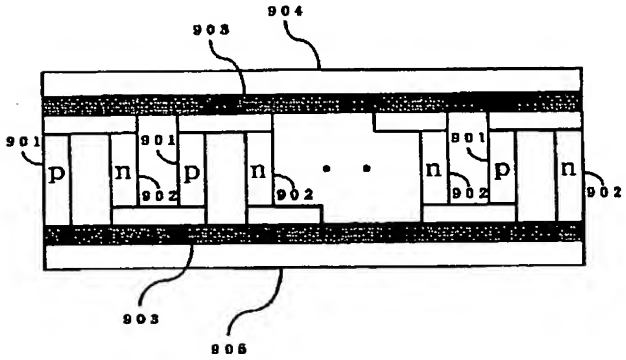
904
903
901
901
901
p
n
p
n
n
p
n
902
902
902
902
903
905

J. Phys.: Condens. Matter 10 (1998) 1013–1032. Printed in the UK PII: S0953-8984(98)82516-2

Crossover from semiconductor to magnetic metal in semi-Heusler phases as a function of valence electron concentration

J Tobołaţ, J Pierre‡, S Kaprzykţ, R V Skolozdra§ and M A Kouacou‡

ţ Faculty of Physics and Nuclear Techniques, Academy of Mining and Metallurgy, alica Mickiewicza 30, 30-059 Kraków, Poland

‡ Laboratoire de Magnetisme L Néel, CNRS, 166X, 38042 Grenoble, France

§ Chemistry Department, I Franko University, Lviv 290005, Ukraine

Received 10 March 1997, in final form 4 November 1997

Abstract. Experimental and theoretical investigations of intermetallic semi-Heusler compounds (CoTiSn, FeTiSb, CoTiSb, NiTiSn, CoNbSn, CoVSb, NiTiSb) and their solid solutions ($CoTiSn_{1-x}Sb_x$, $CoTi_{1-x}Nb_xSn$) are presented. The physical properties of these systems are found to be mostly determined by the number of valence electrons. Resistivity experiments show that compounds with 18 valence electrons are either semiconductors (CoTiSb, NiTiSn) or semi-metals (CoNbSn). The electronic structure calculations performed on 18-valence-electron systems by the KKR method show nine valence bands below the Fermi level and a gap of order 0.4–0.9 eV. A decrease or increase of the number of valence electrons in CoTiSb, NiTiSn or CoNbSn leads in either case to a metallic state and either ferromagnetic (CoTiSn, CoVSb) or paramagnetic (FeTiSb, NiTiSb) properties. The KKR results concerning 17- and 19-valence-electron systems correspond well with experimental characteristics, except in the case of CoVSb which KKR calculations predict to be a half-metallic ferromagnet, which conflicts with experimental data.

Magnetization and resistivity measurements indicate that semiconductor–metal crossovers occur together with the appearance of ferromagnetism in the $CoTiSn_{1-x}Sb_x$ and $Co_{1-x}Ni_xTiSn$ series, for x near 0.4. This behaviour is discussed in the context of the KKR-CPA results.

1. Introduction

Heusler phases are well known ternary intermetallic compounds, with general formula X_2YZ, where X and Y are transition metals and Z is an sp element. Semi-Heusler phases have the same cubic structure, except that one of the X sites is empty, giving a formula XYZ. Due to the vacant site, the overlap between the d wave-functions is smaller, which gives rise to narrower bands and to the appearance of gaps in the energy spectra. This family of compounds attracted wide interest after the discovery for the NiMnSb and PtMnSb ferromagnets [1, 2] of peculiar electronic structure properties, collectively known as half-metallic ferromagnetism. The half-metallic character arises from the magnetic splitting of the bands, which leads to the occurrence of an energy gap at E_F for down-spin electrons, together with a metallic state for up-spin electrons [3, 4].

In this paper we focus on the physical properties of some XYZ compounds, where the transport and magnetic properties are governed by the number of valence electrons (EC). Compounds such as NiTiSn, CoTiSb with EC = 18 were found to be semiconductors (SC) [5, 6]. In the following, we consider how the electronic and magnetic properties are modified

0953-8984/98/051013+20$19.50

on passing to EC = 19 and EC = 17 systems, by adding (removing) one electron to (from) the different crystallographic sites. We shall see how a crossover from a semiconducting to a metallic state occurs, and how it may be related to the onset of weak ferromagnetism.

Measurements of resistivity and magnetization, as well as band-structure calculations by the Korringa–Kohn–Rostoker (KKR) method, were performed for the following ordered samples: CoTiSn, FeTiSb, CoTiSb, NiTiSn, CoNbSn, CoVSb and NiTiSb. Recently [6, 7], insulator–metal crossovers related to the onset of ferromagnetic ordering were detected in $Co_{1-x}Ni_xTiSn$ and $CoTiSn_{1-x}Sb_x$ solid solutions for x near 0.4. However, the concentration dependencies of the magnetic moments and Curie temperatures are not the same in these two series. In this paper the new series of solutions $CoTi_{1-x}Nb_xSn$ is also described, where the substitution is at the Y site, and compared with the previous $Co_{1-x}Ni_xTiSn$ and $CoTiSn_{1-x}Sb_x$ series. As will be shown, the variations of the physical properties with concentration are again different, as it is not equivalent to add one electron to the X site (filling the d shell of Co), to the Y site (enhancing the density of d states at this site), or to the Z site. In order to get a deeper insight into the influence of alloying on electronic structure, band-structure calculations were performed for the above-mentioned alloys using the KKR method with the coherent potential approximation (CPA). As far as possible, the ground-state KKR-CPA results will be compared to observed properties, and some interpretations will be proposed for these series concerning insulator–metal transitions and the onset of ferromagnetism.

Table 1. The lattice parameter (at RT), Curie and Curie–Weiss temperatures, spontaneous magnetization at 0 K and effective paramagnetic moment (per Co/Fe atom), or constant paramagnetic susceptibility (emu mol^{-1}) for XYZ semi-Heusler compounds. The crystallographic positions of inequivalent atoms in the unit cell can be easily derived, since the chemical formula is written as XYZ, where X is at (0, 0, 0), Y is at (1/4, 1/4, 1/4) and Z is at (3/4, 3/4, 3/4) in the unit cell.

Compound XYZ	a (Å)	T_C (K)	$M(0)$ (μ_B)	θ_p (K)	μ_{eff}	$10^4\chi_p$
CoTiSn	5.997	135	0.357	176	1.35	—
CoTiSb	5.884	—	—	—	—	1.7
CoNbSn	5.947	—	—	—	—	0.53
NiTiSn	5.941	—	—	—	—	1.3
CoVSb	5.791	58	0.18	75	1.26	0
NiTiSb	5.872	—	—	—	—	1.4

2. Crystallography and physical properties

Let us first describe some structural aspects of Heusler systems. The unit cell of the true Heusler X_2YZ structure (space group: $Fm\bar{3}m$) consists of four inter-penetrating f.c.c. sublattices. If one of the two equivalent sites (0, 0, 0) or (1/2, 1/2, 1/2) (here, occupied by X atoms) is empty, the semi-Heusler XYZ structure (space group: $F\bar{4}3m$) appears [5, 8]. As we see from table 1, d atoms occupy X and Y sites, while metalloids are located at Z positions. The smallest d metal generally occupies the site (0, 0, 0) related to the vacancy site (1/2, 1/2, 1/2). The XYZ systems are far from compact, and thus are subject to lattice instabilities. From a chemical point of view, they can be stabilized only through covalent bonding. Thus they are encountered when Z = Sn or Sb, and then only within a restricted range of peripheral electron number. The ideal valence electron concentration (EC) is 8 or 18 electrons per formula unit, which corresponds to AgMgAs, NiTiSn, ZrNiSn,

CoTiSb, CoNbSn, etc. It leads to the formation of tetrahedral bonds and sp^3 hybridization around the p element and favours bonding between d metals. Semiconducting properties occur for EC = 18 for some of the above-mentioned compounds, and disappear for other values of EC.

As always for Heusler compounds, the physical properties are strongly dependent on the crystallographic order. Disorder generally occurs between d metals, the more so the closer they are in the periodic table. Some atoms may also occupy a vacancy site. For these reasons, all of the samples investigated in the present work were annealed for a long time (one week to one month) at temperatures between 650 and 800 °C. Nevertheless, some atomic disorder is still observed. It is not possible for instance to obtain intrinsic semiconductors in these systems and band gaps cannot be determined properly from transport experiments below 300 K. Similarly, the residual resistivity of metallic phases remains significant.

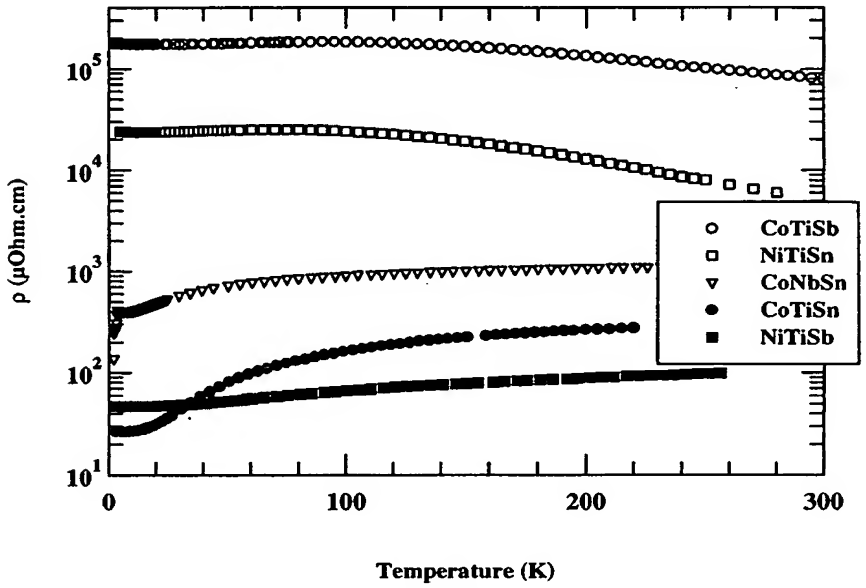

Figure 1. The resistivity for some semi-Heusler compounds.

2.1. The $Co_{1-x}Ni_xTiSn$ series

This series has already been described in previous papers [5, 6]. Here, we recall its basic properties. NiTiSn is a narrow-gap semiconductor (E_g = 0.42 eV according to the KKR calculations [9]). Resistivity measurements show that the intrinsic regime is probably not reached even at room temperature. The experimental gap deduced between 200 and 300 K is only 80 meV, much smaller than calculated. This value may be representative of the activation energy of donor or acceptor levels (figure 1). The susceptibility is nearly constant between 15 and 300 K ($\chi = 1.3 \times 10^{-4}$ emu mol^{-1}) (see table 1). Replacing Ni by Co leads first to the narrowing of the gap, then to metallic conduction and finally to the appearance of weak ferromagnetism for a Co (or hole) concentration of about 0.45. No sharp transition occurs between the SC and metallic phases. The limit between semiconducting and metal-

like behaviours was somewhat arbitrarily set to be the concentration at which the temperature derivative of the resistivity changes from negative to positive, or where the low-temperature resistivity is of the order of the (now historical) Mott limit for metallic resistivity, i.e. a few mΩ cm.

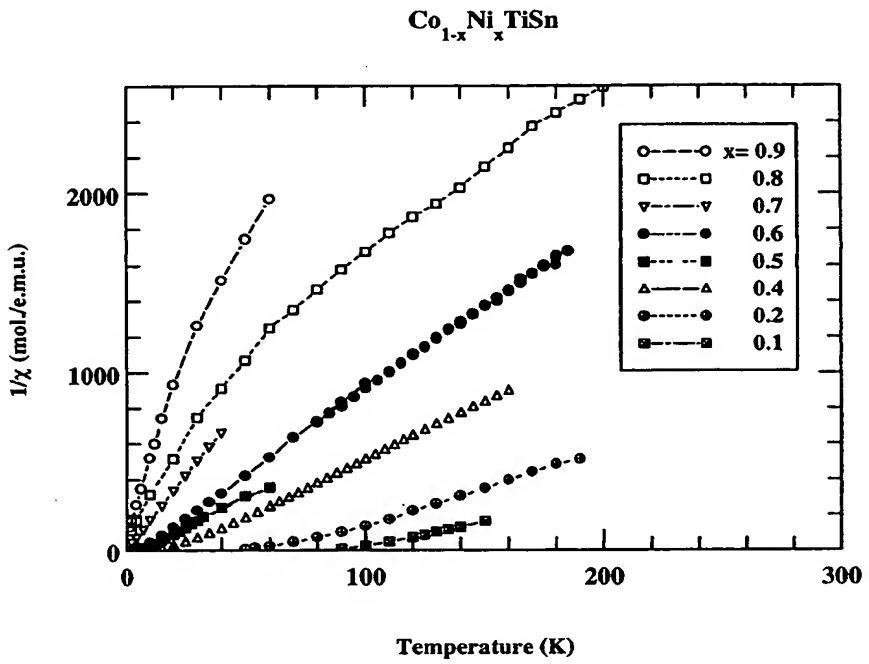

Figure 2. Reciprocal susceptibilities for the $Co_{1-x}Ni_xTiSn$ series.

CoTiSn is a weak ferromagnet, ordering at $T_C = 135$ K, with a moment at low temperature of $M(0) = 0.35\ \mu_B$ (table 2). Co atoms retain a localized moment when diluted in NiTiSn, as shown by the susceptibility of the solutions (figure 2), which exhibit both Curie–Weiss-like and temperature-independent contributions: $\chi = (1-x)C/T + \chi_0$. The Curie constant C per Co ion gives an effective (paramagnetic) moment of Co close to 1.1 μ_B, a value similar to that for pure CoTiSn (1.35 μ_B). Thus the Co paramagnetic moment localizes without a significant change in magnitude when diluted in NiTiSn. In the ferromagnetic range, T_C scales as $M(0)^{1.7}$, which is close to the quadratic behaviour generally observed for localized systems.

2.2. The $CoTiSn_{1-x}Sb_x$ series

Experimental results for this series have already been partly described elsewhere [10]. In this series the solid solution is not continuous: the lattice parameter first decreases regularly on adding Sb up to $x = 0.5$, the phases being metallic. A two-phase region, with two cubic Heusler phases, exists between $x = 0.5$ and $x = 0.6$, then the second semiconducting phase with the smaller lattice parameter continues up to the compound CoTiSb. The SC phase is more compact, which should be ascribed to the bonding mechanism and to the distribution of valence electrons. This SC–metal crossover cannot be a classical Mott transition, since

the SC phase here has a smaller volume than the metallic one and is not magnetically ordered.

The Sn-rich phases order ferromagnetically for $x < 0.5$, but the solutions turn paramagnetic for larger Sb contents. The susceptibility behaviour changes from Curie–Weiss-like in the ferromagnetic range, with an effective moment per Co proportional to the Sn content, to the characteristic behaviour of enhanced paramagnets, with a maximum value in the range 50 to 100 K (figure 3) for SC solutions. A nearly constant susceptibility $\chi = 1.7 \times 10^{-4}$ emu mol^{-1} is observed for the CoTiSb, a result which is close to that ($\chi = 1.14 \times 10^{-4}$ emu mol^{-1}) obtained by Terada *et al* [11]. The magnetic susceptibility of this series as a function of concentration behaves like that of $ZrZn_2$ under pressure [12]. In the ferromagnetic range, T_C is proportional to $M(0)$, a behaviour which was also observed in the metallic solutions between Co_2TiSn and Ni_2TiSn [13].

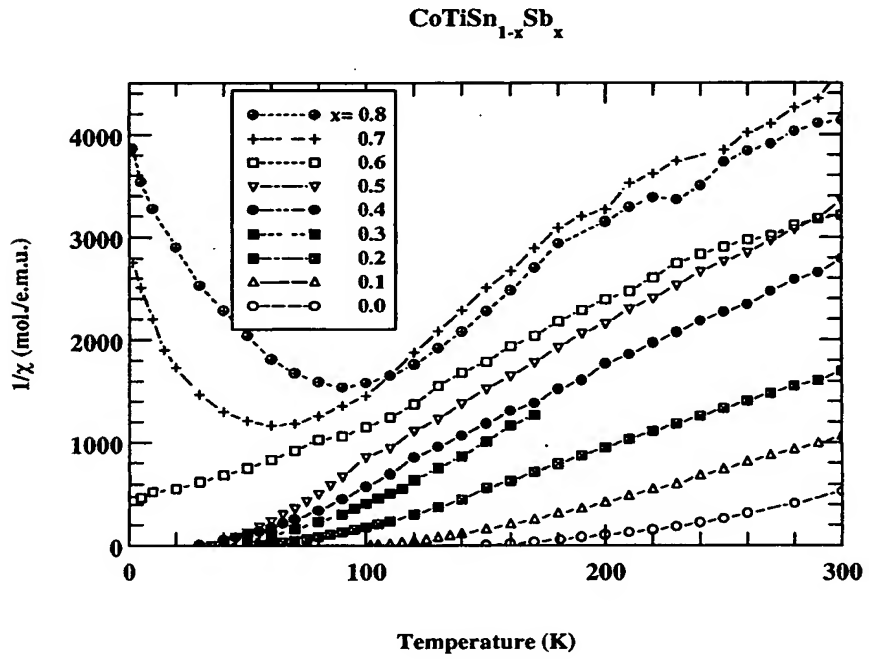

Figure 3. Reciprocal susceptibilities for the $CoTiSn_{1-x}Sb_x$ series.

The resistivity curves of the solutions have a complex behaviour [10]: in the metallic range, the magnetic part of the resistivity becomes larger and larger as the concentration approaches the magnetic–non-magnetic boundary, giving a large T^2-term at low temperature; the S shape of the resistivity is typical of spin fluctuations. For $x > 0.6$, the SC behaviour is recovered.

Thus striking differences are observed between the $CoTiSn_{1-x}Sb_x$ and the $Co_{1-x}Ni_xTiSn$ series. A puzzling feature is that CoTiSb does not order magnetically, and does not even exhibit any localized magnetism (Curie–Weiss susceptibility) whereas Co atoms diluted in NiTiSn do so. A first interpretation would be that an extra electron added to the Z site can be transferred to Co and fills the d shell. We shall see below that this picture is not accurate, and that another interpretation should be given.

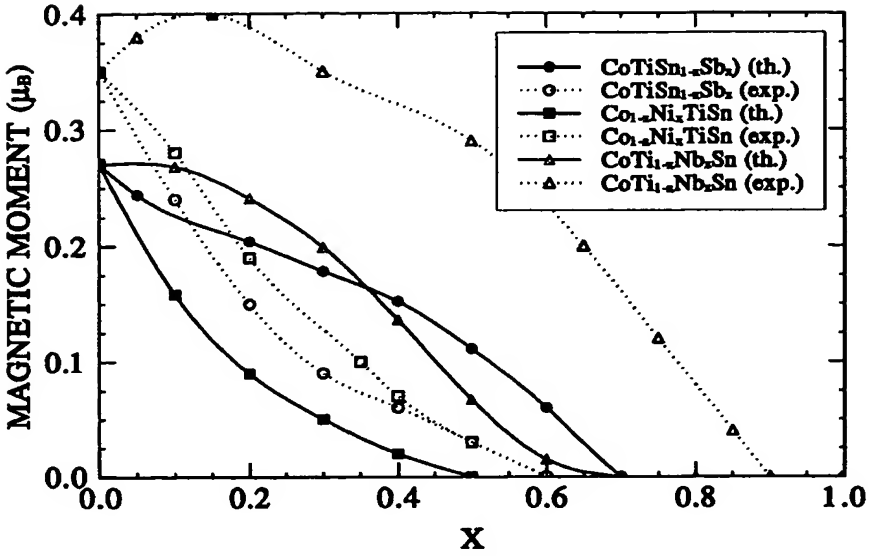

Figure 4. Total magnetic moment variations versus alloy compositions for three isoelectronic series: $Co_{1-x}Ni_xTiSn$ (squares), $CoTiSn_{1-x}Sb_x$ (circles) and $CoTi_{1-x}Nb_xSn$ (triangles). The measured and KKR-CPA points are linked by dotted and solid lines, respectively.

Table 2. Magnetic data for solutions in the $CoTi_{1-x}Nb_xSn$ series.

x (Nb)	T_C (K)	$M(0)$ (μ_B)	θ_p (K)	μ_{eff}
0	135	0.357	158	1.35
0.05	141	0.38	165	1.44
0.15	155	0.40	180	1.51
0.3	120	0.35	151	1.33
0.5	112	0.29	146	1.15
0.65	90	0.20	No CW	—
0.75	23	0.17	—	—
0.85	17	0.12	—	—
0.9	0	0	—	—
1.0	0	0	—	—

2.3. The $CoTi_{1-x}Nb_xSn$ series

A third way to change EC from 17 to 18 is to operate on the third crystallographic site, and to replace Ti by V or Nb. Nb was chosen, since the atomic size of V is smaller than that of either Ti and Nb. In this case, adding a 'd electron' to the Y site should enhance the density of states and correlations on this site. Indeed, the effective moment μ_{eff} per formula unit, θ_p, T_C and $M(0)$ all start to increase with Nb content (table 2, figure 4) up to $x = 0.15$. For $x > 0.15$ all of these quantities decrease, and the ferromagnetism disappears for x between 0.85 and 0.9. The susceptibility of CoNbSn (table 1) is nearly temperature independent and is lower than for other compounds with EC = 18, which may be due to the larger diamagnetic susceptibility of the 4d-metal core. For ferromagnetic samples, the square of the spontaneous magnetization $M(T)$ varies as T^2 for x lower than 0.3, but as

Table 3. The quantities from the band-structure calculations: energy gap E_g, total number of electrons (N_X, N_Y and N_Z), number of d states ($N_{X,d}$, $N_{Y,d}$) inside muffin-tin spheres as well as magnetic moments per formula unit.

Compound	E_g (eV)	N_X	N_Y	N_Z	$N_{X,d}$	$N_{Y,d}$	M (μ_B)
CoTiSn		26.68	20.36	47.83	7.56	1.87	0.28
FeTiSb		25.57	20.38	48.61	6.53	1.96	0.78
CoTiSb	0.95	26.64	20.34	48.52	7.51	1.93	
CoNbSn	0.4–0.6	26.74	38.72	47.82	7.54	2.51	
NbCoSn		39.19	26.42	48.04	2.86	7.44	
NiTiSn	0.42	27.73	20.34	47.87	8.50	1.94	
CoVSb		26.61	21.50	48.41	7.48	2.95	1.00
NiTiSb		27.70	20.33	48.44	8.48	1.96	0.0

$T^{4/3}$ for larger x. This last behaviour was already predicted by Moriya and Kawabata [14] and Lonzarich and Taillefer [15], and attributed to the fluctuations of the order parameter close to the magnetic–non-magnetic crossover.

The resistivity measurements indicate that the metallic character is maintained throughout the series, although the resistivity is much higher for CoNbSn than for metallic CoTiSn or NiTiSb (figure 1). The behaviour observed for CoNbSn implies either a semi-metallic state with a low density of states, or a large atomic disorder which prevents a true semiconducting behaviour. Several CoNbSn samples have been prepared, but even the best one (shown in the figure 1) has a superconducting transition at 3.5 K, a transition temperature which is close to that of Sn. It is probable that some Sn filaments exist between grains and that the stoichiometry of the Heusler phase is not exact. The presence of this spurious phase (undetected by x-rays) may thus explain the metallic-like shape of the resistivity, due to the short-circuit of the primary CoNbSn phase. It may be due to the large difference between the melting points of Sn and Nb, although Co and Nb were first melted together to produce a eutectic with a lower melting point.

Band-structure calculations (see below) show that the inversion of Nb and Co atoms gives rise to a semi-metallic phase instead of a SC one.

2.4. Summary of the experimental results and other compounds

The variation of the ordered magnetic moment $M(0)$ in the three series is plotted in figure 4 as a function of the concentration x (or versus the valence electron number: $17 < EC < 18$). $M(0)$ decreases continuously and almost at the same rate in the $Co_{1-x}Ni_xTiSn$ and $CoTiSn_{1-x}Sb_x$ series, and the ferromagnetic state disappears for x close to 0.6 (EC = 17.6). For the $CoTi_{1-x}Nb_xSn$ series, the magnetization and the Curie temperature first increase as a function of EC, and then drop to zero for EC close to 17.9. As previously mentioned, the last feature is due to the increase in the d DOS at the Y site which reinforces the magnetic interactions.

Compounds like NiTiSb and CoVSb have 19 valence electrons, and thus a reappearance of metallic conduction may be expected. The magnetic properties of these systems have been investigated by Terada *et al* [11]. NiTiSb is a Pauli paramagnet, with $\chi = 1.56 \times 10^{-4}$ emu mol^{-1} as deduced from measurements between 25 and 250 K ($\chi = 1.37 \times 10^{-4}$ emu mol^{-1} from reference [11]). Resistivity measurements show that this compound is a normal metal. The Debye temperature obtained by a Bloch–Grüneisen fit is estimated to be 220 ± 20 K.

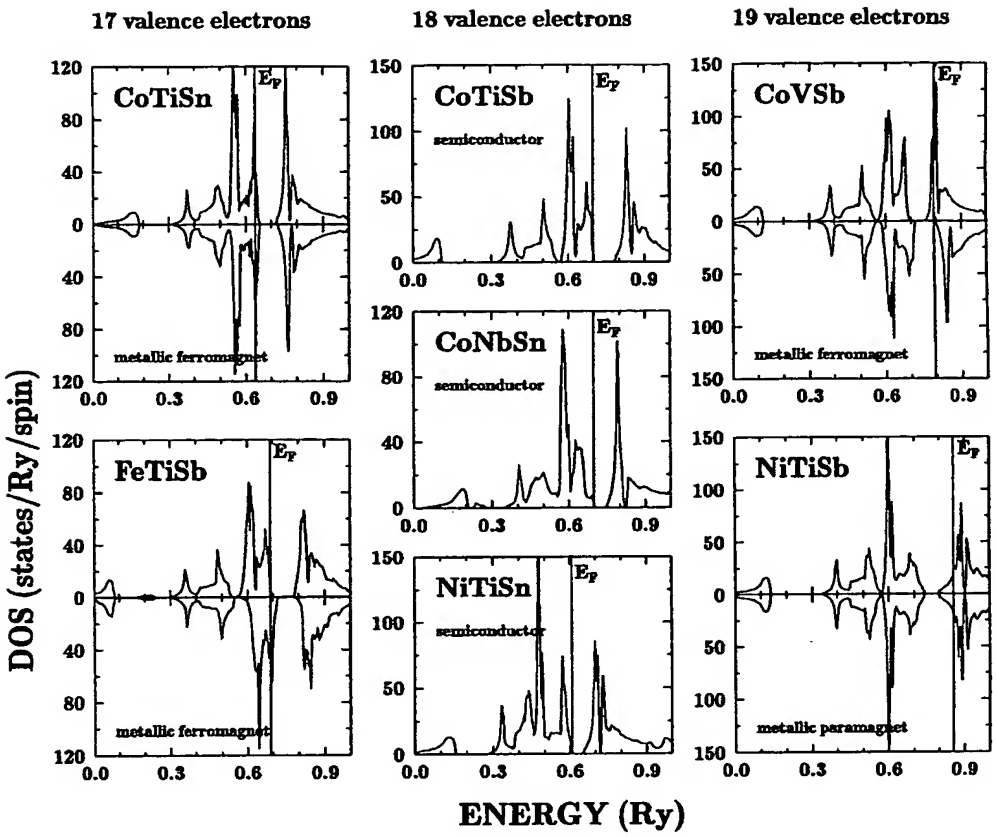

Figure 5. Total densities-of-states spectra of semi-Heusler compounds with various numbers of valence electrons (EC). Each column represents isoelectronic systems. CoTiSn and FeTiSb (EC = 17) are metals, CoTiSb, CoNbSn and NiTiSn (EC = 18) are semiconductors, while CoVSb and NiTiSb (EC = 19) are again metals.

CoVSb is a weak ferromagnet, with $M(0) = 0.18\ \mu_B$, and $T_C = 58$ K [11]. Its effective paramagnetic moment is $1.26\ \mu_B$, close to the values found for CoTiSn and Co diluted in NiTiSn. As for CoTiSn, a fairly large ratio of the paramagnetic to the ferromagnetic moment is observed, which is typical of weak itinerant systems. Finally we observed that FeTiSb (EC = 17) is metallic and exhibits a Curie-like behaviour at low temperatures, but without magnetic order down to 1.5 K.

3. Band-structure studies

We have implemented fully charge and spin self-consistent KKR calculations for CoTiSn, FeTiSb, CoTiSb, CoNbSn, NiTiSn, CoVSb and NiTiSb ordered systems. The computations for $CoTiSn_{1-x}Sb_x$ and $CoTi_{1-x}Nb_xSn$ and the previous ones [9] for $Co_{1-x}Ni_xTiSn$ (with $x = 0.0, \ldots, 1.0$) solid solutions were performed by the KKR-CPA method [16–19]. For compounds as well as for alloys, muffin-tin potentials were constructed within the local spin-density (LSD) approach, using the exchange–correlation part of the von Barth–Hedin

formula [20]. The KKR-CPA self-consistency cycles were repeated for each composition until the difference between input and output potentials was less than 1 mRyd. For the final muffin-tin potentials, the total density of states (DOS), the site-decomposed densities of states (CDOS) and l-decomposed (with $l_{max} = 2$) partial densities of states (PDOS) were computed on a 201-energy-point mesh for the alloys and on a 601-point mesh for the compounds. The integration in k-space was performed using 192 small tetrahedra in (1/48)th of the Brillouin zone, applying the method described in reference [21]. The KKR-CPA code contains the generalized Lloyd formula which permits the precise determination of the Fermi energy, using an elliptic contour in the complex energy plane. In our computations the contour contained 48 energy points and the CPA Green function was computed on a mesh of 75 special k-points in the irreducible part of the BZ for each of the 48 above-mentioned energy points.

In our calculations the experimental lattice constants were generally used. The KKR-CPA calculations for disordered $CoTiSn_{1-x}Sb_x$ were performed with lattice constants corresponding to the values of CoTiSn and CoTiSb compounds successively. This allowed the influence of the lattice parameter to be checked on the electronic structure, an important feature in this case due to the discontinuity of the solid solution. In the $CoTi_{1-x}Nb_xSn$ series the variation of the cell parameter is quite small (table 1). An empty sphere was added at the (1/2, 1/2, 1/2) position in order to improve the filling factor of the WS cell for filling by non-overlapping muffin-tin spheres (for semi-Heusler systems, when using equal radii, this factor is less than 50%; it increases to 68% on adding extra spheres). The radius $r_{mt} = \frac{\sqrt{3}}{8}a$ was chosen for all non-equivalent atoms in the WS cell, although some numerical trials were done for the CoTiSn compound using various muffin-tin radii for Co, Ti and Sn atoms.

The electronic structure of the end-point compounds was also computed using the KKR-CPA code. Such calculations allow the results obtained by the two methods to be compared and show the DOS characteristics for a vanishing or near-vanishing concentration of one dopant. The limit cases ($x = 0$ and $x = 1$) mean that from the KKR-CPA calculations one may recover for instance the DOS of the Nb atom (one-impurity properties) diluted in the pure CoTiSn, i.e. the $CoTi_{1-x}Nb_xSn$ ($x = 0$) case.

The electronic structure of the present semi-Heusler systems is roughly divided into three groups, according to the number of valence electrons (17-, 18- and 19-electron systems). Figure 5 is a kind of phase diagram, which illustrates the electronic structure of systems and their corresponding ground-state properties. CoTiSn and FeTiSb (EC = 17) are found to be metallic ferromagnets, CoTiSb, CoNbSn and NiTiSn (EC = 18) semiconductors, while NiTiSb and CoVSb (EC = 19) are again metals in the paramagnetic and ferromagnetic state, respectively. From a brief comparison we observe that, even for isoelectronic compounds, the magnetic and transport properties strongly depend on the constituent atoms and their crystallographic positions. From the set of pictures in figure 5, we can easily draw all possible 'paths' between the ordered systems, guessing properties of possible solid solutions. Nevertheless, as observed in our experiments, some phase diagrams do not show a continuous solution. In this paper we focus on the series of solid solutions $CoTiSn_{1-x}Sb_x$ and $CoTi_{1-x}Nb_xSn$, which seem the most attractive for our purposes. The $CoV_{1-x}Ti_xSb$ series has not yet been investigated experimentally and will not be presented in this paper.

3.1. CoTiSn and FeTiSb

The spin-projected DOS picture for CoTiSn (the top-left-hand panel in figure 5, also in reference [9]) shows a weak polarization corresponding to a magnetic moment of about

0.28 μ_B per formula, which is mainly localized on the Co site (0.15 μ_B inside the muffin-tin sphere). The conduction band is formed essentially from d states of Co with some admixture of Sn p states and Ti d states, but part of them are observed above a gap. The DOS for spin up abruptly decreases in the vicinity of the Fermi level, whereas for spin down E_F falls almost precisely at a peak of the DOS. Electronic structure calculations close to the SC–metal limit and close to the magnetic instability are highly sensitive to the determination of the Fermi level. The DOS spectra for CoTiSn (the left-hand column in figure 5) and the position of E_F are deduced from the KKR-CPA method (using the generalized Lloyd formula, when determining E_F). The KKR computations of ordered CoTiSn show stronger polarization of bands and result in magnetic moments both on Co (0.41 μ_B) and Ti (0.30 μ_B) atoms. As stated above, the relevant KKR-CPA calculations for CoTiSn show the magnetization to be of order 0.3 μ_B, mainly due to the magnetic moments at Co sites. Recently, the electronic structure calculations have been performed for the Co_2TiSn and Co_2TiAl Heusler systems with the use of the FP-LAPW and the ASW-ASA methods [22]. The comparison shows that the full-potential LAPW computations lead to a total magnetic moment in agreement with experiment in contrast to the ASW-ASA method, which gives non-magnetic ground states for these systems. This result may be influenced by the use of overlapping spheres (ASA) around atoms, which probably cancel some spin-density contributions. The calculations presented in this paper (using muffin-tin potentials inside non-ovelapping spheres) indicate that CoTiSn and Co_2TiSn [9] are weak ferromagnets with the total magnetic moments 0.28 μ_B and 0.90 μ_B (per Co atom) respectively. These values are close to the experimental data (0.35 and 0.96 μ_B [6]) and to the FP-LAPW results [22].

The electronic structure of FeTiSb (the left-hand column in figure 5) is presented for comparison with that of the isoelectronic CoTiSn. FeTiSb is found to be a metallic ferromagnet with a total magnetic moment per formula unit of 0.78 μ_B; the calculated local magnetic moments at the Fe(X) and Ti(Y) sites are 0.66 μ_B and 0.10 μ_B, respectively. As for CoTiSn, E_F lies at the peak of the spin-down DOS. When comparing the component DOS of these two systems (not drawn here), we notice that the d states of Ti more strongly contribute to the conduction band in the FeTiSb system, resulting among other things in a small magnetic moment on Ti. The integrated partial DOS of the Ti d shell up to E_F (table 2) exhibits a higher value for FeTiSb ($N_{Y=Ti,d} = 1.96$) than for CoTiSn ($N_{Y=Ti,d} = 1.86$). This compound indeed exhibits a Curie-like behaviour typical of local magnetic moments at low temperature, with a nearly vanishing Curie–Weiss temperature. However, no magnetic order was detected experimentally down to 1.5 K. As reported in reference [23], the refinement of the diffraction data for FeTiSb seems to show more complex crystallographic structure than the semi-Heusler one (a super-cell or disordered structure). When assuming a disorder on X sites within the X_2YZ-type structure, the KKR-CPA computations show a non-magnetic ground state of $(Fe_{0.5}E_{0.5})_2TiSb$ (E denotes a vacancy), in agreement with the present experiments.

3.2. CoTiSb, CoNbSn and NiTiSn

The KKR studies of semi-Heusler systems possessing 18 valence electrons show the presence of a semiconducting ground state. The basic difference between CoTiSb, NiTiSn and CoNbSn compounds concerns the value of the energy gap E_g, which is biggest (E_g = 0.95 eV) for CoTiSb (see table 2). As can be seen from the dispersion curves, bands for CoTiSb (figure 6) and NiTiSn [9] exhibit an indirect Γ–X gap, while E_g for CoNbSn appears between the W and X points in the Brillouin zone.

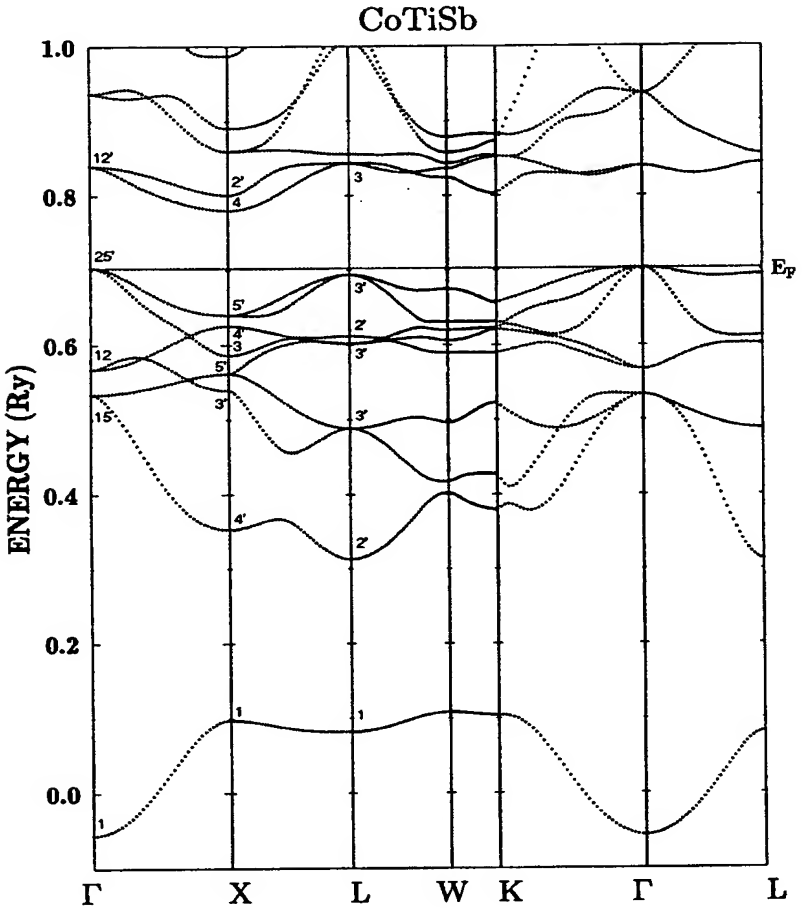

Figure 6. The dispersion curves along high-symmetry BZ directions in the semiconducting CoTiSb. The symmetry labels are assigned according to reference [28].

In this context we recall some limits of the LSD approach in the description of semiconductors. The value of the computed energy gap may be also modified when including the spin–orbit coupling, which is not considered in the present KKR calculations. We expect that upon inclusion of the spin–orbit interaction, the band gaps in semi-Heusler systems may be reduced by about 10–15%, as concluded in reference [24] with respect to the half-metallic PtMnSb.

On the other hand, transport measurements do not give reliable values for the gaps, due to the extrinsic character of the samples (at present, optical measurement results are not available for these systems). Nevertheless, the resistivity values for the three compounds vary in the same sense as the calculated values of the gap (see figure 1 and figure 5).

The CoNbSn compound is near the metal–SC limit, as observed in resistivity measurements. The band-structure studies give an energy gap E_g of the order of 0.4 eV (KKR-CPA) and 0.6 eV (KKR). The disagreement with experiment may arise from the disorder between Co and Nb sites: the KKR computations performed for NbCoSn with

inverted sites (Nb at the X site, while Co is at the Y site) give a semi-metallic state (table 3), with a small DOS at E_F (13 states Ryd^{-1}) mainly due to the Co d contribution.

Both for NiTiSn and for CoTiSb, a dominant character of the electrons (larger mobility, or more donor centres than acceptors) has been observed in the Hall effect. The larger electron mobility may be attributed to the curvature of the valence and conduction bands and to the threefold degeneracy of hole orbitals near the Γ point (the top of the valence band in figure 6), which limits the hole mobility.

For NiTiSn, the main DOS peaks below E_F are principally formed from Ni d states, while above the gap they are due to Ti d states. The situation observed for CoTiSb is slightly different. Here, the gap is two times larger; the electronic spectra deduced from KKR computations also differ from the DOS of NiTiSn. The d states of Co are separated by a gap, and only about 80% of the Co d states are filled below E_F. The main peak of the Co d PDOS is shifted to higher energies, relative to the Ni d PDOS for NiTiSn, due to Co possessing a less attractive potential than Ni. The exact position of the Co d PDOS peak relative to the Fermi energy is also slightly different for CoTiSb and CoNbSn. Moreover, the filling of the d shell of Co in CoNbSn ($N_{Y=Co,d} = 7.54$) is like that in CoTiSb ($N_{Y=Co,d} = 7.51$) (see table 3).

From the DOS spectra for the Y and Z sites in the above-mentioned systems (not drawn here), we see, that replacing Ti by Nb and Sb by Sn leads to a higher increase of d states below E_F than the corresponding decrease of p states at the Z site. Consequently, d states from X and Y sites in CoTiSb and CoTiSn are less hybridized than in CoNbSn.

In this comparison we cannot neglect the influence of the Z position on the formation of the energy gap. The degree of hybridization between d states at X and Y sites and p states at the Z site may control the value of the gap. As can be observed from the p PDOS at the Z site, the hybridization is stronger if Z = Sb than if Z = Sn. Thus CoTiSb (with higher electronegativity of Sb) has a wider E_g than NiTiSn and CoNbSn systems. Nevertheless, the d PDOS are very large on both sides of the gap, and hence its value may also be related to the splitting between bonding/anti-bonding wave-functions of transition metals (see the discussion).

3.3. NiTiSb and CoVSb

Adding one electron more to the semi-Heusler EC = 18 compounds, at either the X or the Z position, turns the system metallic, with only one conduction electron per formula unit. When the density of states at the Fermi level is sufficient, as in CoVSb, Stoner's criterion is met and a ferromagnetic ground state occurs. Calculations show that, surprisingly, the magnetization arises from vanadium atoms. This behaviour may be explained by the fact that E_F falls at a high peak of the d DOS for vanadium. The corresponding density for Co is significantly smaller, and thus the local Stoner criterion is not fulfilled.

Both KKR and KKR-CPA methods indicate that the bands are fully polarized; thus CoVSb should be a half-metallic system (the right-hand column in figure 5) with a magnetic moment per Wigner–Seitz cell equal to 1.00 μ_B. The calculated local magnetic moments on Co, V and Sb are found to be -0.02, 1.03 and -0.03 μ_B, respectively. However, this magnetization value is larger than that observed by Terada *et al* [11]. This disagreement may be due to the very rapidly varying DOS in this compound near E_F: from the total DOS for CoVSb, we also conclude that the half-metallic ferromagnetism here is linked to the highly localized conduction states (a large peak of the DOS at E_F). A different ground state may be favoured in a real system; thus an analysis of the total energy variation as a function of polarization should be undertaken. One other reason for the discrepancy

between experiment and theory may be the atomic disorder between Co and V atoms: V has a smaller radius than other 3d metals which occupy the Y sublattice. It is close to that of Co and this may permit greater disorder.

Now, passing to the NiTiSb system, we notice clearly that adding one electron at the X site (Co replaced by Ni) does not have the same effect as increasing the number of electrons at the Y site by replacing Ti by V. The electronic structure of NiTiSb (figure 5) shows striking differences when compared to that of CoVSb. Spin-polarized KKR computations indicate that the ground state of NiTiSb is non-magnetic. In contrast to the Co d states in CoVSb, the Ni d shell in NiTiSb is more or less filled (as in NiTiSn), and the states above the gap are formed with Ti d states. Due to a small value of the DOS at the Fermi level, neither Ni nor Ti atoms in NiTiSb retain magnetic moments. This result is in agreement with magnetization and resistivity measurements, which indicate vanishing magnetization and metallic character in NiTiSb.

3.4. $CoTiSn_{1-x}Sb_x$ and $CoTi_{1-x}Nb_xSn$ alloys

In this section we compare the electronic structure and magnetic properties derived from KKR-CPA computations for the isoelectronic series of alloys $CoTi_{1-x}Nb_xSn$ and $CoTiSn_{1-x}Sb_x$ (figure 7). In the $CoTi_{1-x}Nb_xSn$ series (the right-hand column in figure 7) an increase of valence electron number is brought about by substitution at the Y site by a d element from the next group in the periodic table (Nb), while in the $CoTiSn_{1-x}Sb_x$ series (the left-hand column in figure 7) it is effected by doping the Z site with Sb.

Due to the different origins of the electrons at the two substitution sites, we expect different behaviours of the electronic structure and magnetism for the series, upon alloying the parent compounds. The total magnetic moment (μ_{tot}) variations versus composition are presented in figure 4 for three series (the $Co_{1-x}Ni_xTiSn$ series was investigated in [9]). As in experiments, the variations of μ_{tot} (more or less proportional to μ_{Co}) change non-linearly in all cases. The alloy compositions for which ferromagnetic ordering disappears are also different for the different series. Taking into account the weak ferromagnetism in all of the samples investigated, the critical concentrations found from KKR-CPA calculations are not far from the experimental results. The starting value of 0.28 μ_B for the magnetic moment of CoTiSn at $x = 0$ also slightly differs from the experimental value (0.35 μ_B), which may modify $\mu_{tot}(x)$ dependencies.

First let us consider $CoTi_{1-x}Nb_xSn$ alloys. Here, an interesting observation concerns the concentration-dependent variation of the total magnetic moment, which exhibits a maximum in experiment and a plateau in the KKR-CPA calculations for Nb concentrations of about 0.1–0.2. This is related to an increase in the d states at Y sites, which generates a small induced magnetic moment at this site for $0 < x < 0.2$. It can be seen from the component DOS (the middle and right-hand columns in figure 8), which exhibits some polarization both at the Co site as well as at the Y site (mainly the Ti site) for $x < 0.3$. For higher Nb content, it is mainly the magnetic moment at the Co site that contributes to the total magnetization, which reaches zero for x-values of about 0.6–0.7. Surprisingly, both the gap between the conduction and valence bands in the $CoTi_{1-x}Nb_xSn$ series (the right-hand column in figure 7 and figure 8) and the exchange splitting become smaller as x increases.

For $x > 0.5$ the density of states at the Fermi level subsequently decreases, reaching zero for $x = 1.0$ (an energy gap of about 0.4 eV occurs). This is supported by resistivity measurements, which show an increase of the resistivity in Nb-rich $CoTi_{1-x}Nb_xSn$ samples although, experimentally, CoNbSn appears to be more or less semi-metallic (see section 2.3).

Crystallographic studies have shown that the solid solution was not continuous between

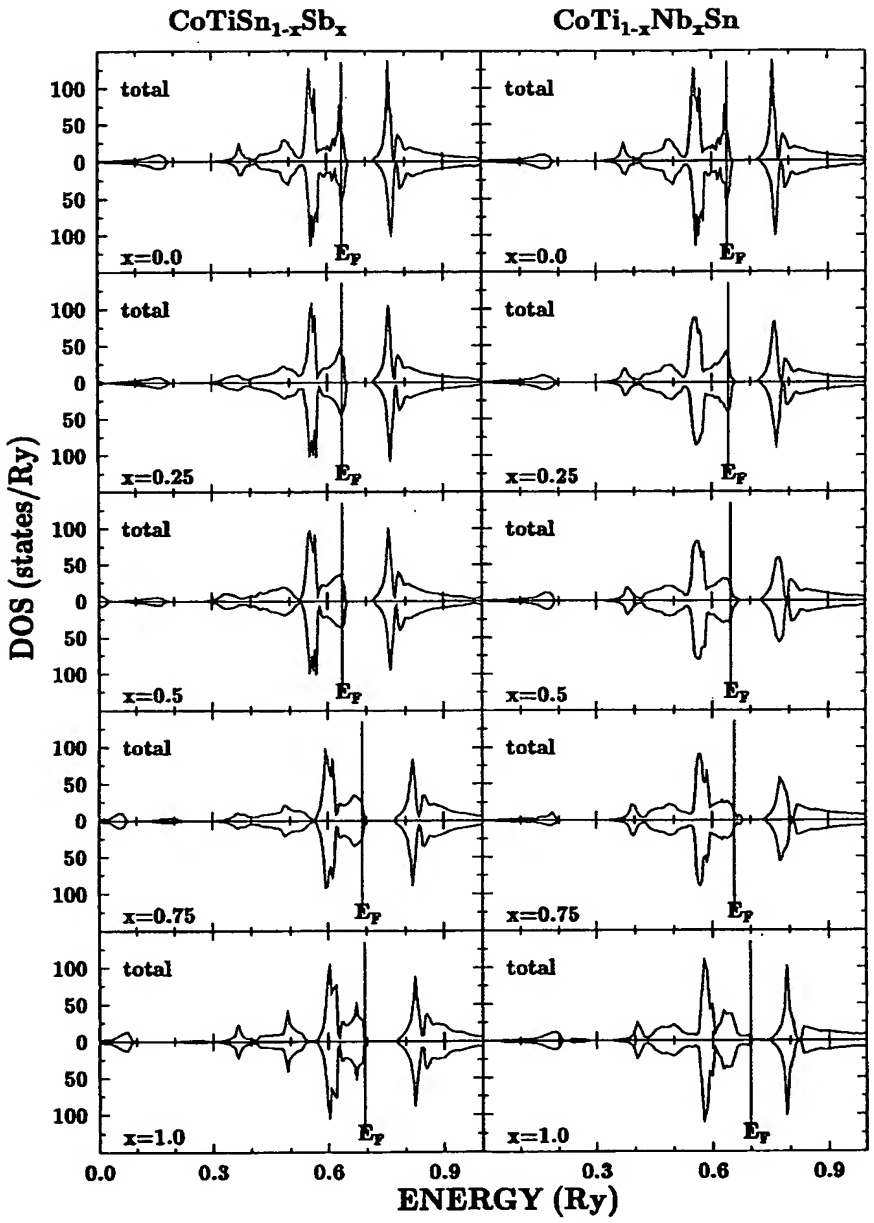

Figure 7. Total densities of states (from the KKR-CPA method) for two disordered series: $CoTi_{1-x}Nb_xSn$ and $CoTiSn_{1-x}Sb_x$.

CoTiSn and CoTiSb. In order to investigate the influence of the lattice parameter on the SC–metal transition, calculations were performed for the $CoTiSn_{1-x}Sb_x$ series with the true parameter (figure 7 and figure 9). The overall DOS shape is not significantly changed (for $x > 0.5$); only a global shift of energies is observed. In the $CoTiSn_{1-x}Sb_x$ series

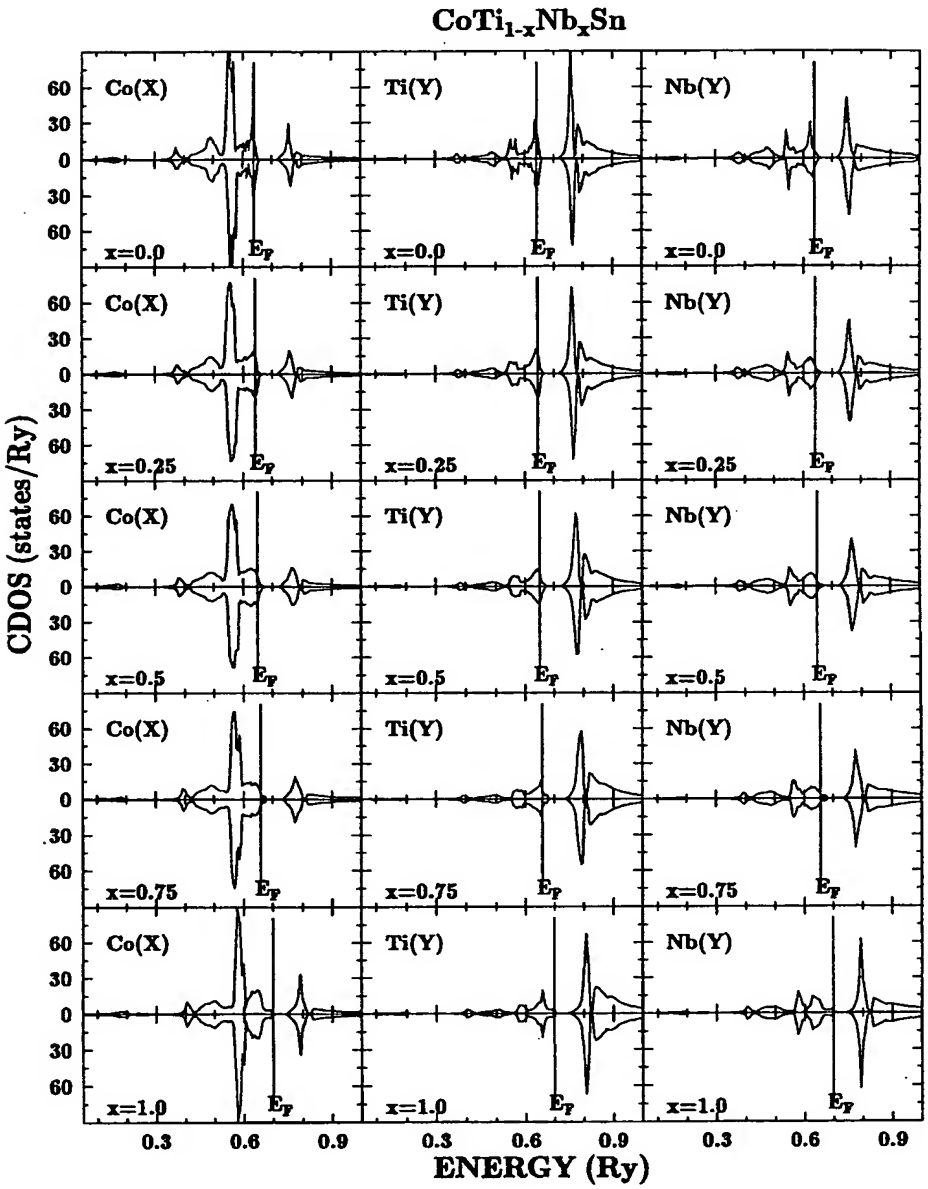

Figure 8. Component densities of states for X and Y sites in the disordered $CoTi_{1-x}Nb_xSn$ series. For borderline concentrations the CDOS of one impurity in the matrix is shown, i.e. Nb in CoTiSn ($x = 0$) and Ti in CoNbSn ($x = 1$).

(oppositely to the previous case), the gap between the conduction and valence bands slightly increases on approaching the CoTiSb compound (the left-hand column in figure 7). The spin polarization continuously decreases, reaching zero for $x \approx 0.7$, which corresponds well to magnetization measurements ($x = 0.6$). Nevertheless, in contrast to the results of the

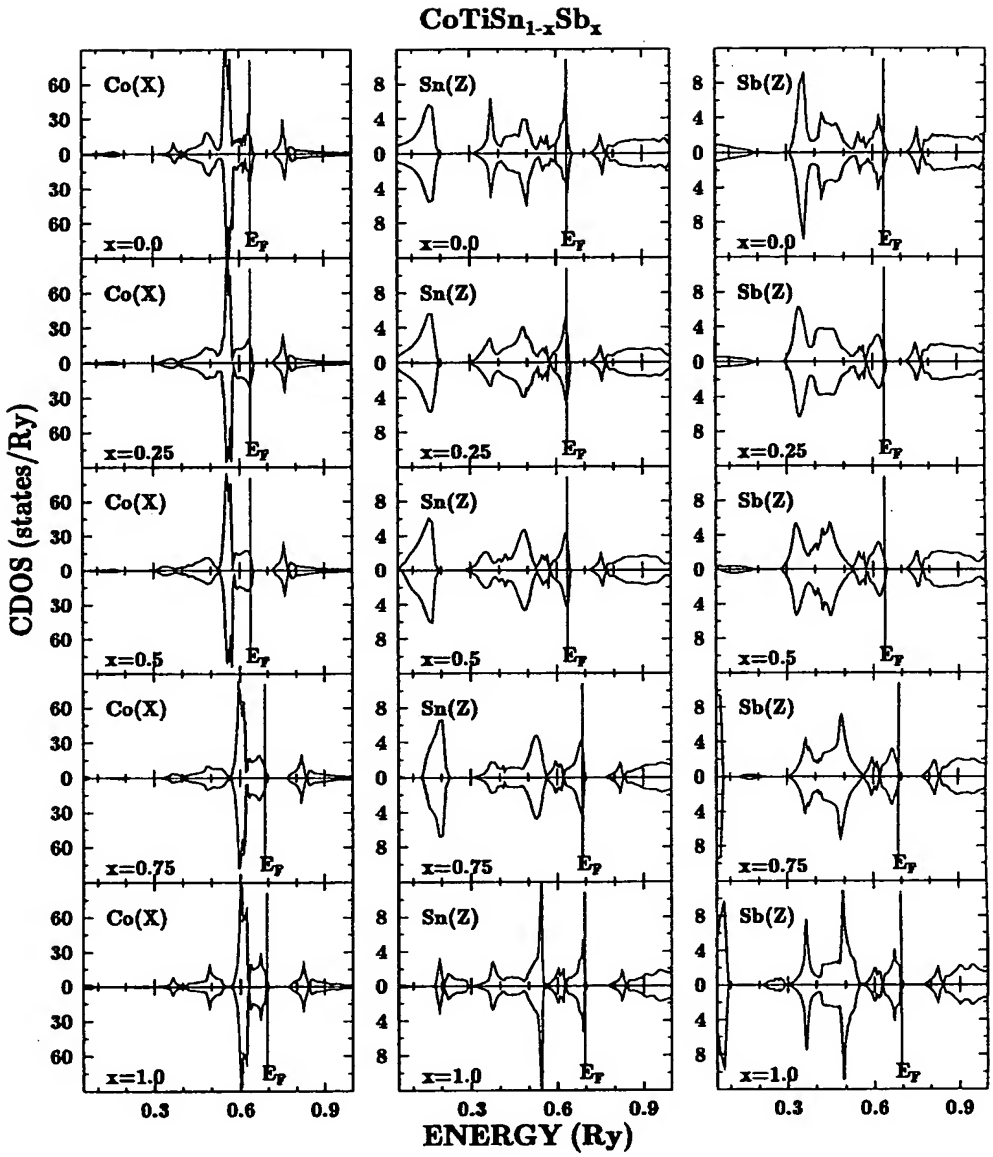

Figure 9. Component densities of states for X and Z sites in the disordered $CoTiSn_{1-x}Sb_x$ series. For borderline concentrations the CDOS of one impurity in the matrix is shown, i.e. Sb in CoTiSn ($x = 0$) and Sn in CoTiSb ($x = 1$).

transport experiments, the crossover to the semiconducting state is not observed in KKR-CPA spectra for intermediate concentrations, mainly due to non-zero contributions of states from Co and Sn atoms (figure 9).

This rigid-band behaviour is a due to eight bands, which are filled for $x = 1.0$, so E_F cannot fall into the gap for $x < 1$. Weakly doped samples probably still have a

semiconducting-like resistivity due to localization arising from the atomic disorder, which will be discussed in the next section.

4. Discussion

Some properties, such as the ferromagnetic–paramagnetic or metal–semiconductor crossovers, can be directly understood from electronic structure calculations, but other results are much less clear and need a more detailed discussion. We will first discuss the transport properties, and next the magnetic properties of these systems.

4.1. Transport properties

We first recall that the gap in the semiconducting phases cannot be properly estimated from our transport experiments below 300 K, due to their extrinsic character. Thus we must rely on the values calculated for the ideal structure within the LSD framework. Nevertheless we observe that the order of magnitude of the measured resistivity goes in the same sense as the calculated value of the gap, both values decreasing from CoTiSb, through NiTiSn, to CoNbSn. This can be simply due to the fact that CoTiSb is better ordered, having fewer impurity states, and CoNbSn is more disordered. One discrepancy between experiments and calculations is the following: when the electron concentration is decreased starting from a SC phase (EC = 18), the resistivity retains a semiconducting-like behaviour (negative temperature derivative) and a large magnitude at low temperatures up to a quite large value for the hole concentration in the lattice. Conversely, in most cases, the CPA calculations indicate that there is a finite DOS at E_F, which implies a metallic state. This should be interpreted in the following way: the CPA calculations do not completely take into account the inhomogeneities in the sample—that is, the different local potentials experienced by carriers due to the chemical disorder—since the environment at an atom is replaced by a mean potential. The resistivity behaviour is indeed caused by the disorder. Anderson and Mott [25] have treated the case of disordered semiconductors, argued for the existence of a mobility edge, and described the mechanism of variable-range hopping (VRH) of carriers, due to localization at the deepest potential wells. In the present system, the typical VRH law: $\ln(R)$ varying as $1/T^{1/4}$ or $1/T^{1/2}$, cannot be observed due to the extrinsic character, but hopping is the common mode of conduction in disordered semiconducting systems [26].

Different types of behaviour are indeed encountered in the present solid solutions. In the case of the $Co_{1-x}Ni_xTiSn$ series, calculations as well as the experimental evidence for a localized moment on Co show that Co levels fall into the former gap of NiTiSn, which is a shortcoming of the rigid-band model. This can explain why the systems remains SC until either a percolation limit is reached, or the Fermi level falls below (for hole doping) the mobility edge, when Co levels collapse into a band. In the case of the $CoTiSn_{1-x}Sb_x$ series, the discontinuity of the lattice parameter of the solid solutions shows that local environment effects must be larger. Conversely, the $CoTi_{1-x}Nb_xSn$ series looks correspondingly more homogeneous and the SC behaviour is indeed rapidly replaced by a metallic state close to the CoNbSn composition.

4.2. Magnetic properties

One first problem is to explain why some compounds present a constant paramagnetism and others a Curie–Weiss behaviour. Moriya and Kawabata [14] have shown that the existence of

strictly localized magnetic moments is not a necessary condition for the existence of Curie–Weiss behaviour. Generally, the Curie–Weiss behaviour has been found to be associated with a sharp peak of the DOS at E_F. Thus we will try to relate magnetic properties to the density of states. We must also explain why localized states of Co diluted in NiTiSn have a small effective moment, why CoTiSb does not show any localized magnetic moments, and also why itinerant magnetic features are observed for narrow bands and, thus, close to a SC–metal transition.

The first observation is that the semiconducting phases NiTiSn and CoTiSb as well as metallic NiTiSb present a susceptibility which does not depend on temperature, whereas CoTiSn and CoVSb present a weak ferromagnetism with a Curie–Weiss behaviour in the paramagnetic range.

Let us first ask what the nature is of the semiconducting phase CoTiSb (charge-transfer, Mott–Hubbard, or another type of semiconductor), and why there is no Curie–Weiss magnetism in this compound. In contrast to the case of Ni in NiTiSn, the d shell of the Co atom is not filled. Electronic structure calculations show (table 3) that there is no more charge transfer from Sb to Co than from Sn to Co in CoTiSn: the number of electrons within the muffin-tin (MT) sphere of Co is the same for the two compounds, and from the partial d DOS the configuration of Co is about $3d^8$. Large electronic correlations within the d shell should maintain a strong intra-atomic coupling. Since Sb p levels are centred well below the gap and have a weak partial DOS on both sides of the gap, we conclude that this gap does not arise only from the charge transfer between Sb and metals. On the other hand, the energy bands (figure 6) show that the splitting between $\Gamma_{25'}$ (occupied t_{2g} states of Co and Ti below E_F) and the unoccupied level Γ_{12} (e_g states above the gap) is about 2 eV. The Co d PDOS is dominant below the gap, and Ti levels dominate above. Thus the gap seems to be due mainly to the hybridization between Co and Ti and the energy difference between bonding and anti-bonding states.

The splitting of d states also indicates that the crystal field around Co is fairly large. In this case, according to Goodenough [27], the spin of the ground state resulting from the crystal field and spin–orbit coupling may be quenched. For a $3d^8$ configuration in a tetrahedral interstice, it has been predicted that the ground state is a non-magnetic singlet (Γ_1 representation), followed by a Γ_4 triplet [27]. This non-magnetic ground state expected for the ionic configuration may tentatively explain why CoTiSb fails to exhibit any Curie–Weiss behaviour, although this ionic picture should be treated with caution due to the strong hybridization with ligands. The hybridization itself, splitting the last occupied bands around the gap, may give rise to this non-magnetic situation.

The constant paramagnetism for other semiconducting phases can be explained as for CoTiSb by a non-magnetic ground state or weak correlations (NiTiSn, CoNbSn), whereas for the NiTiSb metallic phase the more or less uniform Pauli susceptibility is related to a low density of states at E_F.

Conversely, the Curie–Weiss behaviour observed in CoTiSn (or CoVSb) is obviously associated with the presence of a high local density of states at E_F, as revealed by band calculations, and can be rather well understood within the framework of itinerant-electron magnetism. Due to the presence of the gap, only one hole (or electron) participates in conduction and in magnetic ordering, which favours a ferromagnetic type of order. Surprisingly, the magnetic moment in CoVSb is expected to lie on the V atom which has the highest DOS at E_F, rather than on the Co atom. Such a situation should be verified by polarized neutron experiments on single crystals, which is the only way to measure such low ferromagnetic moments.

For solid solutions like $Co_{1-x}Ni_xTiSn$, we pass progressively from one regime to the

other, and the susceptibility can be described by the superposition of a Curie-like term plus a constant susceptibility: $\chi = (1 - x)C/T + \chi_0$. The Curie term comes from the rather well localized Co contribution, the other from other d electrons. This is a typical example of localization without a large change in the Co effective moment (1.1 μ_B for Co diluted in NiTiSn, compared to 1.35 for pure CoTiSn). The KKR-CPA band calculations [9] show that the Co d levels tend to form acceptor levels in the gap of NiTiSn (a shortcoming of the rigid-band model), which gives rise to a non-homogeneous magnetism localized at the Co sites. The ferromagnetic order appears when these impurity states are close enough to give rise to a band and thus to a large enough density of states at E_F. A percolation limit can be defined which corresponds to about 0.4 of a hole per formula unit.

The picture of spin quenching by the crystalline field can also explain, together with the weak ferromagnetism expected from the itinerant model, why the magnetic moment is so low for CoTiSn or for $Co_{1-x}Ni_xTiSn$ solutions. Crystal fields and hybridization give rise to a strong breakdown of Hund's rule and to a low-spin state. One interesting feature is that the effective moment remains close to 1.2 μ_B for CoTiSn, for CoVSb and also for some other weak ferromagnets.

Another peculiar feature is the observation of a susceptibility maximum in the $CoTiSn_{1-x}Sb_x$ series close to CoTiSb. Such a behaviour has also been observed for some enhanced paramagnets (YCo_2 for instance) as for $ZrZn_2$ under pressure [12]. Most probably it is related to a pronounced minimum in the DOS at E_F, giving a positive second derivative $n''(E_F)$; the existence of such a minimum is expected as a consequence of the former gap.

4.3. Conclusions and further developments

In summary, many very different behaviours have been observed in these semi-Heusler phases, from semiconductor to metal, from Pauli-like to Curie–Weiss paramagnet, from paramagnetic to ferromagnetic ground state. An overall agreement has been observed between experimental data and electronic band calculations. Some discrepancies remain, since calculations predict for example a ferromagnetic state for FeTiSb (but a non-magnetic state for $(Fe_{0.5}E_{0.5})_2TiSb$) and a fully polarized state for CoVSb which are not observed. Some of the discrepancies may be attributed to the crystallographic disorder in the real lattices and others to the extreme instability of the magnetic polarization near the magnetic–non-magnetic crossover.

Further experiments are planned to investigate in more detail the appearance of magnetism at the Y site, and to follow by substituting for atoms from Ti to Mn the evolution of the ferromagnetic state from the weak-ferromagnet case to the case of complete ferromagnetic polarization and half-metallic behaviour, as found for NiMnSb.

Acknowledgment

This work was partly realized at CNRS Grenoble thanks to a TEMPRA grant allotted to JT by the Rhone-Alpes Region.

References

[1] de Groot R A, Mueller F M, van Engen P G and Buschow K H J 1983 *Phys. Rev. Lett.* **50** 2024
[2] de Groot R A and Buschow K H J 1986 *J. Magn. Magn. Mater.* **54–57** 1377
[3] Kübler J, Williams A R and Sommers C B 1983 *Phys. Rev.* B **28** 1745
[4] Ishida S, Asano S and Ishida J 1984 *J. Phys. Soc. Japan* **53** 2718

[5] Aliev F G, Kozyrkow V V, Moshchalkov V V, Skolozdra R V and Durczewski K 1990 *Z. Phys.* B **80** 353
[6] Pierre J, Skolozdra R V, Gorelenko Yu K and Kouacou M A 1994 *J. Magn. Magn. Mater.* **134** 95
[7] Pierre J, Skolozdra R V and Stadnyk Yu V 1993 *J. Magn. Magn. Mater.* **128** 93
[8] Booth J G 1988 *Ferromagnetic Materials* vol 4, ed E P Wohlfarth and K H J Buschow (Amsterdam: Elsevier Science) p 211 and references therein
[9] Toboła J, Pierre J, Kaprzyk S, Skolozdra R V and Kouacou M A 1996 *J. Magn. Magn. Mater.* **159** 192
[10] Kouacou M A, Pierre J and Skolozdra R V 1995 *J. Phys.: Condens. Matter* **7** 7373
[11] Terada M, Endo K, Fujita Y and Kimura R 1972 *J. Phys. Soc. Japan* **32** 91
[12] Grosche F M, Pfleiderer C, McMullan G J, Lonzarich G G and Berhoeft N R 1995 *Physica* B **206–207** 20
[13] Pierre J, Skolozdra R V and Kouacou M A 1995 *Physica* B **206–207** 844
[14] Moriya T and Kawabata A 1973 *J. Phys. Soc. Japan* **34** 639
[15] Lonzarich G G and Taillefer L 1985 *J. Phys. C: Solid State Phys.* **18** 4339
[16] Kaplan Th, Leath P L, Gray L J and Diehl H W 1980 *Phys. Rev.* B **21** 4230 and references therein
[17] Kaprzyk S and Bansil A 1990 *Phys. Rev.* B **42** 7378
[18] Bansil A, Kaprzyk S and Toboła J 1992 *Applications of Multiple Scattering Theory in Material Science (MRS Symp. Proc. 253)* (Pittsburgh, PA: Materials Research Society) p 505
[19] Kaprzyk S 1997 *Acta Phys. Pol.* A **91** 135
[20] von Barth U and Hedin L 1972 *J. Phys. C: Solid State Phys.* **5** 1629
[21] Kaprzyk S and Mijnarends P E 1986 *J. Phys. C: Solid State Phys.* **19** 1286
[22] Mohn P, Blaha P and Schwarz K 1995 *J. Magn. Magn. Mater.* **140–144** 183
[23] Szytuła A, Tomkowicz Z and Turowski M 1973 *Acta Phys. Pol.* A **44** 147
[24] Continenza A, de Pascale T M, Meloni F and Serra M 1993 *Japan. J. Appl. Phys.* **32** 240
[25] Mott N F 1974 *Metal–Insulator Transitions* (London: Taylor and Francis)
[26] Pollack M and Shklovskii B (ed) 1991 *Hopping Transport in Solids* (Amsterdam: North-Holland)
[27] Goodenough J B 1963 *Magnetism and the Chemical Bond* (New York: Wiley–Interscience) p 67
[28] Bouckaert L P, Smoluchowski R and Wigner E 1936 *Phys. Rev.* **50** 58